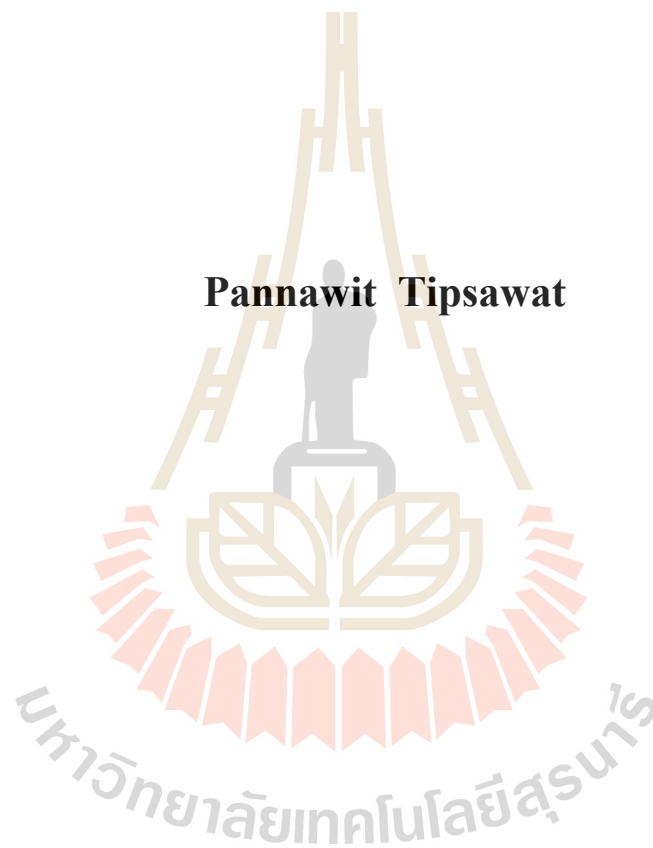


**POINT-DEFECT EQUILIBRIA OF DONORS-TYPE
DEFECTS IN CERIUM (IV) OXIDE**



Pannawit Tipsawat

**A Thesis Submitted in Partial Fulfillment of the Requirement for the
Degree of Master of Science in Physics
Suranaree University of Technology
Academic Year 2018**

สมุดความบกพร่องแบบจุดของความบกพร่องแบบผู้ให้ในซีเรียมออกไซด์



วิทยานิพนธ์นี้เป็นส่วนหนึ่งของการศึกษาตามหลักสูตรปริญญาวิทยาศาสตรมหาบัณฑิต

สาขาวิชาฟิสิกส์

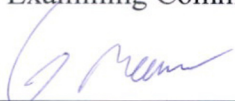
มหาวิทยาลัยเทคโนโลยีสุรนารี

ปีการศึกษา 2561

**POINT-DEFECT EQUILIBRIA OF DONORS-TYPE
DEFECTS IN CERIUM (IV) OXIDE**

Suranaree University of Technology has approved this thesis submitted in partial fulfillment of the requirement for a Master's Degree.

Thesis Examining Committee



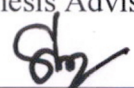
(Assoc. Prof. Dr. Worawat Meevasana)

Chairperson



(Assoc. Prof. Dr. Sirichok Jungthawan)

Member (Thesis Advisor)



(Prof. Dr. Santi Maensiri)

Member



(Asst. Prof. Dr. Michael F. Smith)

Member



(Prof. Dr. Santi Maensiri)
Vice Rector for Academic Affairs
and Internationalization



(Assoc. Prof. Dr. Worawat Meevasana)
Dean of Institute of Science

ปณิธาน วิจัย : สมดุลความบกพร่องแบบจุดของความบกพร่องแบบผู้ให้ในซีเรียมออกไซด์ (POINT-DEFECT EQUILIBRIA OF DONORS-TYPE DEFECTS IN CERIUM (IV) OXIDE). อาจารย์ที่ปรึกษา : รองศาสตราจารย์ ดร.ศิริโชค จิ่งถาวรณ, 81 หน้า.

ซีเรียมออกไซด์/ โพลารอนขนาดเล็ก/ ความบกพร่องแบบจุด/ ผู้ให้/ โลคอลไลเซชัน/ สมบัติการขนส่งอิเล็กตรอน

วัตถุประสงค์ของงานวิจัยนี้คือการศึกษสมบัติการขนส่งและการโลคอลไลเซชันของอิเล็กตรอนในซีเรียมออกไซด์ซึ่งถูกอธิบายด้วยทฤษฎีการกระโดดของโพลารอนโดยซีเรียมออกไซด์เจือแทนทาลัมและทั้งสแตนถูกเตรียมโดยวิธีปฏิกิริยาสถานะของแข็งที่ความเข้มข้นระหว่าง $0.0005 < x < 0.004$

การวิเคราะห์ความบริสุทธิ์ด้วยเทคนิคการเลี้ยวเบนของรังสีเอกซ์ (XRD) ยืนยันความบริสุทธิ์ของสารตัวอย่างโดยปราศจากเฟสเจือปน แลตทิซพารามิเตอร์จากการทดลองและการจำลองจากกลไกการชดเชยของความบกพร่องมีแนวโน้มที่สอดคล้องกัน โดยที่กลุ่มตัวอย่างที่ถูกเจือโดยแทนทาลัมแสดงการหดตัวของแลตทิซพารามิเตอร์ ในขณะที่แลตทิซพารามิเตอร์ของสารตัวอย่างที่เจือด้วยทั้งสแตนนั้นขยายตัวเมื่อความเข้มข้นการเจือเพิ่มขึ้น การเปลี่ยนแปลงของแลตทิซพารามิเตอร์นั้นเกิดจากการมีอยู่ของอะตอมเจือปนและกลไกการชดเชยของความบกพร่อง อย่างไรก็ตามความคลาดเคลื่อนระหว่างการผลจากการทดลองและผลจากการจำลองนั้นมีความเป็นไปได้ที่มาจากความเสียหายไปของความเข้มข้นของ Ce^{3+} ในขั้นตอนการจำลองแลตทิซพารามิเตอร์ สมมติฐานนี้ถูกสนับสนุนโดยผลการวิเคราะห์ปริมาณ Ce^{3+} ซึ่งอัตราส่วนความเข้มข้นระหว่าง Ce^{3+} และอะตอมผู้ให้แสดงผลที่ต่ำกว่าการคาดการณ์แบบจำลองการชดเชยของความบกพร่อง สำหรับการหายไปของความเข้มข้นของ Ce^{3+} นั้นมีข้อสมมติฐานว่าเกิดจากการที่บางส่วนของอิเล็กตรอนจากไอออนของ Ce^{3+} ถูกชดเชยด้วยความบกพร่องประจุบวกชนิดอื่น ตัวอย่างเช่น ความบกพร่องของออกซิเจนแบบแทรก

รูปแบบของความบกพร่องที่เกิดในซีเรียมออกไซด์เจือแทนทาลัมและทั้งสแตนแสดงให้เห็นว่าโพลารอนขนาดเล็กนั้นจะอยู่ตำแหน่งใกล้เคียงกับอะตอมแทนทาลัมในรูปแบบ $(Ce'_{Ce} - Ta'_{Ce})^0$ ในขณะที่ในตัวอย่างไม่ทั้งสแตนโพลารอนชนิดเล็กสองอะตอมนั้นจะอยู่ที่ตำแหน่งถัดไปที่ใกล้ที่สุดกับอะตอมทั้งสแตน $(2Ce'_{Ce} - W''_{Ce})^0$ ซึ่งเป็นการแสดงให้เห็นชัดถึงการมีอยู่ของโพลารอนขนาดเล็กในซีเรียมออกไซด์ประเภทอื่นและยังเน้นชัดถึงอันตรกิริยาระหว่างโพลารอนขนาดเล็กและอะตอมของสารเจือปนแบบผู้ให้ การวิเคราะห์สมบัติการนำไฟฟ้าของซีเรียมออกไซด์

เอกสารผู้ให้แสดงพฤติกรรมการนำไฟฟ้าแบบถูกกระตุ้นด้วยความร้อน ในกราฟแสดงสมบัติการนำไฟฟ้าของสารกลุ่มแทนทาลัมแสดงการมีกลไกการนำไฟฟ้าสองกลไกที่อุณหภูมิต่ำจะมีกลไกการนำไฟฟ้าของสารเจือปน และที่อุณหภูมิสูงขึ้นหรือมากกว่า 150 K จะมีกลไกการนำไฟฟ้าผ่านกระบวนการกระโดดของโพลารอนขนาดเล็ก พลังงานกระตุ้นของโพลารอนขนาดเล็กถูกคำนวณผ่านการคำนวณเชิงเส้น และพล็อตพลังงานกระตุ้นเทียบกับประจุของผู้ให้ (Δq) โดยพลังงานกระตุ้นสูงสุดของโพลารอนขนาดเล็กเท่ากับ $\sim 66 \pm 20$ มิลลิอิเล็กตรอน โวลต์ ยิ่งไปกว่านั้นข้อสันนิษฐานเกี่ยวกับอันตรกิริยาระหว่างโพลารอนชนิดเล็กและอะตอมผู้ให้นั้นถูกยืนยันเมื่อพิจารณาค่าพลังงานยึดเหนี่ยวระหว่างทั้งอะตอมทั้งสองชนิด ซึ่งพบว่าเมื่อประจุของผู้ให้มีความมากขึ้น ผลจากพลังงานยึดเหนี่ยวจะมีอำนาจเหนือกว่าผลจากพลังงานกระตุ้นของโพลารอนขนาดเล็ก ข้อสรุปจากผลการทดลองทั้งหมดนั้นให้เหตุผลสอดคล้องกันว่าอันตรกิริยาของคู่ออมบ์ระหว่างโพลารอนขนาดเล็กและอะตอมเจือปนแบบผู้ให้นั้นมีผลอย่างมีนัยยะสำคัญต่อการเคลื่อนที่ของโพลารอนขนาดเล็ก



สาขาวิชาฟิสิกส์

ปีการศึกษา 2561

ลายมือชื่อนักศึกษา

[Handwritten signature]

ลายมือชื่ออาจารย์ที่ปรึกษา

[Handwritten signature]

ลายมือชื่ออาจารย์ที่ปรึกษาร่วม

[Handwritten signature]

PANNAWIT TIPSAWAT : POINT-DEFECT EQUILIBRIA OF DONORS-
TYPE DEFECTS IN CERIUM (IV) OXIDE. THESIS ADVISOR : ASSOC.
PROF. SIRICHOK JUNGTHAWAN, Ph.D. 81 PP.

CERIUM DIOXIDE/ SMALL POLARON/ POINT-DEFECT/DONORS/
LOCALIZATION/ TRANSPORT PROPERTIES

This work is aiming to understand electron transport and localization of n-type CeO₂ where the small polaron theory mainly contributes to charge transport mechanism. N-type CeO₂ was achieved by donor impurities doping. The donors (Ta and W) doped CeO₂ were prepared by solid-state reaction route with doping concentration limited to dilute regime $0.005 < x < 0.004$.

The purity of obtained ceramic samples was identified using x-ray diffraction while the result showed no observable diffraction of secondary phase. The lattice parameter from x-ray diffraction was compared with the calculated lattice parameter from defect compensation mechanism. The experiment and calculated parameter were in good agreement where Ta doped ceria is distorted as increasing doping concentration and W doped ceria showed expansion trend. This is because the presence of impurities and defect compensation play a role in lattice evolution. However, the deviation of lattice parameter may due to the lack of Ce³⁺ concentration. This is supported by the analysis of Ce³⁺ where both Ta and W doped ceria have ratio between Ce³⁺ and donor impurities lower than expected value from our model. We suggested that the Ce³⁺ ions

are partially compensated with other effective positive defect species such as oxygen interstitial.

The defect formation showed that small polaron localizes at nearest neighbor of Ta as $(\text{Ce}'_{\text{Ce}} - \text{Ta}\bullet_{\text{Ce}})^0$ while two small polarons are sitting near each other at nearest position to W^{6+} ions as $(2\text{Ce}'_{\text{Ce}} - \text{W}\bullet\bullet_{\text{Ce}})^0$. This clarifies the existence of small polaron in n-type CeO_2 and emphasizes the hypothesis of interaction between small polaron and donor impurities. In conductivity analysis, donor doped ceria exhibited thermally activated conductivity. Ta doped ceria's conductivity is linear line with two slopes mean two different thermally activated process where the low and high temperature regimes are impurity conduction and small polaron hopping, respectively. The individually activation energy of small polaron is obtained by the linear fitting of activation energy against effective charge of donor where the upper bound for hopping energy of small polaron is 66 ± 20 meV. Moreover, the binding energy between small polaron and donor impurities is dominant as effective charge increasing. Eventually, all results support the hypothesis that small polaron itinerant is strongly affecting by Coulomb interaction between small polaron and donor impurities.

School of Physics

Academic Year 2018

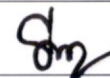
Student's Signature



Advisor's Signature



Co-advisor's Signature



ACKNOWLEDGEMENT

First of all, I would like to express my sincere to my supervisor Assoc. Prof. Dr. Sirichok Jungthawan for teaching me lot of how to work as a good experimentalist and I have gained so many skills working with him. I also would like to thank to my co-advisor Prof. Dr. Santi Maensiri for inspiring my research career since I was a sophomore. Without the kindness of Dr. Taras Kolodiazhnyi, a principal senior research at National Institute for Materials Science (NIMS), Japan, this work and my master's degree could not be done. Working and living in Japan are my life changing point and the most worthful moment of my life. I always felt appreciated with all helps, skills, knowledges Dr. Taras gave me.

This project has a big goal to understand electron localization and transport properties of n-type CeO₂. The number of experimental and theoretical attempts were done, and every step is vital for the work. The preliminary works of Dr. Taras and Miss Thitirat Charoonsuk gave a priceless guiding way for solving the problem of my thesis work. Additionally, the calculation part is a big deal to understand the whole picture of this work, I would say that without spectacular calculation from Mr. Thanundon Kongnok, Asst. Prof. Dr. Sirichok Jungthawan and Dr. Suwit Suthirakun, this work will never be like this.

There are such a people behind the successful of my master's thesis. The supporting from Advanced Materials Physics laboratory (AMP) members is Indispensable and I am grateful to be a part of AMP group. At the beginning of my

master's degree, the short-term research at NIMS cannot happen without all academic staffs from School of Physics and Institute of Science.

I am confident that study environment is a key parameter that shapes my perspective and perform. I would like to mention my friend at School of Physics who are always helping me with every problem, I have faced and my teachers who teach me worthwhile lesson and encourage me to do things I wish.

I would like to thank the Development and Promotion of Science and Technology Talents Project (DPST) for funding my six-month research in Japan and my entire study since a beginning of my bachelor's degree until now. I also would like to acknowledge NIMS for the opportunity of conducting a research at a great research institute with so many well-equipped instruments

Finally, I am thankful for having my family with me and always supports me every step I have taken and every decide I have made.



Pannawit Tipsawat

CONTENTS

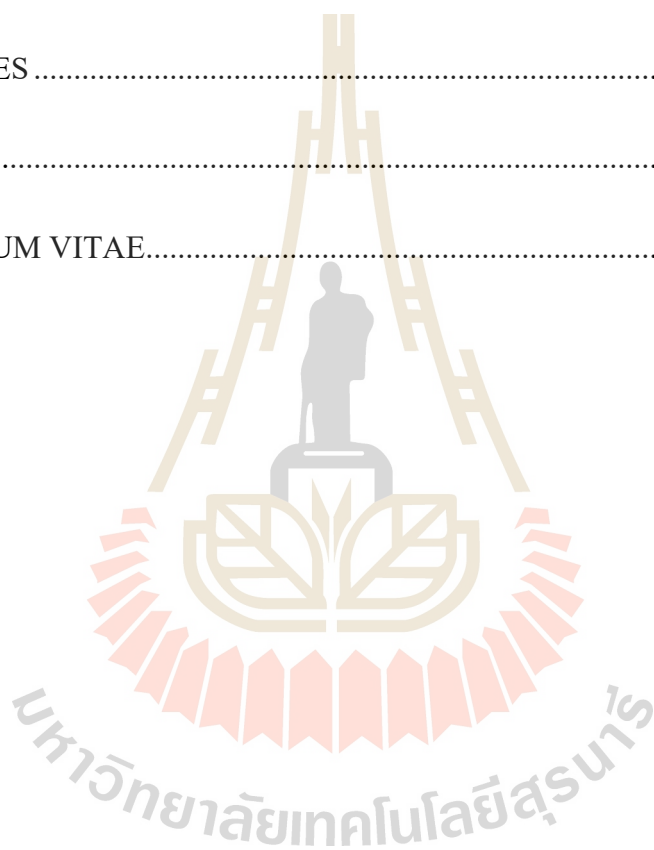
	Page
ABSTRACT IN THAI.....	I
ABSTRACT IN ENGLISH.....	III
ACKNOWLEDGEMENT.....	V
CONTENS.....	VII
LIST OF FIGURES.....	X
LIST OF ABBREVIATIONS.....	XVI
CHAPTER	
I INTRODUCTION.....	1
1.1 Significant and rational of the research.....	1
1.2 Research objective.....	3
1.3 Location of the research.....	4
II THE REVIEWS OF ELECTRON TRANSPORT AND LOCALIZATION IN N-TYPE CERIUM DIOXIDE.....	6
2.1 The concept of small polaron.....	6
2.2 Small polaron in CeO ₂	9
2.3 The additional driven force of electron localization in CeO ₂	16

CONTENS (Continued)

	Page
III	FUNDAMENTAL OF DEFECT CHEMISTRY 19
	3.1 Point defect 19
	3.2 Shallow impurity 23
	3.3 Conductivity 25
IV	RESEARCH METHODOLOGY 32
	4.1 Ceramic sample preparation by solid state reaction 32
	4.2 Characterization 33
	4.2.1 X-ray diffraction spectroscopy (XRD) 33
	4.2.2 Superconducting quantum interference device (SQUID)..... 35
	4.2.3 The electrical impedance spectroscopy 36
V	RESULTS AND DISCUSSION 38
	5.1 Microstructure and defect chemistry of donors doped CeO ₂ 38
	5.1.1 Phase purities and lattice parameter refinement 38
	5.1.2 Magnetochemistry treatment 44
	5.2 Electron transport properties..... 49
	5.3 Discussion..... 52
VI	CONCLUSION & FUTURE DIRECTION OF WORK..... 62

CONTENTS (Continued)

	Page
6.1 Conclusion	62
6.2 Future direction of work	63
REFERENCES	64
APPENDIX	70
CURRICULUM VITAE.....	81



LIST OF FIGURES

Figure	Page
2.1 The re-arranging of atomic position due to the small polaron formation (Emin, 2013).....	7
2.2 (a) The CaF ₂ structure comprises of cations (Ca ions) form face-centered cubic structure with anions (F ions) in tetrahedral voids as simple cubic. (b) The cubic fluorite structure of CeO ₂ where blue and red sphere are cerium and oxygen ions, respectively (Skorodumova et al., 2002).....	9
2.3 The mechanism of Band conductivity of Bloch wave electron compared with hopping conductivity from motion of hopping carrier in localized (Kang et al., 2018).....	12
2.4 The obtained impedance spectra of Ce _{0.85} Gd _{0.15} O _{1.925} with the corresponding equivalent circuit show the contribution of bulk gain, grain boundary and effect of electrode (Zajac and Molenda, 2008).....	14
2.5 The electrical conductivity of Nb and Ta doped CeO ₂ show the transition point in temperature dependent conductivity. The activation energy was derived and divided into two parts as high temperature and low temperature activation energy (Kolodiaznyi et al., 2017).	15

LIST OF FIGURES (Continued)

Figure	Page
2.6 The defect configuration of small polarons and oxygen vacancies are represented as (a) $(V_O^{\bullet\bullet} - 2\text{polaron})^0$, (b) $(V_O^{\bullet\bullet} - \text{polaron})^+$, and (c) $V_O^{\bullet\bullet}$ where grey spheres are Ce atoms, small red spheres are O atoms, dark circles are oxygen vacancies, and small polarons represent yellow spin-up (Sun et al., 2017).	17
3.1 The illustration of inorganic compound with possible point defect species in crystal structure (Tuller and Bishop, 2011).	19
3.2 The demonstration of acceptor impurities shows Boron as acceptor and Silicon is host lattice (Grundmann, 2015).	21
3.3 This illustration is Arsenic as donor impurity in Silicon semiconductor (Grundmann, 2015).	23
3.4 The conductivity process in semiconductor and insulator where (a) at $T = 0\text{ K}$, valence band and conduction band are separated by band gap and (b) the electron is excited from top of valence band across band gap to the conduction band resulting in free electron (Callister, 2007).	24
3.5 The conductivity process of n-type semiconductor arises from impurities state termed donor states where (a) this state positions at	

LIST OF FIGURES (Continued)

Figure	Page
<p>below the conduction band and (b) capable of donating electron to conduction band (Callister, 2007).....</p>	25
<p>3.6 The conductivity process of n-type semiconductor arises from impurity states termed as acceptor states where (a) this state positions at above valence band and (b) capable of accepting an electron from valence band and leaving electron holes (Callister, 2007).....</p>	26
<p>3.7 The conductivity process of n-type semiconductor arises from acceptor states (Callister, 2007).....</p>	27
<p>4.1 The flow chart shows synthesis procedure of ceramics n-type donors doped CeO₂.</p>	30
<p>4.2 The figure shows a schematic of x-ray diffraction (a) and diffractometer (b) (Callister, 2007).....</p>	31
<p>4.3 The represent of SQUID system where (a) the Josephson junction and DC SQUID contained two Josephson junctions (adapted from Jenks et al., 1997) and (b) the experimental measurement system of MPMS equipped with SQUID (Quantum design).</p>	33
<p>4.4 The schematic measurement of Alpha-A impedance analyzer (Friedrich Kremer, 1999).....</p>	34

LIST OF FIGURES (Continued)

Figure	Page
5.1	The XRD spectra of Ta and W doped CeO ₂ compared with main peaks of pure CeO ₂ and internal standard LaB6. 37
5.2	The fitting of Rietveld refinement with (insert) shifting of peak at high angle diffraction of each compositions. 38
5.3	The lattice estimation from defect equation compared with results from Rietveld refinement. 40
5.4	The inverse temperature dependent magnetic susceptibility of Ta and W doped CeO ₂ 44
5.5	The fitting parameter obtained from magnetochemistry method where red rectangular (■) and green circle (●) symbol indicate Ta and W doped CeO ₂ , respectively. Each row indicates different fitting parameter where row a is concentration of Ce ³⁺ (c), row b is crystal field splitting energy between Γ_8 and Γ_7 , row (c) is the susceptibility of temperature-independent paramagnetism constant (χ_{TIP}) and row d is molecular field constant (λ). The solid lines at row an index compensation ratio of Ce ³⁺ :Donors where red line is ratio 2:1 and blue line is ratio 1:1..... 45

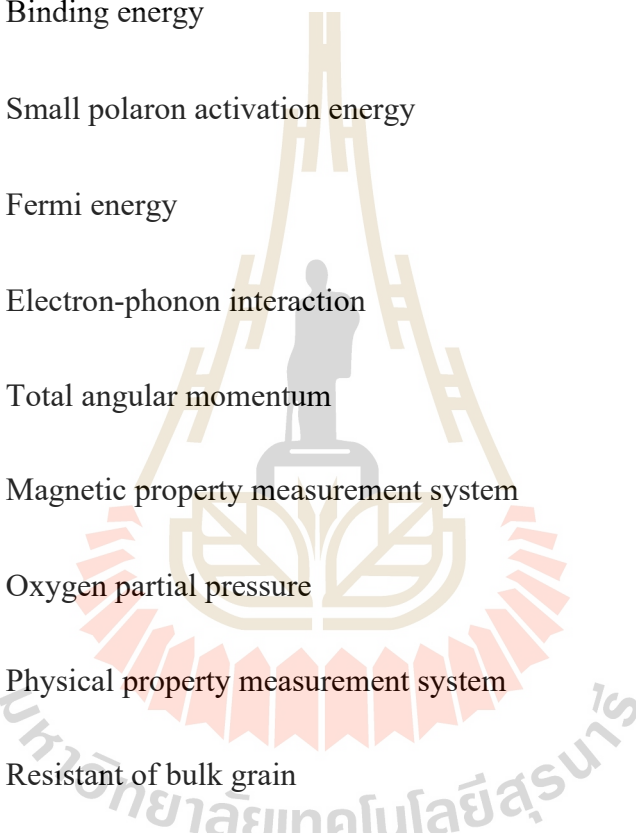
LIST OF FIGURES (Continued)

Figure	Page	
5.6	The selected impedance spectra of W doped CeO ₂ at 200 K demonstrated the semicircle behavior of bulk grain resistance and low frequency effects of electrode interface effect.	46
5.7	The temperature dependent conductivity of Ta and W doped CeO ₂ with obtained activation energy from equation 5.11(a). The activation energy of Ta doped ceria show two distinct activated process in high and low temperature regime (b).	48
5.8	The bound small polaron that confines in potential well induced by lattice distortion (small polaron model) (at top), by the presence of donor (at the middle), and by combing both lattices distort and donor effect (at bottom) (Kolodiazhnyi et al., 2019).	51
5.9	The activation energy plot of donors doped ceria combines the data of U doped ceria from the literature (Stratton and Tuller, 1987) and other Nb from (Kolodiazhnyi et al., 2017).	52
5.10	The density of states (DOS) of (a) Ta and (b) W doped CeO ₂ , respectively. The VBM positioned as zero and dash line indicated the Fermi level where both figure show defect state of small polaron is	

LIST OF FIGURES (Continued)

Figure		Page
	slightly below the conduction band (Kolodiazhnyi et al., 2019).	55
5.11	The calculated formation energy of each configurations compared with fermi energy. This assured that in (a) Ta doped ceria ($\text{Ta}_{\text{Ce}}^{\bullet} - \text{polaron}$) ⁰ is the most stable structure while (b) ($\text{W}_{\text{Ce}}^{\bullet\bullet} - 2\text{polaron}$) ⁰ is W doped ceria favorable defect complex (Kolodiazhnyi et al., 2019).	56
5.12	The calculated spin density of favorable configuration of defect complex: (a) ($\text{Ta}_{\text{Ce}}^{\bullet} - \text{Ce}'_{\text{Ce}}$) ⁰ and (b) ($\text{W}_{\text{Ce}}^{\bullet\bullet} - 2\text{Ce}'_{\text{Ce}}$) ⁰ (Kolodiazhnyi et al., 2019).	56

LIST OF ABBREVIATIONS



E_{σ}	=	Conductivity activation energy
E_b	=	Binding energy
E_h	=	Small polaron activation energy
E_F	=	Fermi energy
EP	=	Electron-phonon interaction
J	=	Total angular momentum
MPMS	=	Magnetic property measurement system
PO ₂	=	Oxygen partial pressure
PPMS	=	Physical property measurement system
R _{bulk}	=	Resistant of bulk grain
R _{ct}	=	Resistant of charge transfer
R _{gb}	=	Resistant of grain boundary
SP	=	Small Polaron model
SQUID	=	Superconducting quantum interference device
XRD	=	X-ray diffractometer

CHAPTER I

INTRODUCTION

1.1 Significant and rational of the research

When consider the electrons in metal, normally the free electrons are delocalized electrons behaving Bloch wave. However, in some semiconductors with incomplete d or f orbital, when electrons are introduced, they tend to form localized states due to the strong interaction between electron and phonon. These localized states determine the metal-insulator transition of semiconductors. One approach to interpret the transport of localized electron is small polaron theory (SP). When extra electron is added to crystal structure and stay adequately long over vibrational period on the host sites, the surrounding atomic hosts will rearrange their position to new equilibrium due to influence of the presence of that electron. This distortion induces a new potential well and electron will be confined by a new induced potential well. This phenomenon was named “*self-trapped*” mechanism. The term “SP” generally refers to both self-trapped electron and atomic distortion. The SP was initiated by a short paper of L. D. Landau (Landau, 1933). The work suggested that the electron motion is considerably slow when travel in insulators such as sodium chloride and this electron could be trapped by the deformation of lattice. One of the most promising properties of SP is transport properties through hopping process. Small polaron itinerants by phonon-assisted jump between the neighbor atom resulting in the overall materials electrical conductivity. The small polaron hopping can be enlarged by thermal energy and yields a

thermally activated conductivity at low temperature regime in semiconductors. However, it has been a puzzling work to study the actual mechanism of SP since both delocalized and small polaron mechanisms can yield thermally activated conductivity. The most obvious example of small polaron is observed in low mobility semiconductor such as n-type cerium dioxide (CeO_2).

CeO_2 has been known as ceria, is a wide bandgap semiconductor with experimental bandgap of 3.2 eV (Orel and Orel, 1994). Ceria possesses the unique cubic fluorite structure (AB_2) with a high reputation in industrial and academic applications due to various types of defect formation in structure. For the academic interest, n-type ceria represents one of the clearest examples of small polaron with two main advantages for studying electron localization and thermally activated conductivity: i) ceria is easily achieving low doping concentration and ii) ceria has empty $4f$ electron system. Firstly, since small polaron is strongly depends on the number and species of defects, the small doping concentration can benefit in restricting the number of defects to proper one. Secondly, ceria has an empty $4f$ electron system so the added electron will occupy at $4f^1$ orbital which is easily to neglect an effect from electron-electron interaction within the band. Although the study of n-type ceria's charge transport mechanism is carried out through decades, the SP is still not well established. The main challenge is a large scattering of observed electrical conductivity activation energy. This deviation is opposing the ideal small polaron transport which based on thermal assisted jump where the activation energy should be independent of impurities species. One of the theories to compensate the lack of understanding in deviation of activation energy is disorder induced random field in defective crystal structure where the interaction of effective positive impurities and trapped electron is significantly strong. To clarify this problem,

the defect chemistry plays an important role as powerful tools to study a system with defects. This tool is significant procedure in establishing knowledge of electron transport and localization in ceria since the electron localization and transport properties in ceria are mainly driven by defect related mechanism.

To distinguish the puzzling mechanism of $4f$ electron mobility in ceria, the n-type ceria was prepared by establishing donors doped ceria system. The donor dopants in this work are comprised of a penta-valence dopant (tantalum) and a hexa-valence dopant (tungsten). The ceramic sample of donors doped ceria was synthesis by simple solid-state reaction. The structural properties were investigated using x-ray diffraction technique (XRD) and Rietveld refinement for calculating the lattice parameter of cubic fluorite. While the paramagnetism was observed by superconducting quantum interference device (SQUID), the obtained magnetic susceptibility was then modelled using magnetochemistry method to reveal the accurate Ce^{3+} concentration. The electron transport properties of n-type ceria were investigated through the electrical impedance spectroscopy. The obtained temperature dependence of conductivity was observed and fitted with the Arrhenius-type behavior for calculating the activation energy. The assumption of defect formation and electron transport were made based on the experimental results together and the supporting first principle calculations precisely.

1.2 Research objectives

The objective of this work is to establish the donors doped ceria comprises of pentavalent and hexavalent impurities with an aim to understand the electron localization and transport properties of $4f$ electron in cerium oxide. The investigation of

electron localization and defect formation are based on the experimental analysis of evolution of lattice parameter by X-ray diffraction spectroscopy and the Ce^{3+} quantity through magnetic study by Superconducting quantum interference devices. The transport properties are carried out by the analysis of temperature dependent conductivity obtained from electrical impedance spectroscopy. The expected results are expected to provided better understanding of the necessary mechanism that contribute to electrical conductivity in donor doped CeO_2 . The observed evidences could lead to the next step of solving electron localization and transport properties in n-type semiconductors.

1.3 Scope of study

This work is limited to study electron transport and localization in ceramic sample of n-type CeO_2 where the donor impurities are tantalum (Ta) and tungsten (W) prepared by solid state reaction in air ambience. Since electron mobility in n-type CeO_2 is extremely low, limit experimental doping concentration (x) is limited dilute regime where $0.0005 < x < 0.004$. All defects in this work are considered the possibility of occurrence at oxygen sufficient condition ($\text{PO}_2 = 0.02 \text{ atm}$).

1.4 Location of the research

The experiments were taken at National Institute for Materials Science (NIMS), 1-1 Namiki, Tsukuba, Japan and Advanced Materials Physics (AMP) Laboratory, School of Physics, Institute of Science, Suranaree University of Technology, 111 University Avenue, Muang District, Nakhon Ratchasima Thailand.

1.5 Outline of thesis

This thesis is divided into six chapters in order to systemically introduce the work of donors doped CeO_2 , coherently. In chapter I, the significant, rational and objective of research is presented with the limited scope so the readers can understand main problem and prepare for our approach to solve that problem in this thesis. Chapter II, the review of electron transport and localization of n-type CeO_2 , this chapter aims to draw of full picture of literature research prior to our work and pointing out a challenge of research in n-type CeO_2 . Essentially, in chapter III, the concept of small polaron formation and transport are gently discussed in detail where the fundament of defect chemistry and charge transport which are main interest in our research are presenting. To be noted that this knowledge is essential tools for fully understand both electron localization and charge transport of small polaron and related mechanism. Chapter IV is research methodology where the synthesis route is presenting along with basic concept of equipped characterization techniques for example, x-ray diffraction spectroscopy, superconducting quantum interference device, and electrical impedance spectroscopy. The most important is chapter V, the results and discussion, where all the experimental results are presented and discussed together with the excellent calculation works to indeed comprehend the electron localization and transport properties of n-type CeO_2 . This chapter evaluates the problem of lattice evolution, defect compensation and formation, driven force for electron localization, and charge transport of n-type CeO_2 . The last chapter is conclusion and future work. The chapter's objectives are to summarize and make suggestion on the picture in electron localization and transport properties of n-type CeO_2 and the benefit this work can contribute to semiconductor research.

CHAPTER II

THE REVIEWS OF ELECTRON TRANSPORT AND LOCALIZATION IN N-TYPE CERIUM OXIDE

This chapter is presenting the fundamental understanding of concepts and problems in small polaron formation, localization and transport properties from the early work back in 1933. Additionally, this chapter is also giving literature reviews of several attempts on clarifying the electronic structure and transport properties of small polaron in n-type CeO₂. The most important point of this chapter is to point out an important of our effort on donors doped system.

2.1 The concept of small polaron

In 1933, L.D. Landau published an initiated work on SP discussing about the localization of slow moving electron in insulator crystal (Landau, 1933). While the electron is slowly moving in lattice, the surrounding atoms then experienced an existence of additional negative charge. Then, the atoms will reposition their equilibrium position. The deformation of atomic position is inducing a new potential well while the delocalized electron will experience this potential well, simultaneously. Specifically, when the induced potential well is deep enough, the electron is then “*self-trapped*” and forming “strong-coupling polaron”. This trapped electron cannot overcome from the potential well without the proper amount of energy. The behavior of

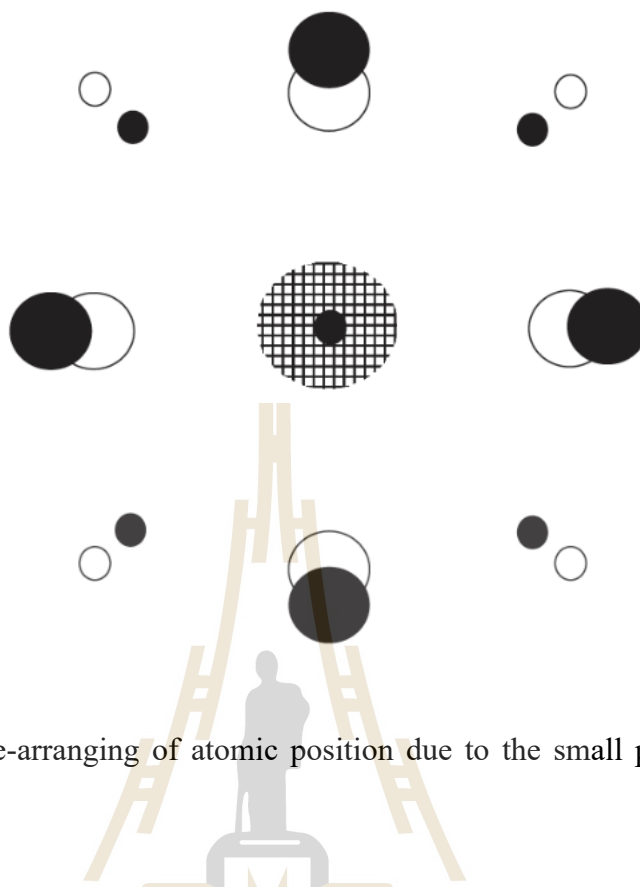


Figure 2.1 The re-arranging of atomic position due to the small polaron formation (Emin, 2013).

polaron is strongly depending on the interaction between electronic carrier and surrounding atoms because this interaction determines potential well's wave function. Generally, the word polaron refers to the unit consisted of a self-trapped electron and associated lattice deformation. The strong-coupling polaron is often referring as "quasi-free carrier", and it can be characterized into two types: large polaron where the self-trapped carrier can extend over several structural unit and small polaron which a self-trapped carrier is confined to one atomic unit. Large polaron motion is coherently moving through several sites and occasionally interrupting by the scattering process. This transport mechanism yields high mobility in materials (higher than $1 \text{ cm}^2/\text{V}\cdot\text{sec}$) and falls with higher temperature. In contrast to large polaron, small polaron transport has lower mobility (lower than $1 \text{ cm}^2/\text{V}\cdot\text{sec}$) since the transport is incoherent motion

driven by occasional succession of phonon-assisted jump through severely localized states.

Phonon-assisted electronic hopping is classified into two types: i) at low temperature, carrier hopping within shallow impurities states (impurity conductivity) and ii) at high temperature, carrier hopping between cations (small polaron). These jumping processes are driven by electron-phonon (EP) interaction and hopping rates is proportional to thermal energy. The required hopping energy is associating with EP interaction. and EP interaction is strong when phonon wavelength is larger than localized electrons. In case of impurity conduction, the radii of shallow impurity normally exceed the interatomic separation, and this results the weak interaction between localized states and phonon. Therefore, each jump only involves an absorption and emission of a single long wavelength phonon during hopping between shallow impurity state. On the other hand, small polaron hopping at high temperature is hopping in the strong localized electronic states with strong electron-phonon interaction. Thus, this process typically requires a number of phonons in absorbed and emitted process. The small polaron phonon-assisted jump process can be divided into three step mechanism: i) surrounding atoms begin to thermally vibrate causing large atomic displacement at nearest a self-trapped electron, ii) with a proper amplitude of fluctuation, a self-trapped electron will transfer to the adjacent sites, and iii) the large displacement eventually relaxes and dissipates the energy to surrounding atoms. This hopping process is rising as temperature is increasing and when temperature exceeds phonon characteristic temperature, this transport mechanism will behave as the Arrhenius-type behavior since the motion of electronic alters to move classically.

2.2 Small polaron in CeO₂

CeO₂ also known as ceria is a wide bandgap semiconductor with a unique cubic fluorite structure. Ceria is well known for technological application due to the defective ability in easily reversible of Ce³⁺ ↔ Ce⁴⁺ states. This ability raised the applications in catalytic properties such as three-way automotive catalytic converter (Kašpar et al., 1999), oxygen sensors (Beie and Gnörich, 1991), low-T electrolyte for SOFC (Tuller and Nowick, 1975), thermochemical redox splitting of H₂O (Muhich and Steinfeld, 2017), oxygen permeation membrane systems (Stoukides, 2000) etc. Moreover, CeO₂ is widely studied as the analogue of radioactive rare earth, UO₂ which shared same cubic fluorite structure and is unsafe for laboratory work (Stennett et al., 2013).

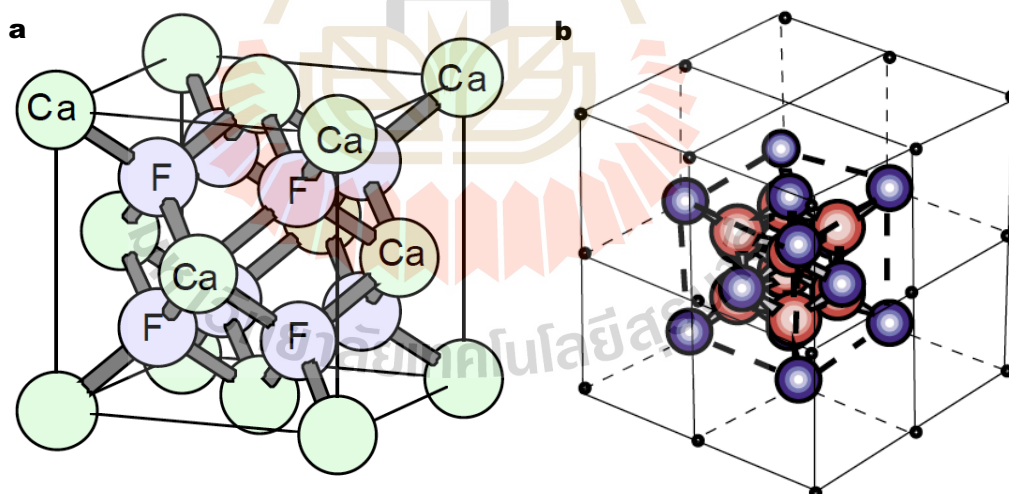


Figure 2.2 (a) The CaF₂ structure comprises of cations (Ca ions) form face-centered cubic structure with anions (F ions) in tetrahedral voids as simple cubic. (b) The cubic fluorite structure of CeO₂ where blue and red sphere are cerium and oxygen ions, respectively (Skorodumova et al., 2002).

Unlike normal lattice structure, a cubic fluorite structure was named after CaF_2 where an occupancy of anion (F ions) in tetrahedral voids of cation (Ca ions) face-centered cubic structure. CeO_2 possesses fluorite structure along with other AX_2 compounds (i.e., ThO_2 , ZrO_2 , PuO_2 , *etc.*) where cerium ions form a face-centered cubic (fcc) structure while oxygen ions form a simple cubic structure and occupy in tetrahedral voids in cerium's fcc structure. This crystal structure of ceria is strongly depending on defects and it gives the most promising application in several industrial usages as mentioned above. So, the investigation on evolution of ceria's crystal structure has been interested since 1995, S. J. Hong (Hong and Virkar, 1995) demonstrated the lattice parameter (a) of cubic fluorite structure by using Shannon and Prewitt effective ionic radii (Shannon and Prewitt, 1969):

$$a = \frac{4}{\sqrt{3}}(r_{\text{cation}} + r_{\text{anion}}) \quad (2.1)$$

Where r_{cation} is radii of cations and r_{anion} is anion ionic radii which is oxygen atoms. However, the study of unusual lattice evolution of Nb doped CeO_2 (Kolodiaznyh et al., 2016) gave the modification factor of CeO_2 lattice parameter based on the experimental results in this study that $a = 5.41075 \text{ \AA}$ where equation 2.1 gives $a = 5.427 \text{ \AA}$. Then the equation 2.1 was multiply with factor 0.99699 as:

$$a = \frac{4}{\sqrt{3}}(r_{\text{cation}} + r_{\text{anion}}) \times 0.99699 \quad (2.2)$$

In 2016, lattice evolution of Ta doped CeO_2 was reported by T. Charoonsuk (Charoonsuk et al., 2017) with the estimation of lattice parameter distortion including the effect from oxygen interstitial and the anion Frenkel defect pair. The r_{cation} is evaluated from the possible defect compensation of Ta and Ce^{3+} by using defect electro-

neutrality. To be noted that the lattice parameter obtained from this approach was more accurate when included the possible oxygen interstitial and the intrinsic anion Frenkel defect pair term into r_{cation} equation. This estimation led to the assumption that the extra electrons from donor impurities are not only compensated with Ce^{3+} but also partially contributed to other defect compensation mechanisms.

One of the most promising academic interest of ceria is that ceria represents as a textbook example of studying small polaron formation and transport. Electron transport in n-type ceria has been widely accepted that originates from small polaron hopping mechanism. However, the conductivity from SP is not similar to the delocalized electron travel in crystal structure as in conventional semiconductors. To clarify this point, the electrical conductivity in materials originates from the motion of free electron above conduction band (delocalized electron) is depicted in figure 2.3a, this mechanism cause the thermally activated conductivity due to the temperature dependence of the electronic carrier concentration. However, the thermally activated conductivity in n-type ceria is a result of the small polaron hopping conductivity. Demonstrating in figure 2.3b, the hopping conductivity is performed the incoherent motion since every jump across the barrier in localized states require the energy and this is where a thermally conductivity arises.

To establish the theory of electronic transport in ceria, n-type ceria generally has been preparing by using reducing method and doping with donor dopants. The reducing method, placing a pristine ceria in low PO_2 atmosphere where oxygen vacancies defect is forming in ceria and yield a non-stoichiometry ceria. The other method is donor

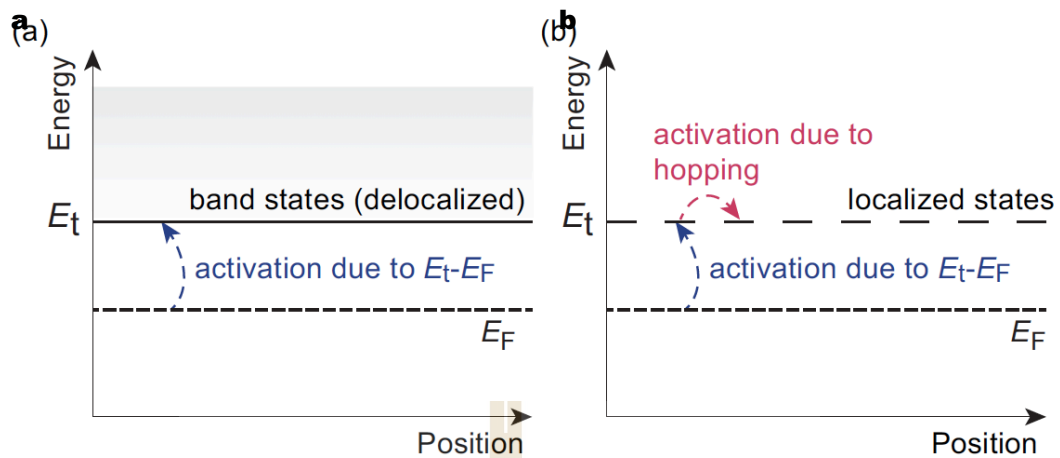


Figure 2.3 The mechanism of Band conductivity of Bloch wave electron compared with hopping conductivity from motion of hopping carrier in localized (Kang et al., 2018).

doping, a high purity ceria is substituted with higher valence cations such as Nb^{5+} , Ta^{5+} , U^{5+} , W^{6+} , etc. After that the successful extra electrons donating from dopants are occupying in a narrow band of an empty Ce 4f electron system. The localization and motion of localized electron play a major role in electrical conductivity of n-type ceria.

The curiosity on the thermally activated conductivity in n-type ceria has been discussed since the pioneer work of H. L. Tuller in 1977 on small polaron hopping in reduced CeO_2 (Tuller and Nowick, 1977). The experiments were carried out on D.C. four probe conductivity measurement at high temperature from 200 to 1150 °C in seal-off specimen system. The thermally activated conductivity was observed where the activation at small doping concentration is 0.40 eV and increasing to 0.52 eV at $x = 0.25$. Following by I. K. Naik in 1978 (Naik and Tien, 1978), the polycrystalline of non-stoichiometric CeO_2 was also studied with four probes D.C. conductivity measurement. The obtained activation energy was increasing with doping concentration which supports the small polaron hopping model. I. K. Naik averred on what had been reported

in the earlier work that the activation energy of 0.20 eV to 0.40 eV in H. L. Tuller work was originated from the mistake in environmental problem of seal-off specimen set-up. The seal-off specimen set-up may cause the oxidation or reduction during the measurement and be directly affecting the conductivity of samples. In 1979, H. L. Tuller published another paper on wider range of non-stoichiometric CeO_2 ($0.00001 < x < 0.25$) to establish the role of oxygen vacancy's favorable formation in reduced CeO_2 (Tuller and Nowick, 1979). This work provided the defect model for singly and doubly oxygen vacancies and quasi-free electron where the doubly oxygen vacancy is dominant at small concentration ($x > 10^{-3}$) and lower than that concentration is the regime of singly oxygen vacancy.

Other significant efforts on study n-type ceria is on donor doped ceria. I. K. Naik arrived with the work on penta-valence donor (Nb_2O_5) doped ceria (Naik and Tien, 1979). The electrical properties were measurement from 800 to 1329 °C with controlled PO_2 ranging from 10^{-19} to 1 atm. They observed that Nb doped ceria has significantly improve in conductivity and this was because the reduction of Ce^{4+} to Ce^{3+} (small polaron). Following by the study of CeO_2 - UO_2 solid solution by T. G. Stratton in 1987. This work presented the hexa-valence (UO_2) as donor for preparing n-type ceria (Stratton and Tuller, 1987) with the observed thermally activated conductivity studied by four probe D.C. technique. The conductivity measurement was evaluated in different temperature spots and varied with PO_2 . A hopping enthalpy of this system was observed to be 0.3 eV for all evaluated region. Following by P. V. Ananthapadmanabhan's work on electrical properties of Ta doped CeO_2 (Ananthapadmanabhan et al., 1992) where the electronic conductivity was reported with 0.2 eV of activation energy. M. R. De Guire

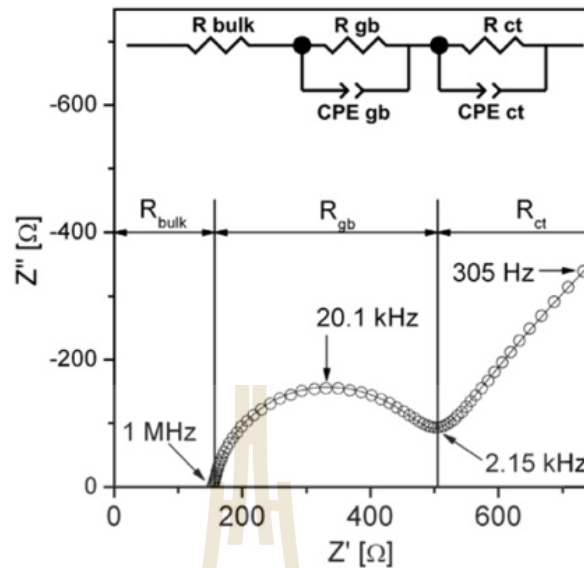


Figure 2.4 The obtained impedance spectra of $\text{Ce}_{0.85}\text{Gd}_{0.15}\text{O}_{1.925}$ with the corresponding equivalent circuit show the contribution of bulk gain, grain boundary and effect of electrode (Zajac and Molenda, 2008).

also reported the electronic conductivity on donors doped ceria with pentavalent (Nb, Ta) and hexavalent (W) (De Guire et al., 1992). These donors doped ceria prepared by two synthesis techniques: a standard mix-oxide method was used for Nb- and W-doped ceria, and a hydroxide coprecipitated was preparing Ta- and Nb-doped. The samples were reported the activation energy in range of 0.32 – 0.40 eV and they gave an interpretation that small polaron played a role in conductivity of these donors doped system.

Specifically, the electrical impedance analysis enables high sensitive approach to probe the electrical properties as demonstrate in acceptors doped ceria by W. Zajac in figure 2.4 (Zajac and Molenda, 2008). The impedance spectra showed almost ideally semicircle impedance with three regimes: i) the high frequency is representing the bulk

grain resistive behavior (R_{bulk}) ii) the medium frequency is a results of grain boundary resistive behavior (R_{gb}), and iii) the low frequency trail show the interfacial interaction between electrode and prepared samples (R_{ct}). In 2012 M. C. Gobel reported electrical impedance study of a thin film Nb doped ceria by pulsed laser deposition (PLD) (Göbel et al., 2012). This work ascribed that PO_2 and microstructure contributed to electrical conductivity of thin film Nb doped ceria where the activation energy was found to be 0.58 – 0.83 eV. The intriguingly idea was proposed by T. Kolodiazhnyi in 2017, the work challenges the role of electron localization and transport properties of ceria that Holstein SP framework is not sufficient for describing in this case. They proposed that other localization mechanism including Anderson localization and Jahn-Teller distortion model are needed to be discussed in order to understand charge transport in n-type CeO_2 . Moreover, the large deviation of activation energy in the previous works on n-type ceria is contradicting the small polaron hopping theory where

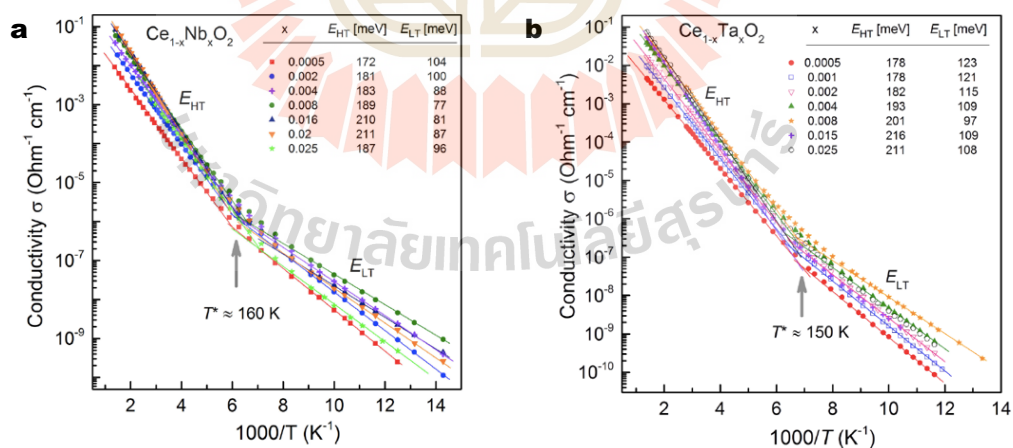


Figure 2.5 The electrical conductivity of Nb and Ta doped CeO_2 show the transition point in temperature dependent conductivity. The activation energy was derived and divided into two parts as high temperature and low temperature activation energy (Kolodiazhnyi et al., 2017).

the hopping is the mechanism under phonon-assisted behavior and the activation energy should be independent of doping species. In this approach, they depicted that the disorder in materials play an important part in both localization and charge transport by introducing the defect-induced random electric fields.

2.3 The additional driven force of electron localization in CeO₂

There are several ideas on the driven force of electron localization in disordered materials. Anderson localization model was proposed in 1958, by P. W. Anderson with the idea of localization induced by random electric field from impurities (Anderson, 1958). The random field is initiated by the scattering of electrons and random defects and resulting in altered the potential. This scattering changes the eigenmodes of delocalized electron from being extended as Bloch wave to be formed a strongly localized state. This idea has been widely accepted for its contribution to localized and transport of electrons in defective materials.

Recently, the attempt on combining Anderson localization and polaron state simultaneously was presented by F. X. Bronold and H. Fehske by using the analytical method (Bronold and Fehske, 2002). Since polaron transport is not well understood especially when consider the additional effect of disorder affecting electron localization. This approach presented the developing the single-particle Anderson-Holstein Hamiltonian with the statistical dynamical mean field approximation (statDMFA). By considering the typical polaron tunneling rate, the breakdown of small polaron is evaluated and results showed that a few of disorder in materials can immobilized the itinerant small polaron by Anderson localization.

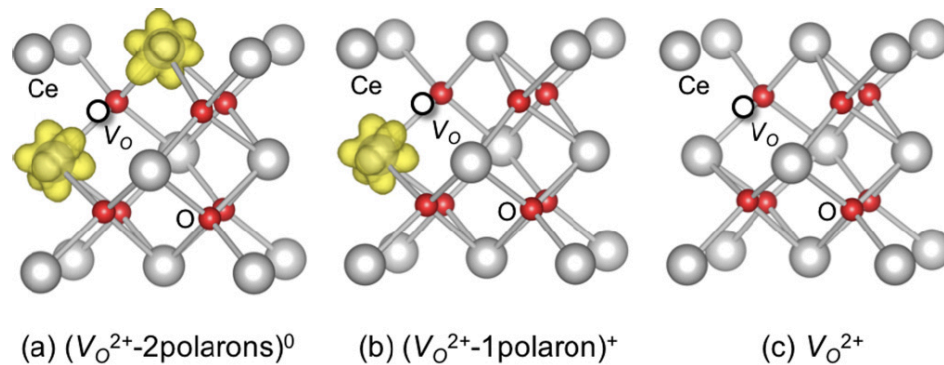
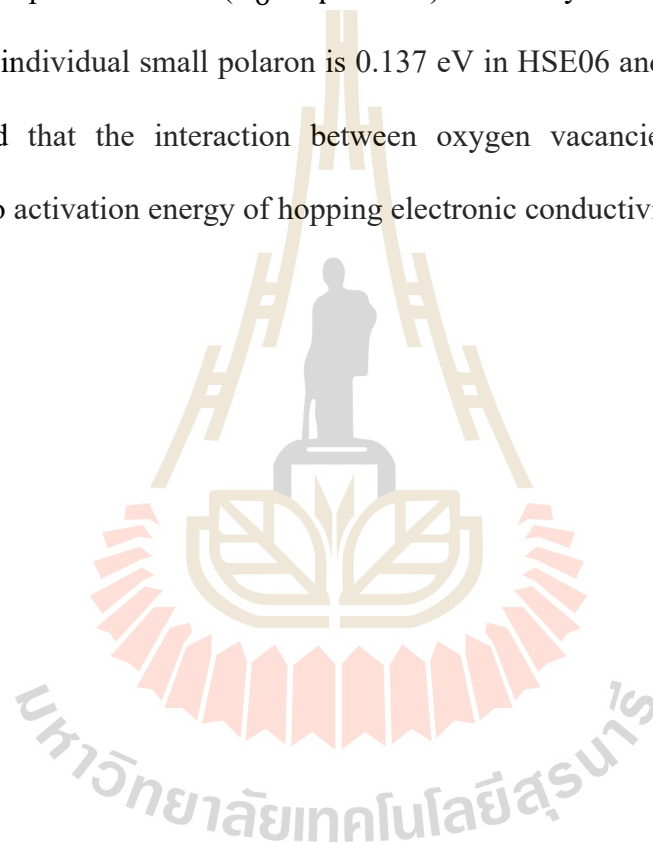


Figure 2.6 The defect configuration of small polarons and oxygen vacancies are represented as (a) $(V_o^{\bullet\bullet} - 2\text{polaron})^0$, (b) $(V_o^{\bullet\bullet} - \text{polaron})^+$, and (c) $V_o^{\bullet\bullet}$ where grey spheres are Ce atoms, small red spheres are O atoms, dark circles are oxygen vacancies, and small polarons represent yellow spin-up (Sun et al., 2017).

While it has been unclear about a role of impurities affecting small polaron, L. Sun evaluated the formation and migration of small polarons and their interaction with effective positive charge defects, oxygen vacancies. Remarkably, fully ionized oxygen vacancy has two effective charge and can bind up to two small polarons. His calculation based on potential function HSE06 and DFT+ U (Sun et al., 2017). In order to assess the interaction between small polaron and oxygen vacancy, the defect formation of oxygen vacancy in CeO_2 and binding energy between oxygen vacancy and small polaron and were calculated since oxygen vacancy can form defect complex with small polaron. In the calculation, it was first obvious that oxygen vacancy is stable in individual doubly charge as $V_o^{\bullet\bullet}$. Oxygen vacancy regularly donates two excess electrons to the system which form as small polaron and when these electron are adding back to oxygen vacancy, this result the defect neutral defect complex $(V_o^{\bullet\bullet} - 2\text{polaron})^0$ and positive complex as $(V_o^{\bullet\bullet} - \text{polaron})^+$. Defect formation with charge distribution of oxygen

vacancies and small polaron in bulk CeO₂ is portrayed in figure 2.6. Apart from the defect formation, the binding energy (E_b) between small polaron and donor impurities (oxygen vacancy) was estimated by taken small polaron out of complex of ($V_{O}^{\bullet\bullet} - 2\text{polaron}$)⁰ one by one. The E_b to remove the first small polaron is found to be significantly high as 0.103 eV in HSE06, and 0.113 eV in DFT + U. The second E_b to remove small polaron from ($V_{O}^{\bullet\bullet} - \text{polaron}$)⁺ which yield doubly charge oxygen vacancy and individual small polaron is 0.137 eV in HSE06 and 0.142 eV in DFT+U. This referred that the interaction between oxygen vacancies and small polaron contributes to activation energy of hopping electronic conductivity.



CHAPTER III

FUNDAMENTAL OF DEFECT CHEMISTRY AND ELECTRICAL CONDUCTIVITY

During the 19th century, crystalline inorganic compounds are systemically arranged in perfect finite pattern where all structural sites are occupied. The idea of stoichiometry was presented that inorganic compound composition was determined by the valence of the constituent atom. Nevertheless, there was a discussion on that inorganic compound probably have variable compositions. The question was clarified in 1930's where Wagner and Schottky evaluated through statistical thermodynamics to demonstrate that the crystal structure can deviate from the ideal structure such as the lattice sites can be empty meanwhile some alien atom can be located in the interstitial space in crystal structure. These imperfections are called "defect" and can be divided to four types: point defect, line defect, planar defect, and bulk defect. In this work, all defects were treated as point defects and the fundamental of defect chemistry is discussing in detail in this chapter in order to give a perspective of equipping defect chemistry in semiconductors.

3.1 Point defect

The deviations from ideal structure is a key parameter from developing materials properties since they exist naturally in all crystalline compound at any temperature.

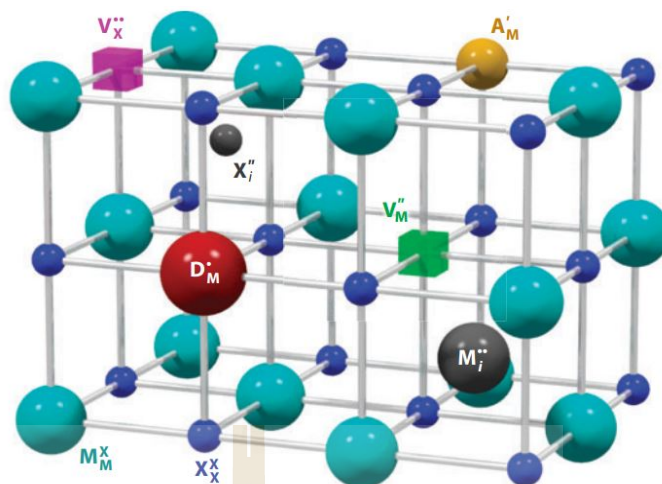


Figure 3.1 The illustration of inorganic compound with possible point defect species in crystal structure (Tuller and Bishop, 2011).

Semiconductor materials properties such as optical properties, magnetic properties, and charge transfer are profoundly depending on the presence of impurity in crystal structure. The crystalline solids contain several types of defects. Thus, in order to study and understand an influence of defects in inorganic materials, the systematic study with well-developed notation of point defects and related atoms is required.

Inorganic compound contains different types of defects as illustrated in figure 3.1. The compound is depicted which M and X stand for cation and anion atom, respectively. Typically, the structural defects that are limited to one structural unit and its vicinity are termed point defect and they can be divided into three main species: i) an absent of atom named vacancy, ii) a presence of atom at void site named interstitial defect, and iii) an alien atom substitute at any atomic site called substitutional defect.

Vacancies (V_X or V_M) are the absence of atom from its own lattice site. When ion is sitting in void of lattice, this is called an interstitial defect (X_i or M_i), noted that

the interstitial can be both host and foreign atom. The presence of foreign atoms of dopants is directly affecting the concentration of native defects in crystalline compound. Mostly valence electron of foreign atom and parent compound are key parameter to determine the defect concentration. Defect chemistry characterizes species of foreign compound by their charge associated to the parent compound where dopant that has equal principal valence electron to host site is termed as “homovalent” while foreign element with unequal valence is defined “aliovalent” or “heterovalent”. The aliovalent impurities can be dissolved into host structure and their deviated of valence electron have made them easier to contribute electronic carrier to the host compound. Aliovalent elements are characterized as donors and acceptors whether they donate or accept extra electrons to host. The dopants with lower valence electron substituting on host atom will be named as “Acceptor” (A_M) while the dopants with higher valence electron is called “Donor” (D_M). In addition to structural defects, crystalline compound contains other defects called electronic defect which is electrons and electron holes. The origin of electronic defect can be from intrinsic excitation of valence electron or results associated with the presence of point defect. The concentration and type of point defect and electronic defect is mostly depending on environmental temperature and oxygen partial pressure.

The most widely accepted model to described defect is “Kröger-Vink notation”. This system described defect in term of structural elements and to be more understandable, defect notations are writing by utilizing perfect crystal as the reference state and considering charge relative to this perfect crystal. This relative charge is termed “effective charge”. “Kröger-Vink notation” is described as a elemental symbol where the main symbol is indicated the impurity species, effective charge, and reference atomic

site. The main symbol comprises of a major letter with subscript and superscript ($X_{\text{subscript}}^{\text{superscript}}$). The main letter denotes a vacancy or an atom while superscript stands for located site of defect. The superscript is the effective charge of defect compared to its reference site and this superscript are denoted as “•” (positive charge), “/” (negative charges), and \times (neutral). To be clearer on effective charge of defect, this notation is ascribed as the difference of defect’s charge and the host’s charge of atom at reference site. For examples, $\text{Ta}_{\text{Ce}}^{\bullet}$ means that Ta^{5+} ions substitute on Ce^{4+} site and effective charge is $1+$. The reason that effective charge is defined as symbol is to disentangle the actual charge of atom from defect relative charge.

The modification of semiconductor generally involves the population of electronic defect or charge carriers. Most of semiconductors contains intrinsically defects. In order to conserve overall electrical charge neutrality and thermodynamic equilibrium of crystal structure, when charged defects are formed, there will always be a complimentary opposite charged defect, coincidentally. These defects normally form as defect pairs. Two defect pairs that are important in metal oxide are Schottky pair and Frenkel pair. The Schottky pair is a pair of opposite charge vacancies as ($V_{\text{M}}^{//} - V_{\text{X}}^{\bullet\bullet}$). This pair are likely to form at outer and inner surface and diffuse into compound structure until compound meet equilibrium. Frenkel pair is a pair of metal vacancies and metal interstitials as ($V_{\text{M}}^{//} - M_{\text{i}}^{\bullet\bullet}$) which likely to happen directly inside materials structure. These defect pair can be from simultaneously, but one specie is normally dominating. The difference is what Schottky are preferring materials that cation and anion are comparable in size but Frenkel pair favored compound that cation and anion size are significantly different.

3.2 Shallow impurity

One of the most important process in semiconductor is the doping which allow us to gently control the concentration of dopant for controlling semiconductor properties. Shallow level impurity generally refers to the substitutional defect such donor and acceptor whose energy level is determined by the long-range Coulomb part of the ion-core potential and the extended wave function is in an order of Bohr radius. These doping species can position within the band gap of interested semiconductor.

The acceptor is a substitutional defect whose valent electron is lower than the host site. This impurity will accept an electron and leave the missing electron (hole) in valence band i.e. the case of Arsenic (III-group) doped Si where As has one valence electron lower than Si atom. In order to form tetrahedral bond within Si, As atom need one more electron and this electron is then borrowed from electron gas by creating a hole carrier. When a hole is ionized to conduction band, the As is leaving with one negative charge as shown in figure 3.2.

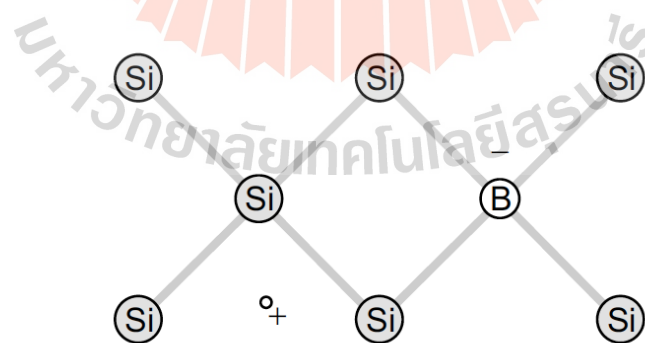


Figure 3.2 The demonstration of acceptor impurities shows Boron as acceptor and Silicon is host lattice (Grundmann, 2015).

The donor impurities are typically the substitutional defects with higher valent electron than after form bonding within their lattice site, they will contain extra electron. These extra electrons will likely be donated to crystal structure. For example, we will discuss the As doped Si as depicted in figure 3.3 when As has 5 valent electron when As successfully substituted Si site, the tetrahedral bond is formed and As has remained one extra electron. When an extra electron of As is ionized, the a positive charge will remained at As. In electronic level, donor energy level normally found located at the upper position of band gap near the conduction band and this impurity donate electron to the conduction band.

The crystal structure generally needs to maintain their electro-neutrality. In case of materials with defect presence, the neutrality is managed through compensation mechanism. When donors and acceptors are coincidentally existed, the recombination between electrons from donors and holes from acceptor will perform. This can determine the types of semiconductor due to the quantity of electron (n-type) and hole (p-type). The charge-neutrality is considered charge from all situation both intrinsic and extrinsic. The most general charge-neutrality is defined as:

$$-n + p + N_D - N_A = 0 \quad (3.1)$$

Where n and p are number of electron (n-type) and hole (p-type) in semiconductor, N_D and N_A is quantity of electron and hole from donor and acceptor, respectively.

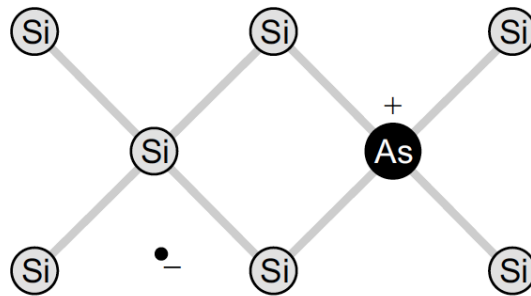


Figure 3.3 This illustration is Arsenic as donor impurity in Silicon semiconductor (Grundmann, 2015).

3.3 Electrical conductivity

The electrical conductivity is used to describe the electrical character of materials that indicates how easy which materials can conduct an electrical current. Specifically, electrical conductivity arises from the motion of mobile charge carriers under the influence of electric field. Ohm's law illustrates the basic concept of the relation of electrical current flowing through materials:

$$V = IR \quad (3.2)$$

where V is the applied voltage and R is the resistant of materials which current is passing. The resistant is materials geometry dependence parameter that can be expressed in term of resistivity (ρ) by:

$$\rho = A/l \cdot R \quad (3.3)$$

where A is cross sectional area perpendicular to the direction of current and l is the length of materials where the voltage is measured. Then, electrical conductivity (σ) is simply the reciprocal of resistivity:

$$\sigma = 1/\rho \quad (3.4)$$

The origin of electrical conductivity in materials is the motion of free electron due to a presence of electrical field and the value of conductivity depends on a number of electrons that available to move. This number of electrons directly relates to nature of materials, electronic structure, the arrangement of electronic states respected to energy levels. Electrical conductivity is important materials' properties since materials

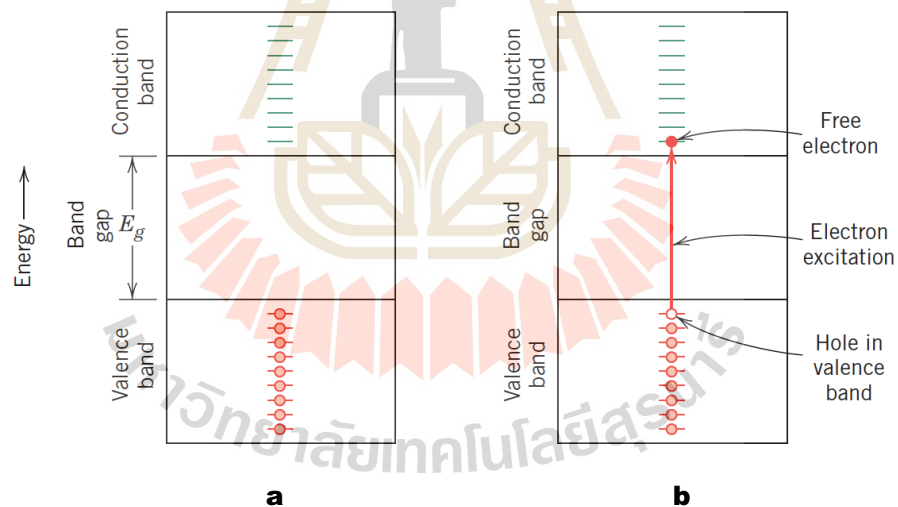


Figure 3.4 The conductivity process in semiconductor and insulator where (a) at $T = 0$ K, valence band and conduction band are separated by band gap and (b) the electron is excited from top of valence band across band gap to the conduction band resulting in free electron (Callister, 2007).

classification is relied on how capable materials can conduct the electrical current. Metals are known as a good conductor because of the abundant number of free electrons in their structure. In contrast to metal, insulating materials exhibit the ultimately low conductivity because the small concentration of available mobile carriers. Semiconductors are positioned between metals and insulators where the origin of charge carriers in semiconductors come from motion of intrinsic and extrinsic charge carriers.

Principally, the semiconductor transport can be pictured by considering energy position of valence band (occupied states), conduction band (empty states), and the distant between these two bands (band gap). The pictorial process of conductivity in semiconductor is depicted in figure 3.4 At $T = 0$ K, figure 3.4a demonstrated the position of the valence band, conduction band and band gap of materials. In order to free electron from occupied states, an occupied electron at top of valance band needs to

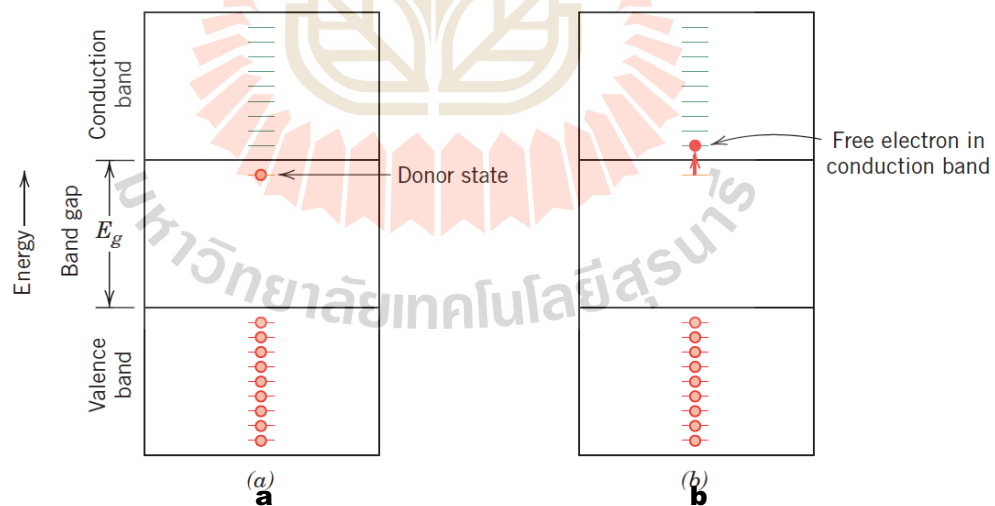


Figure 3.5 The conductivity process of n-type semiconductor arises from impurities state termed donor states where (a) this state positions at below the conduction band and (b) capable of donating electron to conduction band (Callister, 2007).

be activated with amount of energy to promote electron across band gap which can be up to several electron volts. When electron is excited with the proper energy, mobile electron is liberated from localized states as shown in figure 3.5b. The mentioned energy normally comes from an external source such as thermal energy. The possibility that electron can be free is depending on the width of band gap while the wider means the higher energy is needed. Increasing temperature is resulting in increasing thermal energy for activated electron to conduction band which raises a number of electron and yields higher conductivity.

Under the electrical field, the mobiles are accelerated and influenced of periodicity of crystal lattice. In this circumstance, mobile electrons extend in motion of Bloch oscillation as shown in figure 3.7 and should be accelerated as long as electric field is applied. The continuity of carriers' movement is interrupted by the scattering events with imperfect in crystal structure, dislocation, and thermally vibration of atoms. This process lessens electron kinetic energy and alters the direction of electron. The net motion of mobile charge against electric field direction is term "current". This scattering process is responsible for the resistivity in materials and the extent of scattering event is described by "mobility" of electron:

$$\sigma = n|e|\mu_e \quad (3.5)$$

where $|e|$ is magnitude of electron electrical charge, n is electron concentration and μ_e is electron mobility. Electrical properties of semiconductor are controlled by the concentration and types of charge carrier. The extrinsic semiconductor is semiconductor that electrical conductivity normally is determined by the presence of impurities. The conductivity in extrinsic semiconductor is defined as:

$$\sigma = n|e|\mu_e + p|e|\mu_h \quad (3.6)$$

where p are concentration of holes, and μ_h are mobility of electrons holes, respectively. In case of n-type semiconductor, the non-bonding electron which is usually from donor impurity is bound by weakly electrostatic interaction within the forbidden band gap below the conduction band. In this case the activation energy refers to the energy required to excite electron from impurity states to conduction band. Since this impurity states donate an electron to conduction band, the state is named “donor state”. In order to excite a number of electrons from donor states, only thermal energy at room temperature is sufficient then the major carriers from this type of semiconductor are extrinsic electrons ($n \gg p$). Then equation 3.5 can be reduced as:

$$\sigma = n|e|\mu_e \quad (3.7)$$

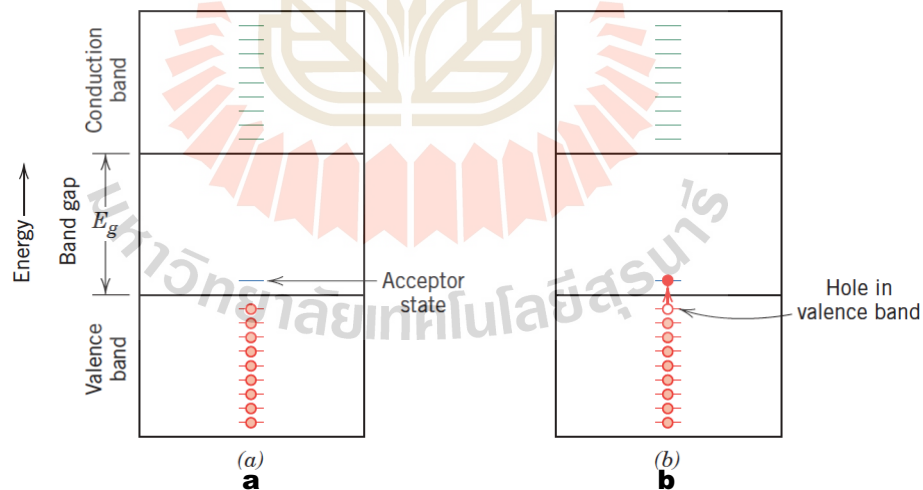


Figure 3.6 The conductivity process of n-type semiconductor arises from impurity states termed as acceptor states where (a) this state positions at above valence band and (b) capable of accepting an electron from valence band and leaving electron holes (Callister, 2007).

On the other hand, p-type semiconductor is extrinsic semiconductor that hole is major carriers. Mostly p-type semiconductors are prepared using acceptor impurities. In band model view, acceptors introduce an energy states within the forbidden gap at nearly top of valence band. By introducing amount of thermal energy, electron at top of valence band jumps to localized at impurities states. This creates the deficiency of electron or holes within valence band. This impurity state is called acceptor states since it capable of accepting electron and leaving hole in valence band. In p-type semiconductor electron holes are the majority electronic defect species ($p \gg n$), then equation 3.5 can be written as:

$$\sigma = p|e|\mu_h \quad (3.8)$$

Apart from delocalized electron wanders through crystal structure, there is other movement that also contribute to charge transport in semiconductor which is a hopping motion. When coherent motion of delocalized electron is interrupted by the presence of strong localized states or impurities, electrons are losing their coherent properties and their motion turn into incoherent. The incoherent transport is the discrete movement that requires amount of energy to perform the motion. Fundamentally, hopping conductivity is driven by electron-phonon interaction in transition of electronic carriers between the localized states. Hopping conductivity can be divided into two regimes: i) an impurity conduction where carrier is hopping between the shallow impurity states at low temperature and ii) carriers hop between cation site at high temperature. This kind of motion is manifested as a reason for conductivity rising in wide band gap semiconductor.

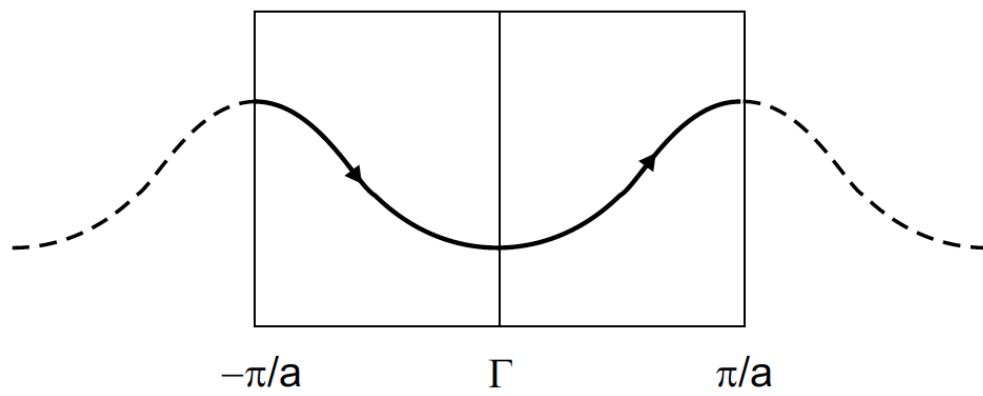


Figure 3.7 The graph represents electron wave function of a Bloch oscillation (Grundmann, 2015).



CHAPTER IV

RESEARCH METHODOLOGY

4.1 Ceramic sample preparation by solid state reaction

Our study consisted of 2 different dopants (M = Tantalum (Ta) and Tungsten (W)). The $Ce_{1-x}M_xO_2$ (M = Ta and W) with $x = 0.0005-0.004$ were prepared by using CeO_2 (99.99% purity, Tokai-Chemy, Japan) as source of CeO_2 while the dopants were derived from Ta_2O_5 (99.99% of CERAC Inc, USA) and WO_3 (99.99% purity, High Purity Chemical, Japan), respectively. The precursors were mixed with ethanol and glided in Y-stabilized mortar and pestle until ethanol totally evaporated for several times. Then, the dried powder was compacted into 20 mm diameter pucks.

After that the pellets were heat-treated at 1300 °C for 10 h in air. Afterward, the pucks were crushed into powder, glided in ethanol, and drying them overnight. The small amount of 5% polyvinyl alcohol (PVA) binder was added to the dried powder before pressing them under 20 MPa in the WC (Fujiloy, Japan). The pellets were stacked on top of each other, placed in pure CeO_2 , and covered by inverted alumina crucible then sintered in air at 1650 °C for 20 h in Ta samples and 1600 °C for 10 h in W samples, then fast-cooled the furnace to room temperature. Then, the sintered samples were obtained.

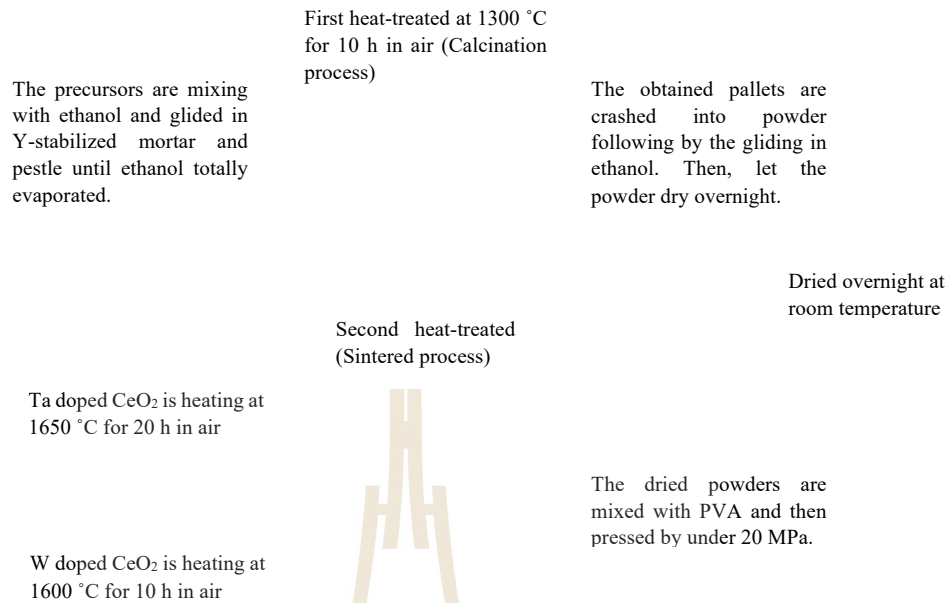


Figure 4.1 The flow chart shows synthesis procedure of ceramics n-type donors doped CeO₂.

4.2 Characterization

4.2.1 X-ray diffractometer (XRD)

The XRD is the most famous characterization techniques in materials field based on the diffraction of x-ray light through solid materials' crystal structure. When the beam of parallel, monochromic, coherent x-ray is penetrating materials and incident on the planes of atoms that separated by interplanar space (d_{hkl}), the resulting diffracted beam is occurring at specific angle (θ) of beam and plane. By collecting the intensity and position of those diffracted beam, the crystal structure of materials is revealed. Moreover, XRD also can identified the characteristic diffraction profiles, lattice

parameter, and geometry of materials. The x-ray diffraction is determined by Bragg's law:

$$2d_{hkl}\sin\theta = n\lambda \quad (4.1)$$

where d_{hkl} is the space between diffraction plane, θ is the incident angle, λ is wavelength of the light source. As shown in figure 4.2b, the diffractometer is functioning to find angle of which diffraction occur where T is light source for x-ray, S is interested specimen, O is rotation axis and C is detector. While the specimen and beam are rotating at θ , the detector is moving at 2θ to maintain the equal of incident and reflection angles.

In this work, we used the commercial diffractometer Rigaku Mini-Flex600 diffractometer with Cu K_{α} x-ray source. A crystallographic program, JANA2006, was employed to perform analysis on the diffraction profile and Rietveld analysis of prepared samples.

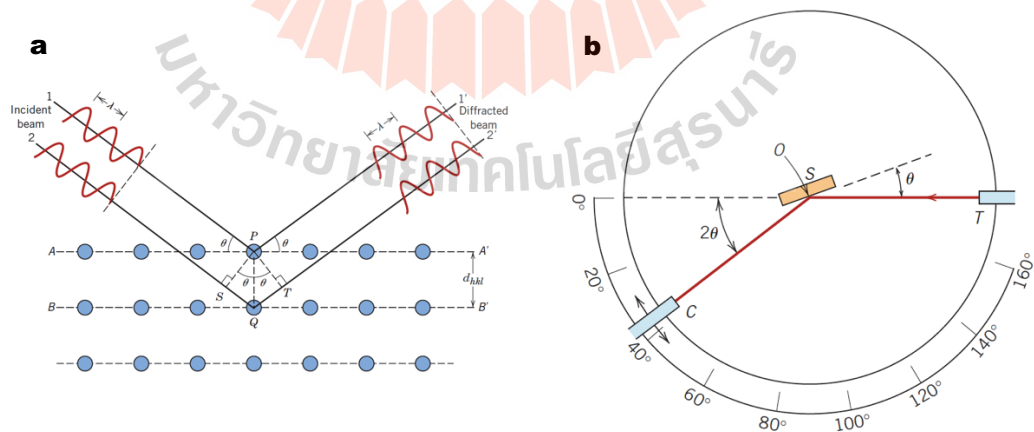


Figure 4.2 The figure shows a schematic of x-ray diffraction (a) and diffractometer (b) (Callister, 2007).

4.2.2 Superconducting quantum interference device (SQUID).

SQUID is known as the highly sensitive magnetic flux-to-voltage transducer operated under the superconducting theory with highly sensitivity that is enough to probe even the biological samples. The superconductivity is a core mechanism of SQUID system and DC SQUID is comprising of two parallel Josephson junctions in a superconducting loop. The property of superconductivity is that when the system is cooled down below a critical temperature, superconductor will generate dc voltage with zero resistance. The maximum current at zero resistant is called the critical current. The mechanism under the measurement employed a quantization of flux through the superconducting loop. The enclosed superconducting loop will contain certain amount of magnetic flux as integer unit of flux quantized which is:

$$\Phi_0 = 2.07 \times 10^{-15} \text{ Wb} \quad (4.2)$$

The flux through the loop is held as constant by superconducting current. Thus, the variation of flux applied to superconducting loop will trigger the current flow to resist the change and cause a phase difference across the junction. The phase difference then gives increasing of measurable voltage across the loop. This causes by the Josephson equation (Jenks et al., 1997):

$$I = I_0 \sin (\theta_1 - \theta_2) \quad (4.3)$$

The magnetic properties are measured from the alteration of magnetic flux as a function of responded current in superconducting loops. Our measurement is carried out by the commercial instrument, the magnetic property measurement system (MPMS, Quantum design), equipped with SQUID at operated temperature range from 2 to 350 K with external magnetic field of 5000 Oe.

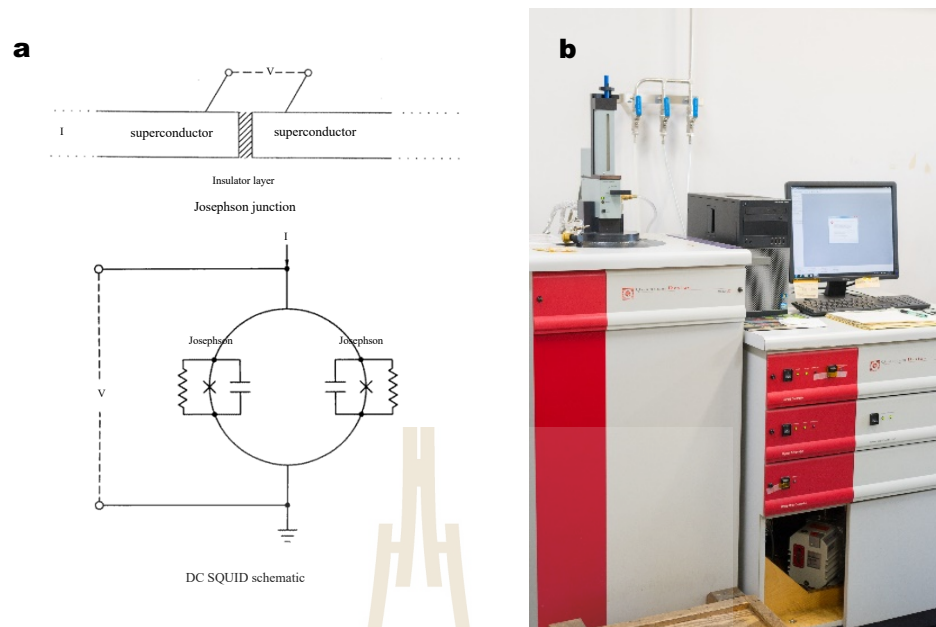


Figure 4.3 The represent of SQUID system where (a) the Josephson junction and DC SQUID contained two Josephson junctions (adapted from Jenks et al., 1997) and (b) the experimental measurement system of MPMS equipped with SQUID (Quantum design).

4.2.3 The electrical impedance spectroscopy

The electrical impedance spectroscopy is one of the most powerful in studying physical properties. In the measurement, the alternate voltage $v(t) = V \sin(\omega t)$ is applied to the system as the stimulus, then the resulted current will be measure as $i(t) = I \sin(\omega t + \theta)$. The impedance will be calculated:

$$Z = \frac{|V|}{|I|} \cdot e^{j(\theta_V - \theta_I)} \quad (4.4)$$

Where Z is complex impedance, $|V|$ is voltage amplitude, θ_V is phase of voltage, $|I|$ is resulted current amplitude, and θ_I is phase of current. The obtained complex impedance is separated into real part ($\text{Re}|Z|$) and imaginary part ($\text{Im}|Z|$) from the relations:

$$\text{Re}[Z] = |Z|\cos(\theta) \quad (4.5)$$

$$\text{Im}[Z] = |Z|\sin(\theta) \quad (4.6)$$

The result of electric impedance spectroscopy normally plotted in the complex plane of $-\text{Im}|Z|$ as y-axis and $\text{Re}|Z|$ as x-axis. As show in fiuger 4.x, the semicircle is found as the result of phase different where $\theta = 0$ mean the pure resistive behavior. The interception at x-axis yields the resistant (R). Then the expected parameter σ (conductivity) was estimated from equation 3.4.

Our set-up is using the alpha impedance analyzer (Novocontrol Technologies) together with the Physical Property Measurement System (PPMS). The Ag paint was deposited into two side of sample pellet surface as the conductive electrode. The Z complex was measured from 1 Hz to 1 MHz frequency range with temperature range of 2 to 350 K.

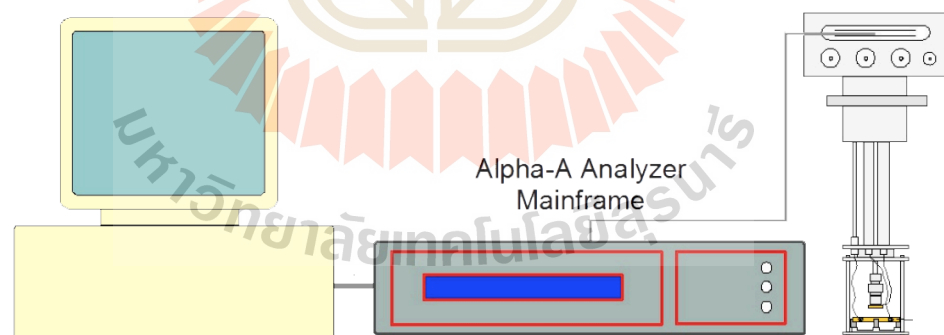


Figure 4.4 The schematic measurement of Alpha-A impedance analyzer (Friedrich Kremer, 1999).

CHAPTER V

RESULTS AND DISCUSSION

This chapter is demonstrating the evidences that donor impurities play a role in lattice distortion and respond for the thermally activated conductivity in n-type CeO₂. The chapter is divided into three separated parts. The first section is experimental result aiming to explain the microstructure and defect chemistry of donors doped CeO₂. This section provides the view of electronic of donors doped ceria and the effect from presence impurities. Second section focuses on the investigation of electron transport properties by using electrical impedance spectroscopy. In this part the experimental activation energy is evaluated through linear fitting from temperature dependent conductivity. The first two sectors present the approach and assumption of experimental results. The last section is discussion section where all the experimental result is analyzed combined with the supportive first principle calculation from our recently published paper (T. Kolodiazhnyi, 2019). The discussion is analyzing of the favorable defect structure in each sample and the effect of impurities on small polaron hopping conductivity of donors doped ceria where the impurities induced potential well play a role in localization of small polaron.

5.1 Microstructure and defect chemistry of donors doped CeO₂

5.1.1 Phase purities and lattice parameter refinement

Electronic structure of donors doped CeO₂ was first investigated for checking

the samples' purity and the effect of impurities to crystal structure. Unfortunately, we observed the severe evaporation of tungsten samples in heat-treatment procedure. To be accurate on doping concentration for W samples, the Inductive Coupling Plasma optical emission spectrometer (ICP-OES) was used to quantify the accurate concentration of W ions in $Ce_{1-x}W_xO_2$ samples. The concentration of W in ceria was quantified by ICP-OES (Hitachi ICP-OES PS3520 UV-DD, Japan). Then, in the following discussion, the doping concentration of W doped ceria will be concentration obtained from ICP. The powder XRD together with Rietveld refinement was performed to clarify the phase purity and lattice parameter evolution. To be noted that the XRD samples were prepared with an internal standard, LaB_6 , for a better resolution in lattice parameter refinement. The XRD spectra clearly confirm the purity of our ceramic samples with no observable of secondary phase as shown in figure 5.1. The spectra are plotted as red cross (+) symbol indicated the main peak of ceria and green vertical bars (|) indexes the major peak position of LaB_6 .

To study the effect of donor impurities on lattice distortion, Rietveld refinement was employed to calculate lattice parameter (a) from XRD results by using Jana 2006 software. Figure 5.2 shows the quality of experimental data and fitting results where experimental data and fitting results are plotted as + symbols and solid line, respectively. The solid line at bottom of figure 5.2 shows the difference between the fit and experimental data while the insertion of figure 5.2 is high diffraction peak indicates the slightly distortion of lattice parameter in each sample. The obtained lattice parameters from Rietveld refinement indicates the evolution of lattice parameter where Ta doped ceria show the contraction trend and W doped ceria's lattice parameter is expanding as a function of doping concentration. This question is strongly depending on a presence

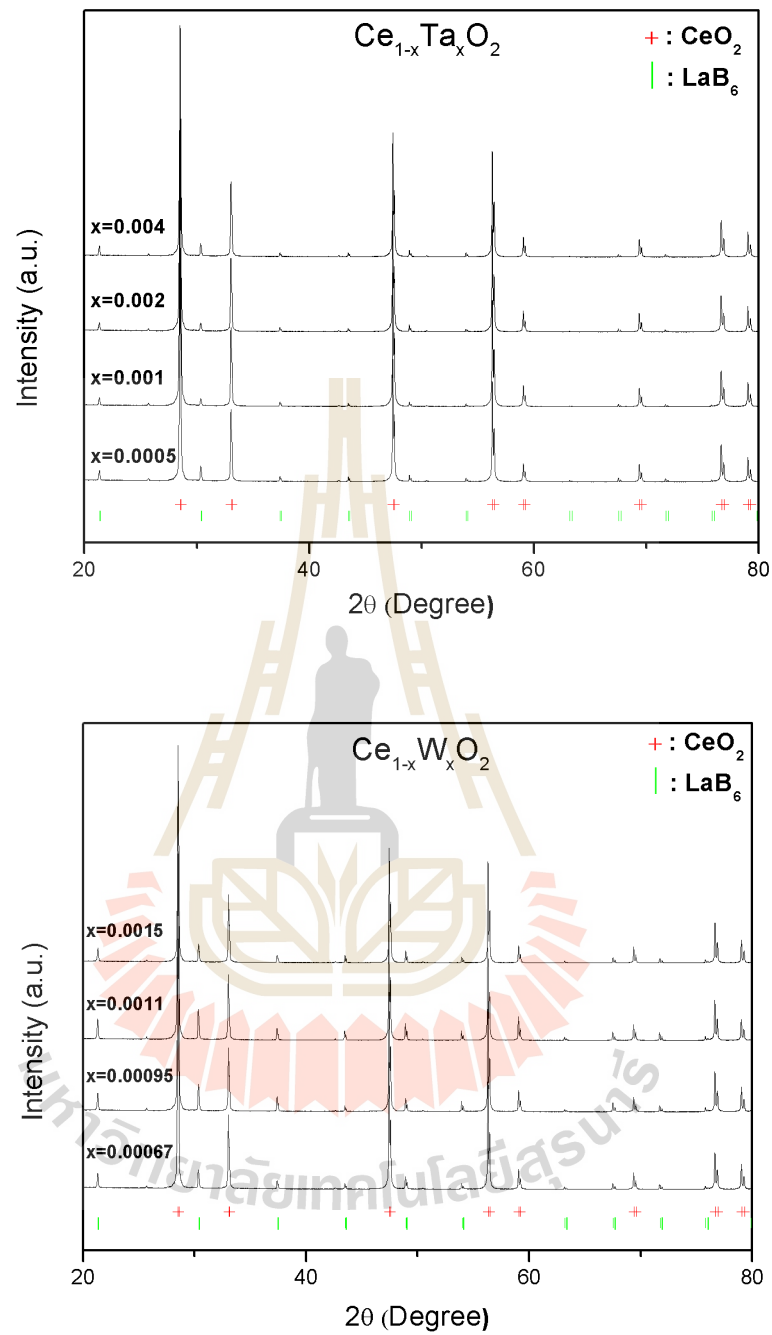


Figure 5.1 The XRD spectra of Ta and W doped CeO_2 compared with main peaks of pure CeO_2 and internal standard LaB_6 .

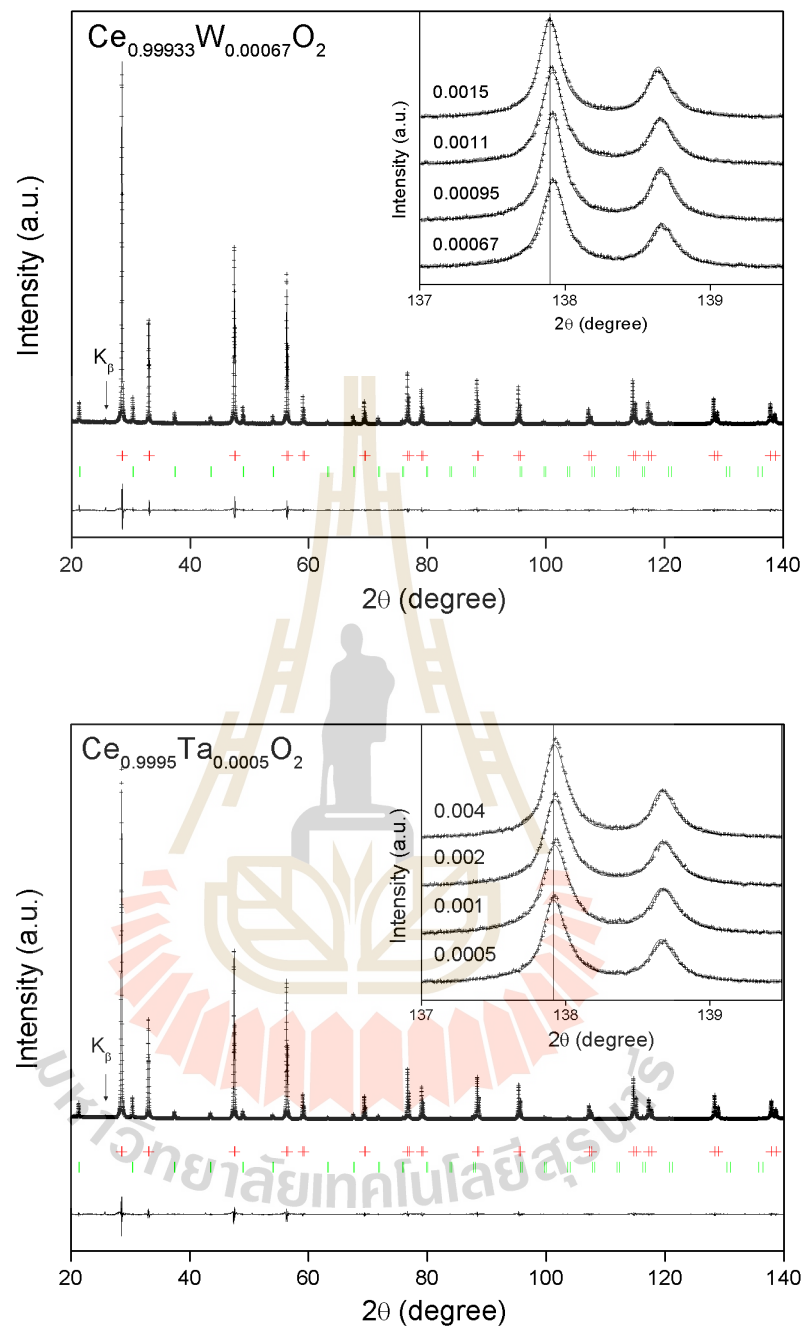


Figure 5.2 The fitting of Rietveld refinement with (insert) shifting of peak at high angle diffraction of each compositions.

of impurities in each sample. To understand the distortion of lattice parameter of donors doped ceria, we employed the defect chemistry as a tool to model the distortion by considering a defect compensation mechanism under defective environment.

First, an electro-neutrality condition for point defect in Ta doped CeO₂ is described as:

$$[\text{Ta}_{\text{Ce}}^{\bullet}] + [\text{V}_{\text{O}}^{\circ}] + 2[\text{V}_{\text{O}}^{\bullet\bullet}] = [\text{O}_{\text{i}}'] + 2[\text{O}_{\text{i}}''] + 4[\text{V}_{\text{Ce}}'''] + 3[\text{V}_{\text{Ce}}''] + 2[\text{V}_{\text{Ce}}'] + [\text{V}_{\text{Ce}}] + [\text{Ce}'_{\text{Ce}}] \quad (5.1)$$

The electro-neutrality condition for W doped ceria is:

$$[\text{W}_{\text{Ce}}^{\bullet}] + 2[\text{W}_{\text{Ce}}^{\bullet\bullet}] + [\text{V}_{\text{O}}^{\circ}] + 2[\text{V}_{\text{O}}^{\bullet\bullet}] = [\text{O}_{\text{i}}'] + 2[\text{O}_{\text{i}}''] + 4[\text{V}_{\text{Ce}}'''] + 3[\text{V}_{\text{Ce}}''] + 2[\text{V}_{\text{Ce}}'] + [\text{V}_{\text{Ce}}] + [\text{Ce}'_{\text{Ce}}] \quad (5.2)$$

The electro-neutrality shows all possible defect species in interested compound but in heat treatment, our synthesis system was performed at air ambient ($\text{PO}_2 = 0.02$ atm) where oxygen condition is in sufficient condition then defects related to oxygen deficiency condition can be eliminate. In this treatment, we presumed that donor impurities considered as dominant species and the substitution of donor impurities cause a major distortion to Ta and W doped ceria. Hence, the lattice parameter modelling is initially considering the simplest criteria of compensation mechanism in Ta and W doped ceria involving individually between donor defects and electronic defect. The hypothesis is an electron from $\text{Ta}_{\text{Ce}}^{\bullet}$ defect is compensated by one Ce^{4+} forming Ce'_{Ce} while two electrons from $\text{W}_{\text{Ce}}^{\bullet\bullet}$ defect are forming two Ce'_{Ce} as listed below:

$$[\text{Ta}_{\text{Ce}}^{\bullet}] = [\text{Ce}'_{\text{Ce}}] \quad (5.3)$$

$$[\text{W}_{\text{Ce}}^{\bullet\bullet}] = 2[\text{Ce}'_{\text{Ce}}] \quad (5.4)$$

This treatment obeyed the Shannon and Prewitt ionic radii when an ideal lattice parameter of fluorite structure is:

$$a = \frac{4}{\sqrt{3}}(r_{cation} + r_{anion}) \times 0.99699 \quad (5.5)$$

From equation 5.3, r_{anion} for Ta doped ceria is:

$$r_{anion} = xr_{Ta^{5+}} + xr_{Ce^{3+}} + (1 - 2x)r_{Ce^{4+}} \quad (5.6)$$

From equation 5.4, r_{anion} for W doped ceria is:

$$r_{anion} = xr_{W^{6+}} + 2xr_{Ce^{3+}} + (1 - 3x)r_{Ce^{4+}} \quad (5.7)$$

where $r_{anion} = r_{O^{2-}} = 1.380 \text{ \AA}$, $r_{Ta^{5+}} = 0.74 \text{ \AA}$, $r_{Ce^{3+}} = 1.14 \text{ \AA}$, $r_{Ce^{4+}} = 0.97 \text{ \AA}$, and x is doping concentration. All mentioned cations have coordination number (CN)

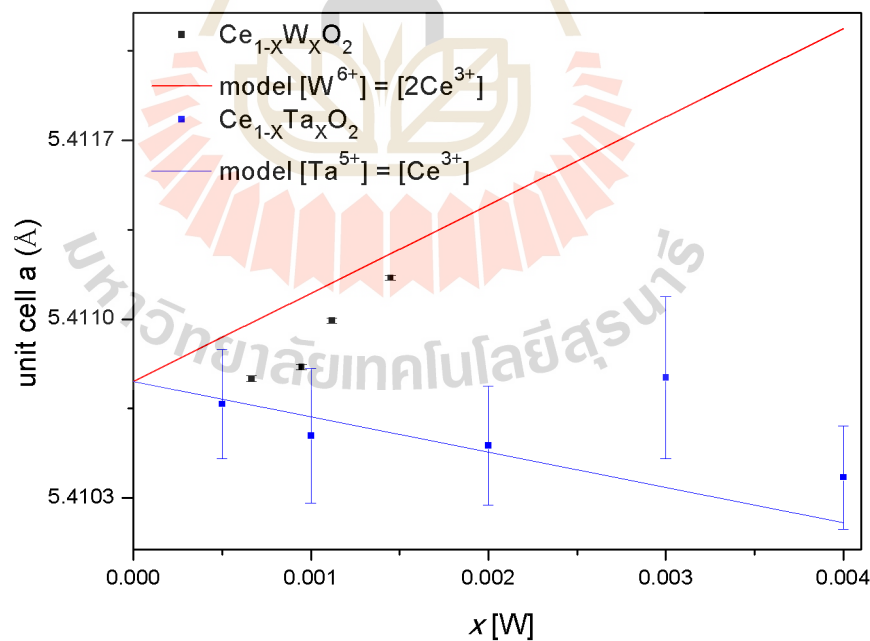


Figure 5.3 The lattice estimation from defect equation compared with results from Rietveld refinement.

of 8; however, the Shannon and Prewitt ionic radii has no data for $r_{W^{6+}}$ having 8 CN. We then did the linear fitting for radii and the result is $r_{W^{6+}} = 0.78 \text{ \AA}$. All fitting results from equation 5.6 and 5.7 were plotted against data from Rietveld data as a function of dopant in figure 5.3. The Rietveld lattice parameter of Ta doped ceria shows distraction trend and W doped ceria lattice parameter is enlarging as a function of doping concentration.

5.1.2 Magnetochemistry treatment

The magnetic properties of donors doped ceria were measured by MPMS system equipped with SUIDs to observe the response of magnetic properties under an influence of external magnetic field. Then, the magnetic susceptibility (χ) is calculated from the relation of magnetization (M) and external filed (H):

$$\chi = M/H \quad (5.8)$$

The inverse magnetic susceptibility as a function of temperature of Ta and W doped ceria is showed in figure 5.4. Remarkably, magnetic susceptibility showed paramagnetism behavior and at low temperature χ showed dramatically increase, Curie-like tail. The Curie-like tail is resulting from the donor species inducing unpair electrons ($4f^1$) in form of Ce^{3+} ions followed equation 5.3 and 5.4. This clarified that magnetic properties of CeO_2 is depending on concentration of Ce^{3+} . To quantify the concentration of Ce^{3+} , we equipped the Magnetochemistry. This method was introduced by T. Kolodiazhnyi (Kolodiazhnyi et al., 2016) in his work on pure and Nb doped ceria. The origin of paramagnetism in n-type ceria arises from i) the origin of partially covalence nature of ceria, ii) van Vleck paramagnetism. While the concentration of Ce^{3+} induced by donor dopants plays an important role in drastically decreasing of susceptibility at

low temperature. Thus, the fitting of magnetic susceptibility can gain the quantity of Ce^{3+} . This approach quantified concentration of Ce^{3+} by consider the free-ion form Ce^{3+} has 6-fold degenerate ground state separated from first excited multiplet by 0.28 eV (Herrmann et al., 1966). The model of magnetic susceptibility, that the first and second order of Zeeman terms are included by the perturbation method in which a weak magnetic field from thermal energy is applied along z-axis, is introduced by the van Vleck fomula:

$$\chi_{CEF} = \frac{N_A g_J^2 \mu_B^2}{Z} \left\{ \frac{1}{k_B T} \sum_{n,k} \sum_{k'=1}^{\omega_n} |\langle \psi_{n,k} | J_z | \psi_{n',k'} \rangle|^2 e^{-\frac{E_n}{k_B T}} + \right. \\ \left. 2 \sum_{n,k} \sum_{n' \neq n} \sum_{k'=1}^{\omega_{n'}} \frac{|\langle \psi_{n,k} | J_z | \psi_{n',k'} \rangle|^2}{E_{n'} - E_n} e^{-\frac{E_n}{k_B T}} \right\} \quad (5.9)$$

where N_A is an Avogadro's number, g_J is a Landau g-factor, μ_B is a Bohr magneton, $|\psi_{n,k}\rangle$ is n-th state relative to the wave function k, E_n is energy of n-th state, ω_n is the multicity and Z is a partition function given by:

$$Z = \sum_n \omega_n e^{-\frac{E_n}{k_B T}} \quad (5.10)$$

In order to solve the susceptibility of van Vleck paramagnetism, the crystal electric filed (CEF) treatment was utilized. In the treatment, the symmetry of free-ion form Ce^{3+} which has 6-fold degenerate ground states ($J = 5/2$) will split into 4-fold degenerate states (Γ_8) and 2-fold degenerate excited states (Γ_7) by crystal electric filed. As the Ce^{3+} ion is in a cubic fluorite crystal the Γ_8 will be ground state. The wave function and energy of each states were solved using Hamiltonian from Stevens operator equivalents:

$$H_{CEF} = \sum_{n=0}^6 \sum_{m=0}^n B_n^m O_N^m \quad (5.11)$$

where O_N^M are the Stevens operators and B_O^M are the CEF parameters. The calculated wave function of Ce^{3+} in cubic symmetry from Steven operator was substituted into equation 5.9. The results of magnetic susceptibility contributed from Ce^{3+} is equal to

$$\chi_{CEF} = \frac{N_A g^2 \mu_B^2 c}{4 + 2e^{-\frac{\Delta}{K_B T}}} \left\{ \frac{\frac{65}{9} + \frac{25}{18} e^{-\frac{\Delta}{K_B T}}}{K_B T} + \frac{80(1 - e^{-\frac{\Delta}{K_B T}})}{9\Delta} \right\}, \quad (5.12)$$

where c is Ce^{3+} concentration, Δ is energy gap between Γ_8 and Γ_7 magnetic multiplets, K_B is a Boltzmann constant, and T is the absolute temperature. Consequently, the obtained temperature dependent magnetic susceptibility is given by:

$$\chi_{Total} = (\chi_{TIP} + \chi_{CEF}) - \lambda \quad (5.13)$$

where χ_{Total} is total magnetic susceptibility, χ_{TIP} is temperature-independent paramagnetism susceptibility, χ_{CEF} is a crystal field effect magnetic susceptibility and λ is molecular field constant.

Figure 5.5 shows calculated parameters obtained through magnetochemistry method. Figure 5.5a show the Ce^{3+} content where in W doped samples, the ratio between Ce^{3+} ions and W^{6+} ions seem to better agree with 1:1 ratio rather than 2:1 as it was expected from the lattice parameter prediction. Moreover, the ratio in Ta^{5+} ions to Ce^{3+} ions is also lower than expected ratio (1:1). Thus, the results imply that not all excess electrons from donor impurities are charge compensated by Ce^{3+} . Figure 5.5b, the crystal field splitting energy show an almost independence of doping concentration because the interaction between donor ions and Ce^{3+} is considerably weak in both Ta and W doped ceria. Figure 5.5c, the temperature-independent paramagnetism constant (TIP) is observed in all samples this can be the reason of partially covalent nature in

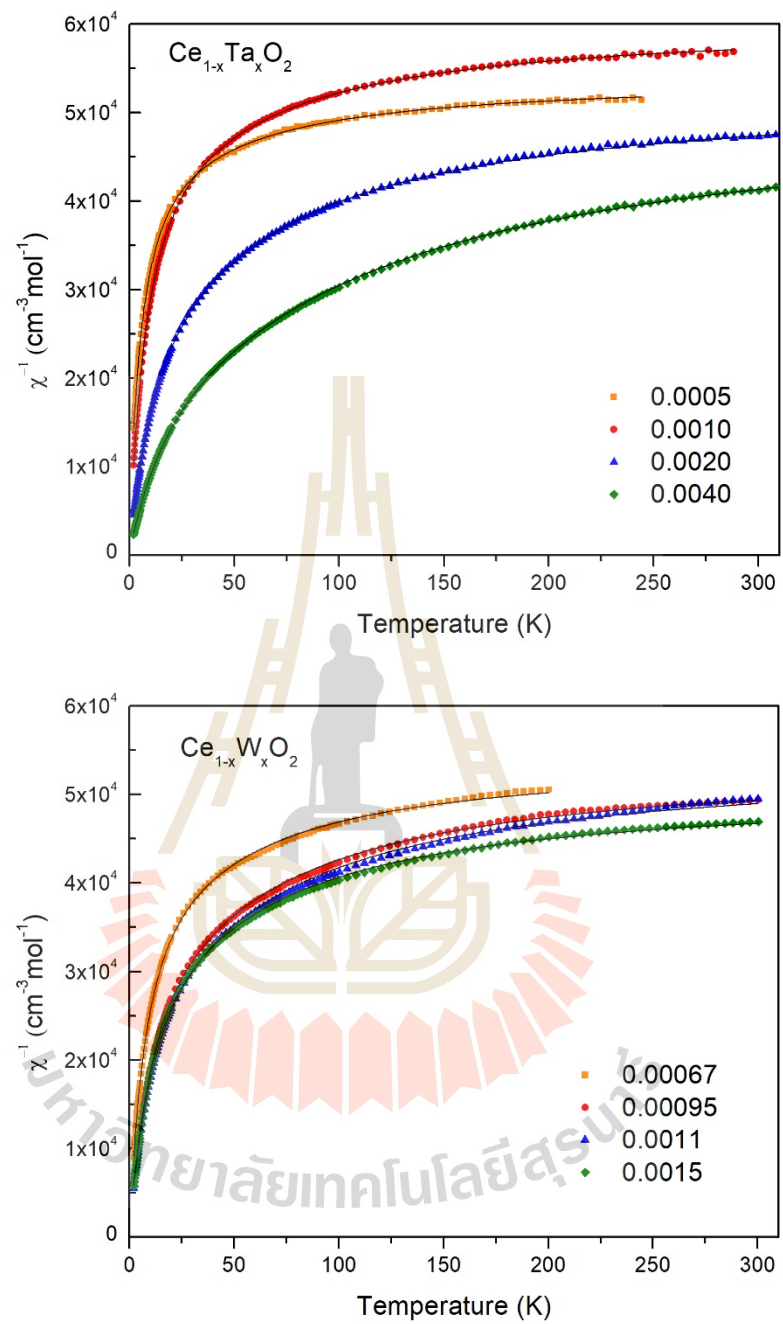


Figure 5.4 The inverse temperature dependent magnetic susceptibility of Ta and W doped CeO_2 .

samples chemical bonding of ceria. In figure 5.5d, molecular field constant indicated the nature of the exchange interaction of Antiferromagnetism materials.

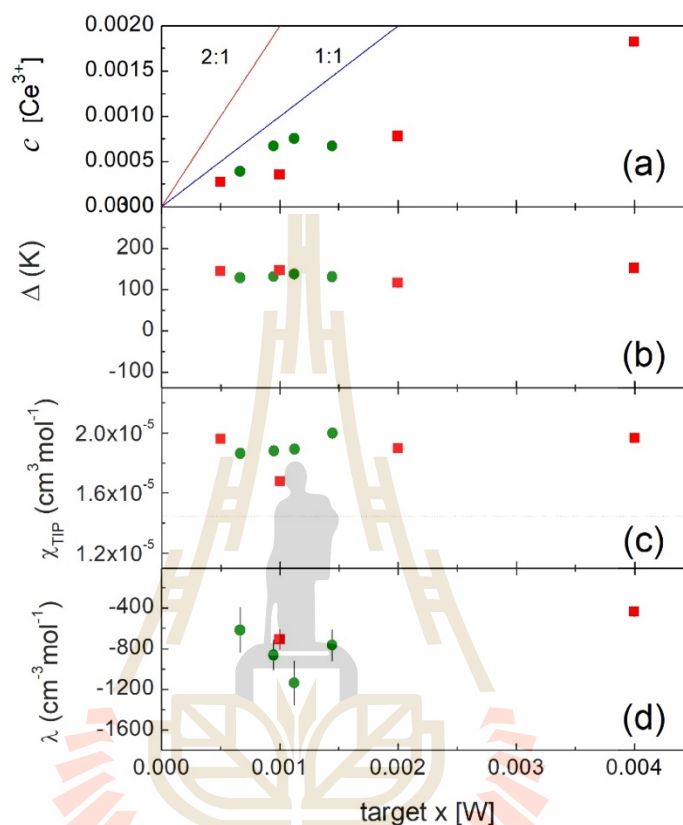


Figure 5.5 The fitting parameter obtained from magnetochemistry method where red rectangular (■) and green circle (●) symbol indicate Ta and W doped CeO_2 , respectively. Each row indicates different fitting parameter where row a is concentration of Ce^{3+} (c), row b is crystal field splitting energy between Γ_8 and Γ_7 , row (c) is the susceptibility of temperature-independent paramagnetism constant (χ_{TIP}) and row d is molecular field constant (λ). The solid lines at row an index compensation ratio of Ce^{3+} :Donors where red line is ratio 2:1 and blue line is ratio 1:1.

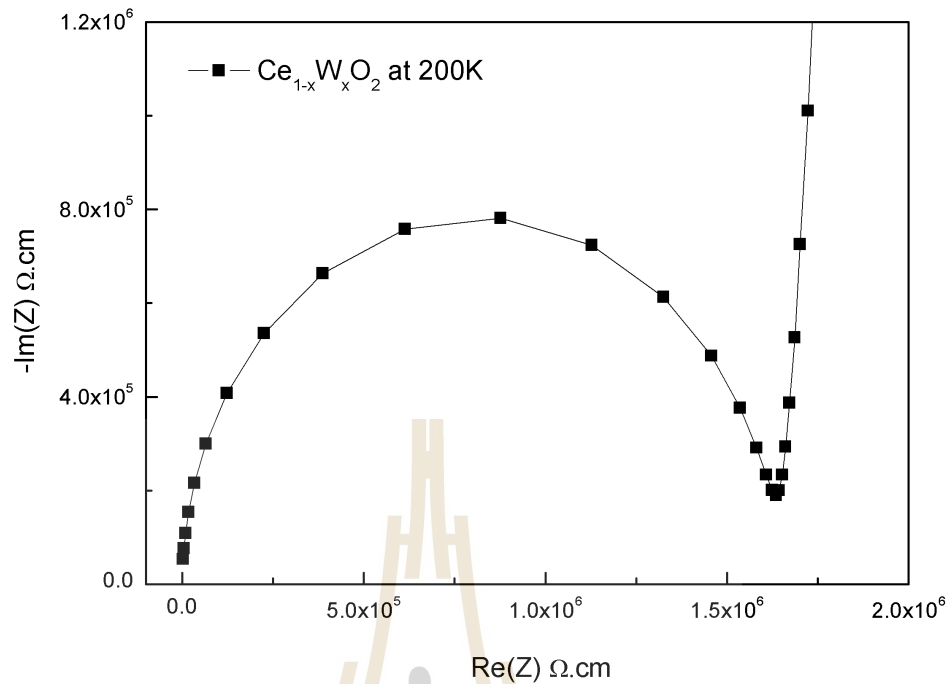


Figure 5.6 The selected impedance spectra of W doped CeO_2 at 200 K demonstrated the semicircle behavior of bulk grain resistance and low frequency effects of electrode interface effect.

5.2 Electron transport properties

Impedance analysis were performed to obtain electrical temperature dependence of conductivity of samples. The obtained impedance spectra were showed in figure 5.6. By consider semicircle behavior of bulk gain resistance of samples, we them selected the point on x-axis ($\text{Re}[Z]$) of characteristic arc corresponding to bulk gain resistance. At this point, the impedance was simply assumed that samples exhibited pure resistive behavior (the phase different is zero). Then, the selected $\text{Re}[Z]$ was converted into electrical conductivity (ρ).

The obtained electrical conductivity showed in figure 5.7a presented the temperature dependence with simple Arrhenius-type behavior as shown below:

$$\sigma = \sigma_0 e^{\left(\frac{-E_\sigma}{KT}\right)}, \quad (5.14)$$

where σ is electrical conductivity, σ_0 is conductivity constant, and E_σ is conductivity activation energy. This activated process occurs through the transport in ceria may originate from two different mechanism: i) small polaron hopping conductivity and ii) the bound small polaron due to interaction of donor impurities. So, the activation energy is defined as:

$$E_\sigma = E_h + E_b, \quad (5.15)$$

Where E_h is small polaron hopping conductivity and E_b is binding energy of small polaron and donor impurities caused bound small polaron (BSP). As illustrated by T. Kolodiazhnyi (Kolodiazhnyi et al., 2019), the bound small polaron (BSP) is the small polaron state that confine with the impurities state due to the Coulomb interaction. Thus, the energy requires to escape from this potential well is higher than expect from SP individually.

To find the total activation energy of donors doped ceria, the conductivity from equation 5.15 is modified into:

$$\ln\sigma = -E_\sigma\left(\frac{1}{KT}\right) + \ln\sigma_0 \quad (5.16)$$

The conductivity activation energy can be obtained by performing linear fitting of temperature dependent conductivity. The activation energy of each donor species

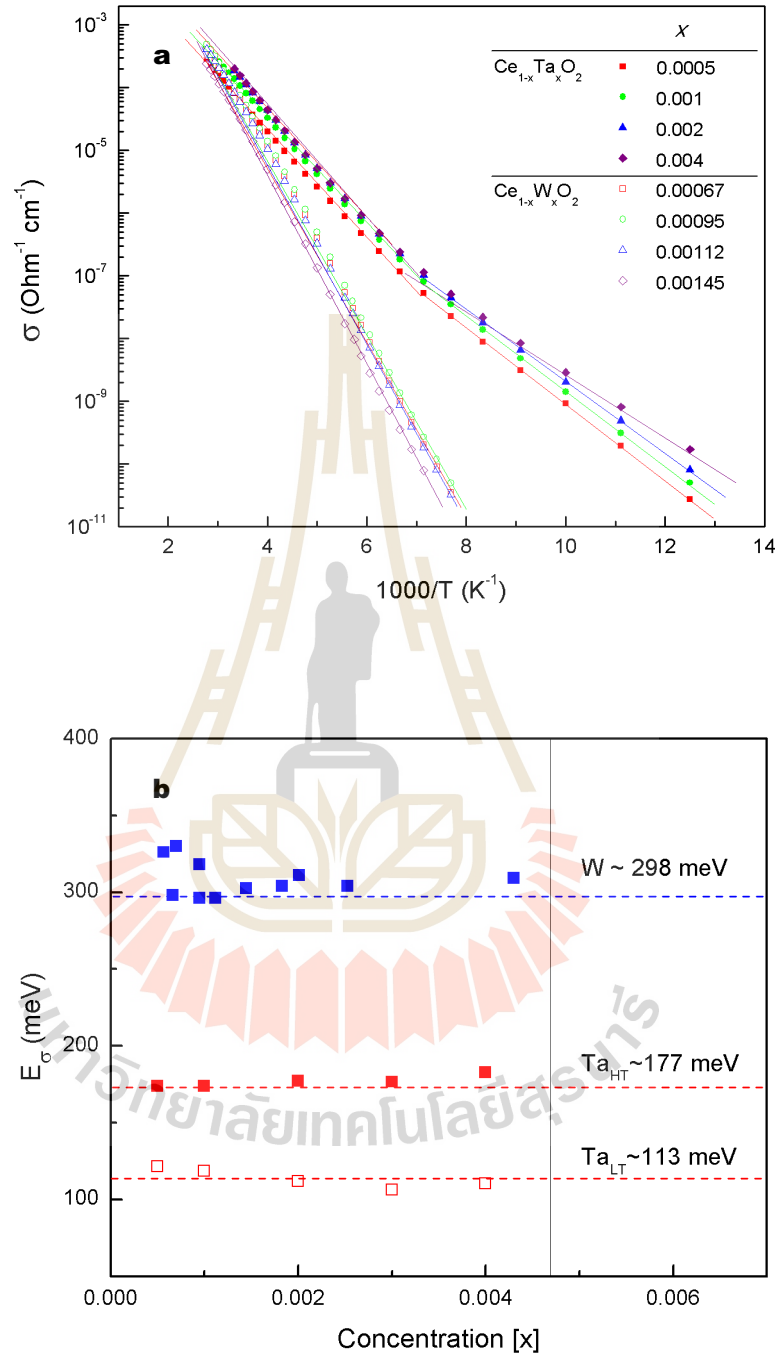


Figure 5.7 The temperature dependent conductivity of Ta and W doped CeO_2 with obtained activation energy from equation 5.11(a). The activation energy of Ta doped ceria show two distinct activated process in high and low temperature regime (b).

are showed in the label in figure 5.7a where the activation energy at each substitutional concentration insignificant difference. To clarify the different of E_{σ} , all observed E_{σ} are plotted together in figure 5.7b including some of preliminary work done by Dr. Taras Kolodiazhnyi. It is remarkably clear that the conductivity of Ta doped ceria showed two slopes with the transition energy near $\sim 150 \pm 10$ K. This indicates that in this observed temperature Ta doped ceria has two different processes that contribute to charge transport. The E_{σ} in Ta doped ceria are denoted as E_{HT} and E_{LT} for activation energy in high temperature and low temperature, respectively. The high temperature activation energy (E_{HT}) is 0.177 eV and low temperature regime (E_{LT}) is 0.113 eV. Surprisingly, in W doped ceria the activation energy is 0.298 eV which is almost two time higher than E_{HT} of Ta doped samples.

5.3 Discussion

All the major diffraction peaks observed in XRD spectra were well fitted with ICSD database no. 182988 for pristine CeO_2 . The lattice distortion obtained from Rietveld refinement obtained from XRD data shows the evolution of unit cell where Ta doped ceria is contracting as increasing the doping concentration and W doped ceria is expanding against doping concentration. Our lattice parameter model derived from defect compensation has similar trend with results obtained from the refinement. According to equation 5.6, Ta ions are dominant species in the system, and these yield the distraction in Ta doped ceria samples. Conversely, the W doped ceria is expanding because Ce^{3+} ions induced by W^{6+} ions are dominant, and the ionic radius is bigger than surrounding atoms. The deviation showing in figure 5.3 is because the concentration of

Ce^{3+} is partially compensated with other relatively positive defect such as oxygen vacancies which is supported by the lattice evolution treatment (Charoonsuk et al., 2017) and the appearance of oxygen interstitial observed from nuclear magnetic resonance (NMR) (Heinzmann et al., 2016).

The hypothesis that Ce^{3+} is only partially compensated with donor impurities is also supporting by the result from magnetochemistry as depicted in figure 5.5a. The fitting lines of ratio between the concentration of donor and Ce^{3+} are showed. These lines aim to indicate the ratio of compensation where one Ta^{5+} ion is expected to compensate with one Ce^{3+} ion and one W^{6+} ion compensates with two Ce^{3+} ions. However, both Ce^{3+} concentration is low than the expected line. This may interpret that certain amount of Ce^{3+} is compensated with other defects as stated above.

In conductivity analysis, the donors doped ceria both obey the simple Arrhenius-type behavior of temperature dependent conductivity where the obtained activation energy is showed in figure 5.7b. In Ta doped ceria, the conductivity shows two separated mechanism with the transition temperature around 150 ± 10 K. This may come from the different types of hopping conductivity rising in two temperature regimes. As mentioned in the earlier section, the small polaron and impurity conduction are dominate differently because the different in required hopping energy relates to EP interaction. In small polaron, the interaction between electron and phonon is stronger than the EP interaction in impurity conduction. This mean small polaron requires much higher energy to excite from localized states than impurity conduction. So, at high temperature conductivity of Ta doped ceria is considered as small polaron hopping and at low temperature regime, impurity conduction is dominant. To be comparative of E_{σ} , we will limit the discussion

to activation energy of Ta doped ceria only at high temperature regime (E_{HT}). Next point to discuss is the different in E_{σ} between Ta and W doped ceria. What contradicting the SP is that the high activation energy of W doped ceria which is almost two time higher than E_{HT} of Ta doped samples. The discussion on additional driven forces for electron localization in n-type ceria is needed to be discussed since the hopping of small polaron are the phonon-assisted mechanism and this should be independent of dopant species. The reason responds for that deviation is that driven forces of localized electron are more than single process of small polaron. The idea of impurities induced potential well is considered as illustrated in figure 5.8, this idea was proposed by T. Kolodiazhnyi et al., 2019. The top row of figure 5.8 shows incoherent transport of small polaron transport with hopping energy (E_h) corresponding to EP interaction. The middle row of figure 5.8 depicts the picture of trapped electron by Coulomb potential induced by donor impurities with energy barrier E_C . The bottom row of figure 5.8 draws our hypothesis that the potential induced by donor dopants enlarge self-induced potential of small polaron. When mobile small polaron faces the distortion of potential, the self-trapped electron is then bound to deeper induced potential well and termed as the bound small polaron state (BSP). BSP requires higher energy to hop across the new induced potential which equal to sum of small polaron hopping energy and binding energy due to Coulomb interaction between self-trapped electron and donor as mentioned in equation 5.16. To determine the effect of donors to the activation energy from the hypothesis, the activation energy of donor doped ceria is plotted against effective charge (Δq) of each donor species. 1987. Since the observed activation energy of hexa-valence is two time higher than penta-valence, we assume that the activation energy is proportional to:

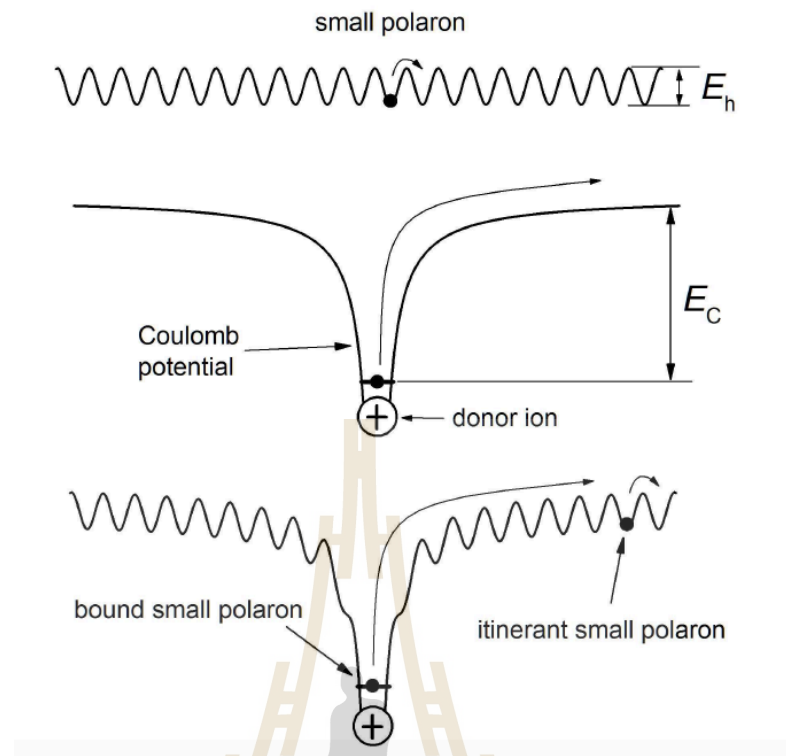


Figure 5.8 The bound small polaron that confines in potential well induced by lattice distortion (small polaron model) (at top), by the presence of donor (at the middle), and by combining both lattices distort and donor effect (at bottom) (Kolodiazhnyi et al., 2019).

$$E \propto \Delta q / r \quad (5.17)$$

where r is the distance between impurity and self-trapped electron. To gain a complete set of data, we included the activation energy from literature reviews of penta-valence (Nb) donor doped ceria from Kolodiazhnyi et al., 2017 and hexa-valence (U) doped ceria from Stratton and Tuller, 1987. The linear fitting of activation energy is performed against effective charge of donor as shown in figure 5.9. At $\Delta q = 0$ where no impurity contributes to activation energy, the pure activation energy of small polaron was obtained to be $\sim 66 \pm 20$ meV while E_C for pent-valent and hexa-valent dopant are 121 and 243, respectively.

To discuss electron localization and charge mobility in ceria, we employed the first principle calculation from the recent published paper in Physical Reviews B titled “Disentangling small-polaron and Anderson-localization effect in ceria: Combined experimental and first-principles study” (Kolodiazhnyi et al., 2019). The calculation was done by Mr. Thanandon Kongnok, Assoc. Prof. Sirichok Jungthawan from School of Physics and Dr. Suwit Suthirakun from School of Chemistry, Suranaree investigate electron localization in donors doped CeO₂ base on density function theory (DFT) The exchange and correlation energies functional is Perdew-Burke-Ernzerhof generalized gradient approximation. This calculation of polaron in donor doped ceria is in the super cell size of 2 x 2 x 2. The plane-wave expansion’s cut off energy as 400 eV

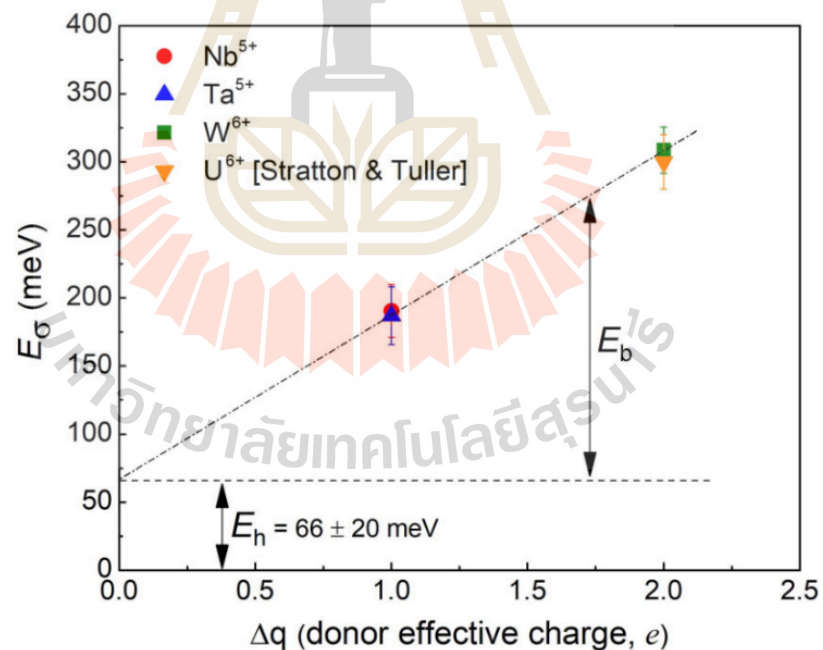


Figure 5.9 The activation energy plot of donors doped ceria combined the data of U doped ceria from the literature (Stratton and Tuller, 1987) and other Nb from (Kolodiazhnyi et al., 2017).

and $2 \times 2 \times 2$ mesh of special k -point was utilized. For better accuracy in density of states (DOS) calculation, a denser $3 \times 3 \times 3$ k -point was employed. In case of Ce $4f$ orbitals, a Hubbard-like term was used for on-site Coulomb interactions ($U_{\text{eff}} = 4.5$ eV) because of the lack of Coulomb self-interaction.

Since the most remarkable behavior in SP is self-trapping mechanism, the calculated self-trapped energy (E^{ST}) of polaron in supercell was defined as:

$$E^{ST} = E_{\text{tot}}(\text{polaron}) + E_{\text{tot}}(\text{delocalization}) \quad (5.18)$$

where $E_{\text{tot}}(\text{polaron})$ is the total energy of supercell with small polaron and $E_{\text{tot}}(\text{delocalization})$ is the total energy of supercell with delocalized electron in conduction band. Another problem is a defect structure in donors doped ceria, in order to understand the formation of defect, the formation energy (E^f) of impurities substitutes at Ce atom is calculated as:

$$E^f = E_{\text{tot}}(M^q) - [E_{\text{tot}}(\text{bulk}) + \mu_M - \mu_{\text{Ce}}] + q(E_{VBM} + E_F) + \Delta^q \quad (5.19)$$

where $E_{\text{tot}}(M^q)$ is the total energy of supercell containing defect of charge state q , $E_{\text{tot}}(\text{bulk})$ is the total energy of perfect bulk ceria with the same supercell and μ_M is chemical potential of dopant M ($M = \text{Ta}$ and W) that substitute in Ce atom with a chemical potential μ_{Ce} . Fermi energy and the valence band maximum of bulk ceria were denoted as E_{VBM} and E_F , respectively while the charge-state dependent correction due to the finite size of super cell is Δ^q .

It is well known that the bandgaps calculated from DFT are usually underestimate. As mentioned earlier, the experimental ceria bandgap is 3.2 eV where in the calculated bandgap from this DFT calculation is 2.56 eV. Generally, ceria is known

for the flat conduction band of Ce 4*f*. As shown in figure 5.10 DOS of Ta and W doped CeO₂ showed additional defect states of Ce 4*f* at slightly below the fermi level where the excess electron from donor impurities can then localized and forming small polaron formation. In addition to the electronic structure, the self-trapping energy for ceria was calculated as -0.14 eV while the calculation by L. Sun showed higher results as -0.30 eV in HSE06 and -0.54 in DFT+*U*.

The formation of defect structure was carried out by calculating formation energy and plotting against fermi energy (E_F) as depicted in figure 5.11. In Ta doped CeO₂, figure 5.11a, the most stable defect formation at high E_F is neutral charge of defect pair that contain tantalum being ionized as 5+ and donate an extra electron to the nearest neighbor Ce ions forming defect pair $(\text{Ce}'_{\text{Ce}} - \text{Ta}^{\bullet}_{\text{Ce}})^0$ as shown in figure 5.11b. Similarly, in W doped CeO₂ the most stable defect structure at high E_F is $(2\text{Ce}'_{\text{Ce}} - \text{W}^{\bullet\bullet}_{\text{Ce}})^0$ as illustrated in figure 5.11b. After that the favorable configurations were employed to calculate the spin density where only one spin occupied in impurity state as seen in DOS in figure 5.10. The favorable defect structure with calculated spin density is illustrated in figure 5.12. For Ta doped ceria, figure 5.12a, the polaron is localized at nearest-neighbor Ce atom where W doped ceria has the two polaron localized at nearest-neighbor Ce atom and another at the nearest-neighbor Ce atom that close to the first one as shown in figure 5.12b.

As L. Sun demonstrated in his work on the interaction between oxygen vacancies and small polaron in reduced ceria. the E_b as in order to remove first and second small polaron from defect complex between small polaron and effective positive charged defect is:

$$E_b^{1st} = E_{tot}[M_{Ce}^{n+} - (n - 1) polaron^{1+}] + E_{tot}(polaron) - E_{tot}[M_{Ce}^{n+} - n polaron^0] - E_{tot}[bulk] \quad (5.20)$$

and:

$$E_b^{2nd} = E_{tot}[M_{Ce}^{n+} - (n - 2) polaron^{1+}] + E_{tot}(polaron) - E_{tot}[M_{Ce}^{n+} - (n - 1) polaron^0] - E_{tot}[bulk] \quad (5.21)$$

The calculated E_b for Ta doped ceria is 0.516 eV and for first and second polaron in W doped ceria is 0.256 and 1.107 eV. These number are in good agreement with our hypothesis that the interaction between polaron and donor impurities need to be considered when study the localization and transport of small polaron motion in ceria.

All the works need to be summarized both theoretical and experimental work for better understanding of defect formation and electron transport properties of n-type ceria. The favorable formation of defect structure of Ta and W doped ceria was proposed



Figure 5.10 The density of states (DOS) of (a) Ta and (b) W doped CeO_2 , respectively. The VBM positioned as zero and dash line indicated the Fermi level where both figure show defect state of small polaron is slightly below the conduction band (Kolodiazhnyi et al., 2019).

from defect chemistry approach that one small polaron should compensated one extra electron from $\text{Ta}_{\text{Ce}}^{\bullet}$ and formed as defect pair $(\text{Ce}'_{\text{Ce}} - \text{Ta}_{\text{Ce}}^{\bullet})^0$. Meanwhile two small polarons should compensated two extra electrons from $\text{W}_{\text{Ce}}^{\bullet\bullet}$ and form a strength line of defect complex as $(\text{Ce}'_{\text{Ce}} - \text{W}_{\text{Ce}}^{\bullet\bullet} - \text{Ce}'_{\text{Ce}})^0$. These assumptions agree with favorable defect formation of Ta doped ceria since small polaron is likely sitting at nearest neighbor to Ta^{5+} ion. However, W doped ceria are slightly interesting since small polaron form the complex of two Ce^{3+} and the near each other as $(2\text{Ce}'_{\text{Ce}} - \text{W}_{\text{Ce}}^{\bullet\bullet})^0$ rather than form the strength line of defect complex.

In conductivity analysis, the first principle calculation was confirming two important evidences to electron localization and transport properties in n-type ceria. The

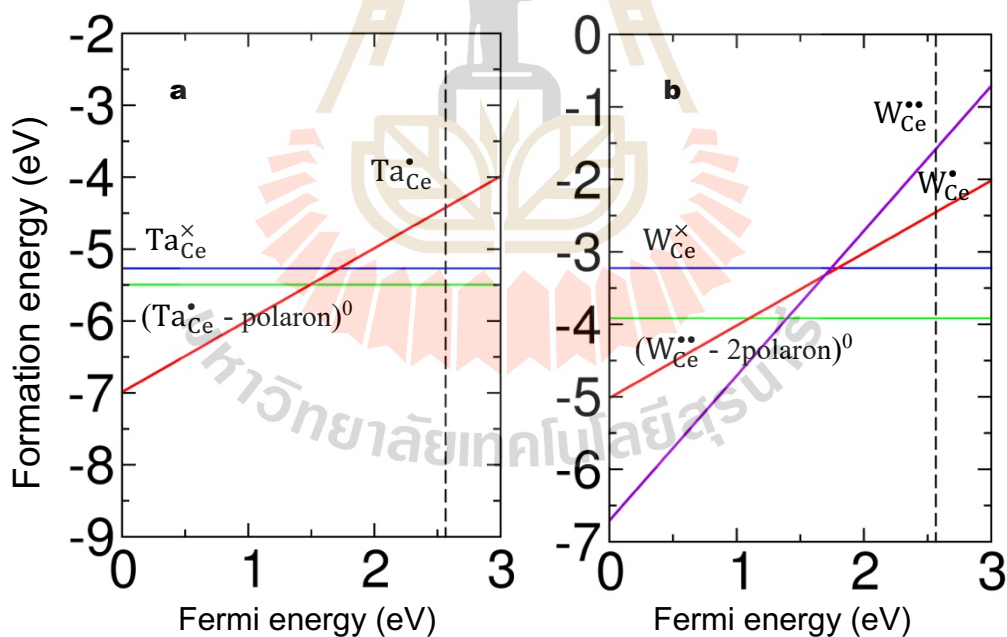


Figure 5.11 The calculated formation energy of each configurations compared with fermi energy. This assured that in (a) Ta doped ceria $(\text{Ta}_{\text{Ce}}^{\bullet} - \text{polaron})^0$ is the most stable structure while (b) $(\text{W}_{\text{Ce}}^{\bullet\bullet} - 2\text{polaron})^0$ is W doped ceria favorable defect complex (Kolodiazny et al., 2019).

existence of localized state as small polaron in $4f$ electron system were portrayed in DOS and spin density calculation showing the occupied $4f^1$ electron localized in forbidden gap near conduction band. Additionally, the effect of Coulomb interaction between donor impurities also was confirmed to be significantly large compared to small polaron hopping activation energy which opposes the conventional SP. According to defect complex formation, the effective charge can be reduced by the formation of defect. This leads to an assumption that the small polaron hopping energy (E_h) is vanishing and value of $66 \pm \text{meV}$ is settled as the upper bound of E_h . Meanwhile, the experimental works on activation energy also give another remarkable assumption while the effect from E_b is larger as increasing effective charge (Δq). This concludes that at higher Δq the affect from donor impurity is dominant compared to small polaron hopping process.



Figure 5.12 The calculated spin density of favorable configuration of defect complex:

(a) $(\text{Ta}_{\text{Ce}}^{\bullet} - \text{Ce}'_{\text{Ce}})^0$ and (b) $(\text{W}_{\text{Ce}}^{\bullet\bullet} - 2\text{Ce}'_{\text{Ce}})^0$ (Kolodiazhnyi et al., 2019).

CHAPTER VI

CONCLUSION & FUTURE DIRECTION OF WORK

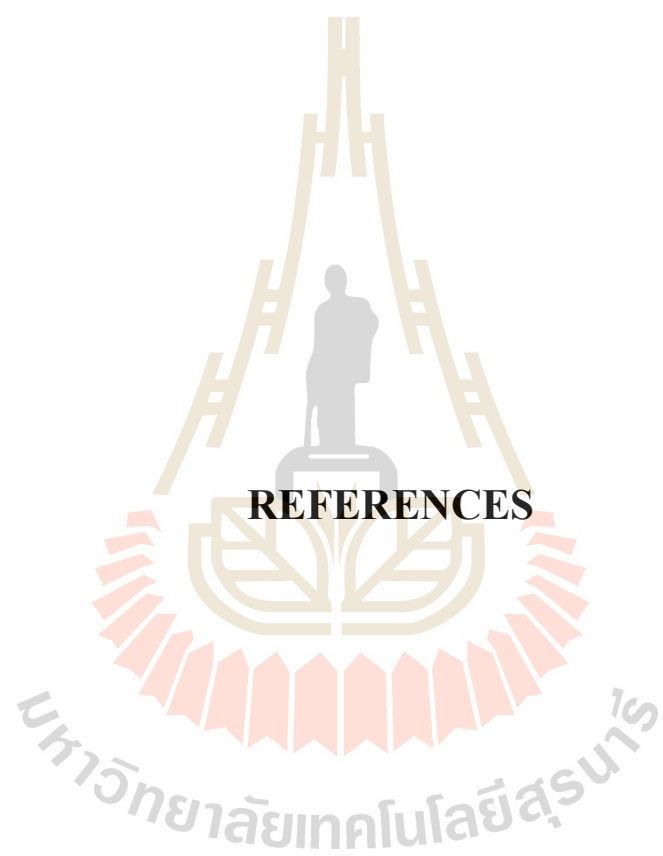
6.1 Conclusion

The studies of evolution of lattice parameter obtained from Rietveld refinement and defect chemistry treatment is in the same trend as Ta doped samples show the contraction and W doped samples are expanding. The deviation suggests that there is other defect compensation in our samples such as oxygen vacancies. This supports with the concentration of Ce^{3+} obtained from magnetochemistry where the ratio of donor ions and Ce^{3+} is lower than the expected ratio (1:1 for Ta sample and 2:1 for W sample). Moreover, the crystal field splitting energy shows the deviation as plot against doping concentrations where this can presume that the interaction between donor impurities and Ce^{3+} should be considered. In conductivity analysis, donors doped ceria both obey the simple Arrhenius-type behavior of temperature dependent conductivity with the different activation energy. As combining our results with data from literature reviews, the individual activation energy for small polaron effect is obtained by the linear fitting of activation energy against effective charge of donor (Δq) where at $\Delta q = 0$ implies no effect of induced-potential well from donor impurities an upper bound for $E_h \sim 66 \pm 20$ meV. This can be more clearly by coincidentally considering the supportive works based on first principle calculations. The result of the calculations shows the E_b between small polaron and effective positive donor impurities is considerably large compared to

total activation energy which support the assumption that donor impurities play a significant role in localized of small polaron. The defect favorable formation was also estimated against the fermi level shows that the system likely to form the $(\text{Ta}_{\text{Ce}}^{\bullet} - \text{Ce}'_{\text{Ce}})^0$ and $(\text{W}_{\text{Ce}}^{\bullet\bullet} - 2\text{Ce}'_{\text{Ce}})^0$. The calculated spin-density illustrated the defect complex of donor impurities and small polaron where the formation can be future model for study the dielectric behavior induced by small polaron in future work.

6.2 Future direction of work

The future work is dividing into two themes: an electronic structure of n-type and a charge transport of small polaron. Since high energy spectroscopies can reveal the actual structure of inorganic, these techniques are interesting for studying the complicated electronic structure of n-type ceria. Moreover, the defect chemistry treatment can be more specific to the species of defect such as oxygen interstitials and intrinsic defect pairs. While the transport properties of n-type ceria are still unclear on several point like the deviation between experimental and simulations activation energy, the efforts on investigate both experimentally and theoretically are required. In this work we demonstrated have demonstrated the effect of donor impurities on the potential well that trapped small polaron forms bound small polaron which is normally ignored in other studies. We hope that this work will enable new aspect of working with the localization and transport properties of incomplete *d*- and *f*-orbital in cubic fluorite materials.



REFERENCES

REFERECES

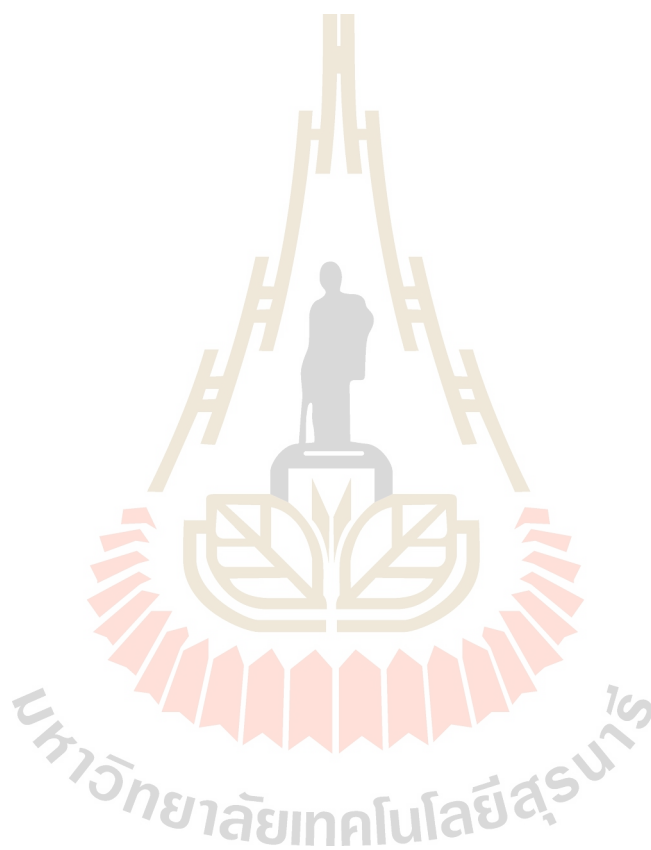
- Ananthapadmanabhan, P. V., Menon, S. B., Patil, D. S., Venkatramani, N., and Rohatgi, V. K. (1992). Electrical conductivity of cerium dioxide doped with tantalum pentoxide. **Journal of Materials Science Letters**. 11(8): 501-503.
- Anderson, P. W. (1958). Absence of diffusion in certain random lattices. **Physical Review**. 109(5): 1492-1505.
- Beie, H. J., and Gnörich, A. (1991). Oxygen gas sensors based on CeO₂ thick and thin films. **Sensors and Actuators B: Chemical**. 4(3): 393-399.
- Bronold, F. X., and Fehske, H. (2002). Anderson localization of polaron states. **Physical Review B**. 66(7): 073102.
- Callister, W. D. & Rethwisch, D. G. (2007). **Introduction to materials science and engineering**. In electrical conductivity, John Wiley & Sons, Hoboken, NJ, pp. 721-727.
- Charoonsuk, T., Vittayakorn, N., and Kolodiazhnyi, T. (2017). Lattice evolution and point defect chemistry in Ta-doped ceria. **Journal of Alloys and Compounds**. 695: 1317-1323.
- De Guire, M. R., Shingler, M. J., and Dincer, E. (1992). Point defect analysis and microstructural effects in pure and donor-doped ceria. **Solid State Ionics**. 52(1): 155-163.
- Emin, D. (2013). **Polarons**. In Succinct overview, Cambridge University Press, New York, pp. 2.

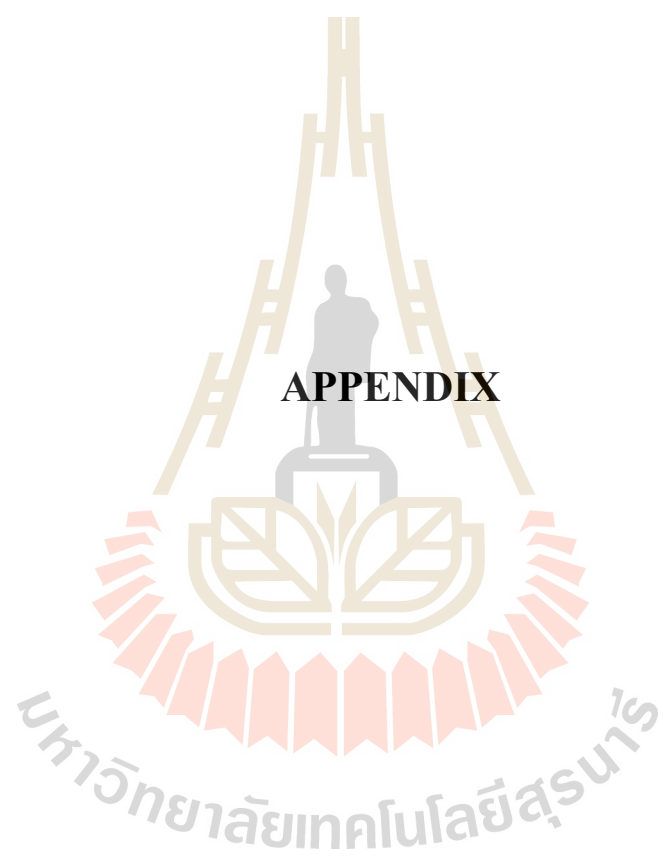
- Friedrich Kremer. (1999). High performance dielectric, conductivity and electrochemical impedance analyzers. Retrieved from https://www.novocontrol.de/php/ana_alpha.php.
- Göbel, M. C., Gregori, G., and Maier, J. (2012). Electronically blocking grain boundaries in donor doped cerium dioxide. **Solid State Ionics**. 215: 45-51.
- Grundmann, M. (2015). **The physics of semiconductors: an introduction including nanophysics and applications**. Springer.
- Heinzmann, R., Issac, I., Eufinger, J.-P., Ulbrich, G., Lerch, M., Janek, J., and Indris, S. (2016). Observing Local Oxygen Interstitial Diffusion in Donor-Doped Ceria by ^{17}O NMR Relaxometry. **The Journal of Physical Chemistry C**. 120(16): 8568-8577.
- Herrmann, G. F., Pearson, J. J., Wickersheim, K. A., and Buchanan, R. A. (1966). Crystal Field Effects for Ce^{3+} and Yb^{3+} in the Garnets. **Journal of Applied Physics**. 37(3): 1312-1313.
- Hong, S. J., and Virkar, A. V. (1995). Lattice parameters and densities of rare-earth oxide doped ceria electrolytes. **Journal of the American Ceramic Society**. 78(2): 433-439.
- Jenks, W. G., Sadeghi, S. S. H., and Wikswo, J. P. (1997). SQUIDs for nondestructive evaluation. **Journal of Physics D: Applied Physics**. 30(3): 293-323.
- Kang, S. D., Dylla, M., and Snyder, G. J. (2018). Thermopower-conductivity relation for distinguishing transport mechanisms: Polaron hopping in CeO_2 and band conduction in SrTiO_3 . **Physical Review B**. 97(23): 235201.
- Kašpar, J., Fornasiero, P., and Graziani, M. (1999). Use of CeO_2 -based oxides in the three-way catalysis. **Catalysis Today**. 50(2): 285-298.

- Kolodiazhnyi, T., Charoonsuk, T., Seo, Y.-S., Chang, S., Vittayakorn, N., and Hwang, J. (2017). Magnetic, optical, and electron transport properties of n-type CeO₂: Small polarons versus Anderson localization. **Physical Review B**. 95(4): 045203.
- Kolodiazhnyi, T., Sakurai, H., Belik, A. A., and Gornostaeva, O. V. (2016). Unusual lattice evolution and magnetochemistry of Nb doped CeO₂. **Acta Materialia**. 113: 116-123.
- Kolodiazhnyi, T., Tipsawat, P., Charoonsuk, T., Kongnok, T., Jungthawan, S., Suthirakun, S., Vittayakorn, N., and Maensiri, S. (2019). Disentangling small-polaron and Anderson-localization effects in ceria: Combined experimental and first-principles study. **Physical Review B**. 99(3): 035144.
- Landau, L. D. (1933). Electron motion in crystal lattices. **Physikalische Zeitschrift der Sowjetunion**. 3: 664.
- Muhich, C., and Steinfeld, A. (2017). Principles of doping ceria for the solar thermochemical redox splitting of H₂O and CO₂. **Journal of Materials Chemistry A**. 5(30): 15578-15590.
- Naik, I. K., and Tien, T. Y. (1978). Small-polaron mobility in nonstoichiometric cerium dioxide. **Journal of Physics and Chemistry of Solids**. 39(3): 311-315.
- Naik, I. K., and Tien, T. Y. (1979). Electrical conduction in Nb₂O₅-doped cerium dioxide. **Journal of The Electrochemical Society**. 126(4): 562-566.
- Orel, Z. C., and Orel, B. (1994). Optical properties of pure CeO₂ and mixed CeO₂/SnO₂ thin film coatings. **physica status solidi (b)**. 186(1): K33-K36.
- Shannon, R. D., and Prewitt, C. T. (1969). Effective ionic radii in oxides and fluorides. **Acta Crystallographica Section B**. 25(5): 925-946.

- Skorodumova, N. V., Simak, S. I., Lundqvist, B. I., Abrikosov, I. A., and Johansson, B. (2002). Quantum origin of the oxygen storage capability of ceria. **Physical Review Letters**. 89(16): 166601.
- Stennett, M. C., Corkhill, C. L., Marshall, L. A., and Hyatt, N. C. (2013). Preparation, characterisation and dissolution of a CeO₂ analogue for UO₂ nuclear fuel. **Journal of Nuclear Materials**. 432(1): 182-188.
- Stoukides, M. (2000). Solid-electrolyte membrane reactors: current experience and future outlook. **Catalysis Reviews**. 42(1-2): 1-70.
- Stratton, T. G., and Tuller, H. L. (1987). Thermodynamic and transport studies of mixed oxides. The CeO₂-UO₂ system. **Journal of the Chemical Society, Faraday Transactions 2: Molecular and Chemical Physics**. 83(7): 1143-1156.
- Sun, L., Huang, X., Wang, L., and Janotti, A. (2017). Disentangling the role of small polarons and oxygen vacancies in CeO₂. **Physical Review B**. 95(24): 245101.
- Tuller, H. L., and Bishop, S. R. (2011). Point defects in oxides: tailoring materials through defect engineering. **Annual Review of Materials Research**. 41(1): 369-398.
- Tuller, H. L., and Nowick, A. S. (1975). Doped ceria as a solid oxide electrolyte. **Journal of The Electrochemical Society**. 122(2): 255-259.
- Tuller, H. L., and Nowick, A. S. (1977). Small polaron electron transport in reduced CeO₂ single crystals. **Journal of Physics and Chemistry of Solids**. 38(8): 859-867.
- Tuller, H. L., and Nowick, A. S. (1979). Defect structure and electrical properties of nonstoichiometric CeO₂ single crystals. **Journal of The Electrochemical Society**. 126(2): 209-217.

Zajac, W., and Molenda, J. (2008). Electrical conductivity of doubly doped ceria. **Solid State Ionics**. 179(1): 154-158.





APPENDIX

APPENDIX

PUBLICATION AND PRESENTATION

A.1 Publication

Kolodiazhnyi, T., Tipsawat, P., Charoonsuk, T., Kongnok, T., Jungthawan, S., Suthirakun, S., Vittayakorn, N., and Maensiri, S. (2019). Disentangling small-polaron and Anderson-localization effects in ceria: Combined experimental and first-principles study. **Physical Review B**. 99(3): 035144.

A.2 Oral presentation

Tipsawat P., Kolodiazhnyi T., and Maensiri S., Anomalous low-temperature dielectric properties of W doped CeO₂". Oral presenter at The First Materials Research Society of Thailand International Conference, Chiang Mai, Thailand.

Tipsawat P., Kolodiazhnyi T., and Maensiri S., Defect chemistry analysis of low-temperature dielectric properties in n-type CeO₂". Oral presenter at International Conference on the 4th Industrial Revolution and its Impacts, Nakhon Si Thammarat, Thailand.

Disentangling small polaron and Anderson localization effects in ceria: Combined experimental and first-principles study

Taras Kolodiazhnyi,^{1,*} Pannawit Tipsawat,² Thitirat Charoonsuk,³ Thanundon Kongnok,⁴ Sirichok Jungthawan,⁴ Suwit Suthirakun,⁴ Naratip Vittayakorn,⁵ and Santi Maensiri⁴

¹National Institute for Materials Science, 1-1 Namiki, Tsukuba, Ibaraki, 305-0044, Japan

²School of Physics, Institute of Science, Suranaree University of Technology, Nakhon Ratchasima, 30000, Thailand

³Electroceramic Research Laboratory, College of Nanotechnology,

King Mongkut's Institute of Technology Ladkrabang, Bangkok 10520, Thailand

⁴Institute of Science, Suranaree University of Technology, Nakhon Ratchasima, 30000, Thailand

⁵Department of Chemistry, Faculty of Science, King Mongkut's Institute of Technology Ladkrabang, Bangkok 10520, Thailand

By comparison of the electrical conductivity of ceria doped with penta- and hexa-valent ions, we separate the total electron localization energy into the two contributions originating from the small polaron effects and the Coulomb interaction with the donor ions. The upper bound of the itinerant small polaron hopping energy is estimated at 66 ± 20 meV. The binding energy of the $\text{Ce}^{3+}\text{-}M^{5+/6+}$ defect complex increases from 121 meV for $M = \text{Nb}^{5+}/\text{Ta}^{5+}$ to 243 meV for $M = \text{W}^{6+}/\text{U}^{6+}$. The first-principles simulations are in qualitative agreement with the experimental findings. At low temperatures the f electrons bound to the donor defects show dielectric relaxation with the lowest activation energy of 2.7 and 17 meV for Nb(Ta)- and W-doped ceria, respectively. Remarkably, these energies are significantly smaller than the hopping energy of the itinerant small polarons. While both the electron-lattice and the electron-defect interactions cause the f -electron localization in real-case ceria, the latter effects seem to be the dominant.

I. INTRODUCTION

Electron localization plays a central role in the metal-insulator transition in solids. Carrier localization can be driven by spin/charge density waves, Mott transition, small polaron formation, lattice disorder, etc. For example, manifestation of the Anderson-type localization¹ is found in random-field-induced carrier localization in doped Si, and random-bond-induced localization in sulfur². On the other hand, n -type CeO_2 has been considered a textbook example of a small polaron (SP) model³ where $4f$ electrons are localized at the Ce^{3+} ions as a result of a strong electron-phonon interaction and local lattice distortions of the nearby ions⁴.

Very recent studies of n -type ceria, however, reveal that, in addition to the small polaron effects, electrons may localize next to the donor ions (or oxygen vacancies) forming a bound small polaron (BSP)⁵ as illustrated in Figure 1. In the latter case, the main cause of the BSP formation could be disorder-induced Anderson localization of the f electron next to the donor/defect site. Indeed, as was pointed out in Ref.⁶, both SP and Anderson localization effects are intertwined in the partially disordered solids. The first attempt to disentangle these two effects using the first-principles calculations of reduced ceria was reported recently in Ref.⁷ It was found that the f electron localization is caused by both the polaronic effects ($E_h \approx 120$ eV) and the binding to the donor defect, e.g., oxygen vacancy ($E_b \approx 137$ meV), where E_h is the SP hopping (diffusion) energy and E_b is the binding energy of the localized $4f$ electron to the nearest donor defect (not to be confused with the binding energy of SP).

In this contribution we attempt to disentangle the SP

and the Anderson disorder effects and to get an experimental estimate of the E_h and E_b using a series of donor-doped ceria with different donor effective charges. We complement our experimental findings with the results of the first-principles calculations. Our results indicate that both the electron-lattice and electron-defect interactions contribute to the total localization energy of the f electron in ceria. However, with an increase in the effective charge of the donor ion, the electron-defect interaction becomes the dominant one. As such, the ideal small polaron picture is inadequate and requires to include the defect-induced disorder effects which dominate the electron localization in a real-case ceria.

II. MATERIALS AND METHODS

Polycrystalline $\text{Ce}_{1-x}M_x\text{O}_2$ ceramics, where $M = \text{Nb}$, Ta and W, with target $x = 0 - 0.01$ were used for this study. Nb- and Ta-doped CeO_2 samples were the same as those reported in Ref.⁵. The details of their preparation can be found elsewhere⁵. W-doped ceramics were prepared at identical conditions to those of Nb- and Ta-doped CeO_2 . The 99.99% pure WO_3 from High Purity Chemicals, Japan was used as a source of W^{6+} ion.

The concentration of Ce^{3+} ions in the sintered ceramics was determined by fitting the dc magnetic susceptibility with the van Vleck equation taking into account the crystal field effects as described in Ref.⁸ Magnetic moment in the 2 - 300 K range was measured using the Magnetic Properties Measurements System (MPMS-XL, Quantum Design, USA) at 5000 Oe. Electrical conductivity of polycrystalline ceramics were extracted from the complex impedance, Z^* , measurements in the 1 Hz - 1 MHz frequency range. The Physical Property Measure-

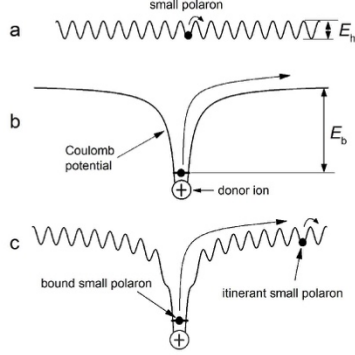


FIG. 1. Schematics of the itinerant SP (a) and the SP bound to donor defect (c) by Coulomb potential (b).

ment System (PPMS, Quantum Design, USA) was used to control the sample temperature in the 2 – 360 K interval.

The electron localization in doped CeO_2 was also modelled by using Vienna ab initio Simulation Package (VASP)^{9,10} based on density functional theory (DFT)^{11,12}. The Perdew-Burke-Ernzerhof (PBE) generalized gradient approximation (GGA) was employed as the exchange and correlation energies^{13–15}. The $2 \times 2 \times 2$ supercell was used to simulate the defect and the polaron formation of doped CeO_2 . The cut-off energy for planewave expansion was set to 400 eV and $2 \times 2 \times 2$ mesh of special k-points was used. A denser $3 \times 3 \times 3$ k-points mesh was used for better accuracy in density of states (DOS) calculations. Due to the lack of cancellation of the Coulomb self-interaction, a Hubbard-like term¹⁶ was introduced to account for the on-site interactions ($U_{eff} = 4.5$ eV in the case of Ce $4f$ orbitals).

The polaron formation is investigated by calculating self-trapping energy of an excess electron (E^{ST}), i.e., the energy gained by a small polaron formation, that is defined as⁷

$$E^{ST} = E_{\text{tot}}(\text{polaron}) - E_{\text{tot}}(\text{delocalized}), \quad (1)$$

where $E_{\text{tot}}(\text{polaron})$ is the total energy of the supercell containing a small polaron, and $E_{\text{tot}}(\text{delocalized})$ is the total energy of supercell with an extra electron delocalized in conduction band⁷. The positive/negative value of E^{ST} indicates that the polaron formation is unfavorable/favorable with reference to the delocalized electronic state. The formation energy of a dopant M substituting for Ce atom, $E^f(M^q)$, where $M = \text{Nb}, \text{Ta}, \text{W}$ and U , is given by

$$E^f = E_{\text{tot}}(M^q) - [E_{\text{tot}}(\text{bulk}) + \mu_M - \mu_{Ce}] + q(E_{\text{VBM}} + E_F) + \Delta^q, \quad (2)$$

where $E_{\text{tot}}(M^q)$ is the total energy of the supercell containing the defect in the charge state q (Note that this charge state is not the oxidation number), and $E_{\text{tot}}(\text{bulk})$ is the total energy of perfect bulk CeO_2 with the same supercell. The μ_M , where $M = \text{Nb}, \text{Ta}, \text{W}$ and U , is a chemical potential of a dopant that substitutes Ce atom with a chemical potential μ_{Ce} . The value of chemical potential is irrelevant when comparing the relative stability of a similar defect for different charge states. In this study, the formation energies reported here were obtained by setting chemical potential of all elements to zero. The Fermi level, E_F , representing the energy of the electron reservoir is a variable in this formalism and referenced to the valence band maximum (VBM, E_{VBM}) of bulk. Finally, Δ^q is the charge-state dependent correction due to the finite size of the supercells^{17,18}.

III. RESULTS AND DISCUSSION

A. Experimental results

Temperature dependence of electrical conductivity, σ , for selected Nb-, Ta- and W-doped CeO_2 is shown in Figure 2. The activation energy of conductivity, E_σ , for $\text{Ce}_{1-x}\text{W}_x\text{O}_2$ extracted from the Arrhenius-type dependence is 309 ± 17 meV. This energy is notably higher than the $E_\sigma \sim 190 \pm 21$ meV found in Nb- and Ta-substituted CeO_2 ⁵. A large difference between the activation energies of Nb(Ta)- and W-doped CeO_2 is highly unusual for a small polaron model of ceria which claims that the SP hopping energy is independent on the type of the donor dopant. This claim is based on the major assumption that the SP hopping energy in ceria is determined by the electron-phonon interactions, whereas the defects and disorder are of secondary importance. While this assumption may still be valid for ideal, defect-free ceria, the experimental data for a real-case ceria points to a different picture.

In contrast to what would have been expected in the ideal SP scenario, we speculate that the large difference in the E_σ for n -type ceria comes from the different type of the donor dopants. In particular, the different values of E_σ for Nb(Ta)- and W-doped CeO_2 may be associated with the different effective charges, Δq , of the donor ions. For a purely ionic picture, the Δq for $\text{Ta}^{5+}(\text{Nb}^{5+})$ and W^{6+} ions substituting for Ce^{4+} host is $+1|e|$ and $+2|e|$, respectively.

To address both the itinerant SP and the defect-bound SP effects, the SP conductivity in ceria can be expressed as:

$$\sigma = e\mu n \approx e\mu_0 \exp(-E_h/k_B T) [\text{Ce}^{3+}] \exp(-E_b/k_B T), \quad (3)$$

where the term $\mu_0 \exp(-E_h/k_B T)$ accounts for the SP mobility and the term $[\text{Ce}^{3+}] \exp(-E_b/k_B T)$ accounts for the concentration of the *itinerant* small polarons. The $[\text{Ce}^{3+}]$ is the concentration of the Ce^{3+} ions, k_B is the

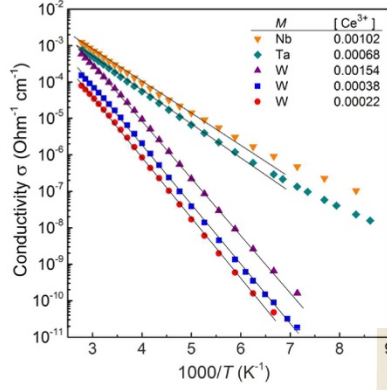


FIG. 2. (Color online) Electrical conductivity of $\text{Ce}_{1-x}\text{M}_x\text{O}_2$, $M = \text{Nb}, \text{Ta}$ and W , as a function of reciprocal temperature. The concentration of Ce^{3+} per formula unit is indicated in the legend.

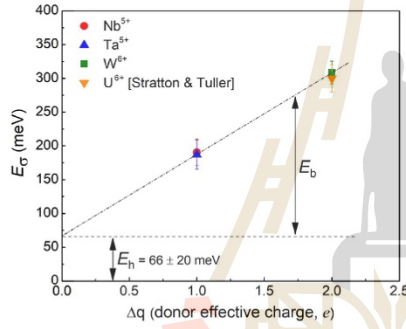


FIG. 3. Activation energy of the conductivity of the donor-doped ceria as a function of the effective charge of the donor ion, Δq .

Boltzmann constant and T is the absolute temperature. According to Eq. 3, the total activation energy of conductivity, E_σ , is the sum of the SP hopping and defect binding energies: $E_\sigma = E_h + E_b$. As shown schematically in Figure 1, the SP transport occurs by the bound SP first becoming itinerant by breaking away from the donor defect followed by the phonon-assisted hopping of itinerant SP.

How one can distinguish experimentally between the E_h and E_b ? One has little control over the SP hopping (diffusion) energy, E_h , as it is not easy to modify the op-

tical and acoustic phonons under ambient pressure. We focus, therefore, on the $4f$ electron-defect binding energy, E_b . Here we make a major assumption that the main contribution to E_b comes from the electrostatic interaction between the donor defect and the $4f$ electron. We believe that this assumption is justified by the strongly localized nature of the $4f$ electron. In this case, E_b will depend on the effective charge of the donor defect, Δq , as:

$$E_b \propto \Delta q / r, \quad (4)$$

where r is the distance between the donor defect and the Ce^{3+} ion (i.e., $r \sim 3.83 \text{ \AA}$ when donor is located on the cation site). Therefore, by varying the donor effective charge, Δq , one can vary the E_b .

The experimental E_σ for the different values of the effective donor charge are summarized in Figure 3 for Nb-, Ta- W- an U-doped CeO_2 . The E_σ for U-doped ceria was adapted from Ref.¹⁹ Remarkably, the experimental values of activation energy of conductivity for W^{6+} - and U^{6+} -doped ceria agree within the standard deviation as do the E_σ values for the Nb^{5+} - and Ta^{5+} -doped ceria.

We speculate that the higher E_σ values for W(U)-doped ceria as compared to the Nb(Ta)-dopants are attributed to the higher Δq in the former compounds and serve as an indirect support for our assumption that the main contribution to the E_b comes from the Coulomb interactions of point defects. A linear extrapolation of E_σ to $\Delta q = 0$ in Fig. 3 yields $E_h \sim 66 \pm 20 \text{ meV}$, which is the estimated hopping energy of the itinerant SP in ceria. The E_b values obtained from Fig. 3 for Nb(Ta)- and W(U)-doped ceria are 121 and 243 meV, respectively. A two-fold enhancement in E_b for W(U) dopants as compared to the Nb(Ta) dopants is in quantitative agreement with that predicted by Eq. 4.

This excellent agreement, however, might be somewhat accidental because of the rather crude assumptions made in the estimation of the donor effective charge. This is particularly relevant to the W^{6+} defect which is charge compensated by the two Ce^{3+} ions. Assuming the coaxial configuration of the $\text{Ce}^{3+}\text{-W}^{6+}\text{-Ce}^{3+}$ defect, the effective charge of the $\text{W}^{6+}\text{-Ce}^{3+}$ defect dipole felt by the second Ce^{3+} ion will be reduced by ca. 25%. Importantly, this will lead to the *vanishing* of the E_h energy estimated from Fig. 3. We conclude, therefore, that if the SP effects are present in ceria, they should probably contribute less than 66 meV to the SP hopping energy and that the $E_h \sim 66 \text{ meV}$ should be considered as the upper bound limit of the f electron localization caused by the SP effects.

Next, we examine the dynamics of the bound small polaron (BSP) in ceria at low temperatures. According to a simple model of the charged point defects, the $[\text{Ce}^{3+}\text{-M}^{5+}]$ defect complex (where $M = \text{Nb}, \text{Ta}$) can be treated as an electric dipole with a fixed M^{5+} position as depicted in Figure 4a. In case of an ideal non-interacting dipoles, in the absence of the small polaron effects, (i.e. no local lattice distortion), the f electron can occupy 12

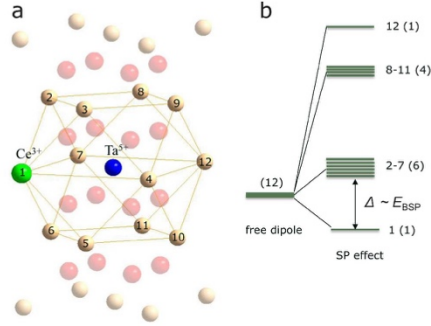


FIG. 4. (a) Schematic of the $\text{Ce}^{3+}\text{-M}^{5+}$ dipolar defect in ceria. (b) Energy diagram of the $\text{Ce}^{3+}\text{-M}^{5+}$ dipole. The degeneracy of the energy levels is indicated in the brackets.

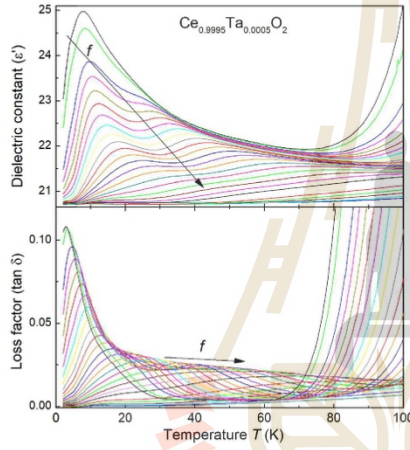


FIG. 5. Low-temperature dependence of the dielectric constant (top panel) and dielectric loss, $\tan \delta$ (bottom panel) of $\text{Ce}_{0.9995}\text{Ta}_{0.0005}\text{O}_2$ ceramics measured at selected ac frequencies, f , from 1 Hz to 1 MHz.

equivalent Ce sites next to the M^{5+} donor and the energy of the 'free' dipole will be twelve-fold degenerate (Fig. 4b). When the SP effects and dipole-dipole interactions come into play, the degeneracy will be (partially) removed as depicted in Fig. 4b. The ground state will be separated from the first excited 6-fold degenerate states by the energy $\Delta = E_{\text{BSP}}$, where E_{BSP} is the energy required to move the bound small polaron along with the

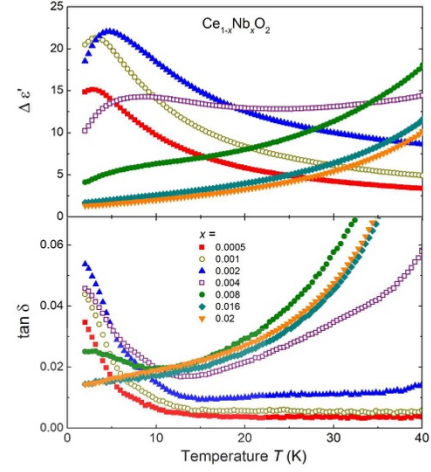


FIG. 6. (top panel) Low-temperature dependence of $\Delta \epsilon' = \epsilon'_0 - \epsilon'_\infty$, where ϵ'_0 was measured at 1 Hz and ϵ'_∞ was measured at 1 MHz. (bottom panel) Dielectric loss, $\tan \delta$ of $\text{Ce}_{1-x}\text{Nb}_x\text{O}_2$ ceramics measured at $f = 1$ Hz.

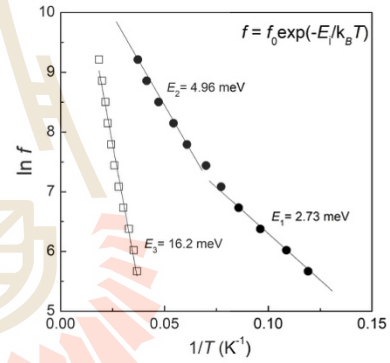


FIG. 7. Frequency dependence of the $\tan \delta$ peak as a function of $1/T$ for $\text{Ce}_{0.9995}\text{Ta}_{0.0005}\text{O}_2$ ceramics.

local lattice distortion from the ground state 1 to one of the six equivalent neighbour Ce sites labelled as 2,3,...7 in Fig. 4a. The next excited state is 4-fold degenerate and requires the higher energy to move the BSP from the site 1 to one of the four equivalent next-neighbour Ce sites labeled 8, 9...11. in Fig. 4a. The hopping of the

f electron between the 12 Ce sites bound to the donor defect can be viewed as a re-orientation (i.e., rotation) of the electric dipole which can be detected by the dielectric spectroscopy if the E_{BSP} is not too large.

Figure 5 shows an example of the low- T dependence of the real part of the dielectric constant, ϵ' , and dielectric loss, $\tan \delta$, for $\text{Ce}_{0.9995}\text{Ta}_{0.0005}\text{O}_2$ ceramics measured at selected ac frequencies, f , from 1 Hz to 1 MHz. In contrast to undoped CeO_2 whose ϵ' is temperature- and frequency-independent (not shown), the donor-doped ceria shows a pronounced low- T dielectric anomaly at $T < 70$ K (Fig. 5). At higher temperatures, the ϵ' increases dramatically due to the Maxwell-Wagner effect. We attribute the low-temperature $\epsilon'(T)$ anomaly to the dielectric relaxation of the dipolar defects associated with the localized hopping of the bound small polaron trapped next to the (donor) defect cite. Similar dielectric anomaly due to the relaxation of the bound small polarons is found in Nb-doped ceria. With increasing donor content, the $\Delta\epsilon' = \epsilon'_0 - \epsilon'_\infty$, (where ϵ'_0 and ϵ'_∞ are the low- and high-frequency dielectric constants, respectively) in $\text{Ce}_{1-x}\text{M}_x\text{O}_2$ goes through the maximum at $x \sim 0.002$ and decreases at $x > 0.004$ (Fig. 6). The decrease in the $\Delta\epsilon'$ at higher x is associated with the dipole-dipole interactions and disorder effects as the concentration of the defects increases.

To estimate the energy scale of the relaxation dynamics of the BSP we follow the frequency dependence of several $\tan \delta$ peaks that can be seen in Fig. 5. The frequency at which $\tan \delta$ shows a maximum at $T = T_m$ is plotted as a function of $1/T$ in Fig. 7. The f vs. $1/T$ dependence was fitted with the Arrhenius equation:

$$f = f_0 \exp\left(-\frac{E_a}{k_B T}\right), \quad (5)$$

where f is the applied frequency, f_0 is the attempt frequency of dipole re-orientation, E_a is the energy barrier of the re-orientation process and T is the temperature of the $\tan \delta$ maximum. The fit to Eq. 5 yields activation energies of ca. 2.73, 4.96 and 16.2 meV (Fig. 7). These are attributed to the (hopping) energies separating the BSP ground state from the several BSP excited states depicted in Fig. 4 b.

It is interesting that the hopping energy of the BSP (i.e., ~ 3 -16 meV) is significantly lower than that of the hopping energy of the itinerant SP (~ 66 meV). Although the BSP and the itinerant SP will experience different local lattice environment and, therefore, will have different hopping energy, it is still somewhat surprising that the energy difference is so large. It is quite plausible that we have overestimated the hopping energy of the itinerant SP as discussed above.

In contrast to the Nb(Ta)-doped ceramics, the W-doped ceria demonstrates significantly weaker dielectric relaxation at low T as shown in Fig. 8. Both the ϵ' and $\tan \delta$ anomalies in W-doped CeO_2 are more than one order of magnitude smaller than those found in Nb(Ta)-doped ceria (compare with Figs. 5 and 6). The activa-

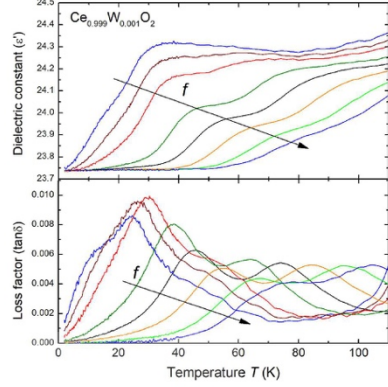


FIG. 8. Low-temperature dependence of the dielectric constant (top panel) and dielectric loss, $\tan \delta$ (bottom panel) of $\text{Ce}_{0.999}\text{W}_{0.001}\text{O}_2$ ceramics measured at selected ac frequencies, f , from 4 Hz to 5 kHz.

tion energies of the series of the low- T dielectric relaxations estimated from the frequency dependence of the $\tan \delta$ peaks in $\text{Ce}_{0.999}\text{W}_{0.001}\text{O}_2$ ceramics are ~ 17 , 27 and 62 meV; that is higher than those found in the Nb(Ta)-doped samples. A much weaker dielectric anomaly in W-doped ceria can be understood from the geometric considerations: In contrast to the $\text{Ce}^{3+}\text{-Nb}^{5+}$ defect, the co-axial $\text{Ce}^{3+}\text{-W}^{6+}\text{-Ce}^{3+}$ defect has zero total electric moment and, therefore, cannot contribute to the dielectric relaxation unless it adopts a non-co-axial geometry (as found in our first-principles simulations). Moreover, we expect that part of the W^{6+} ions will be partially compensated by accidental acceptor impurities and oxygen interstitials, thus creating a small concentration of the $\text{W}^{6+}\text{-Ce}^{3+}$ dipolar defects which can contribute to the weak dielectric relaxation in the W-doped CeO_2 . The higher activation energies of the dipolar relaxation may be attributed to larger random fields and local lattice distortions experienced by the BSP in the W-doped CeO_2 . The first-principles findings discussed below largely corroborate these experimental-based conclusions.

B. Results of the first-principles simulations

CeO_2 has experimental bandgap of 3.2 eV²⁰ with flat conduction bands of localized electrons⁷. The localized electrons distort the neighboring O atoms around Ce^{3+} called a small polaron. The calculated self-trapping energy of an excess electron in CeO_2 is -0.14 eV in our calculation (-0.30 eV in HSE06 and -0.54 eV in DFT+

TABLE I. Bond length of M -O $_i$ for polarons shown in Fig.10 (a), (b), (c), and (d) where 1,2,3...8 indicates the position of the O atom as labeled in Fig. 10(a). The calculated bond length of Ce-O of pristine ceria is 2.343 Å. E^{ST} represents energy difference between polaron state and delocalized state. For Nb, Ta, and W doped ceria, the four O atoms that form a tetrahedral configuration around the dopant are underlined.

Configuration	$M - O_i$ bond [Å]	E^{ST}
$[\text{Nb}^{1+} - \text{Ce}^{3+}]^0$	2.337, <u>1.978</u> , <u>1.954</u> , 2.514, 2.541, <u>2.002</u> , <u>1.979</u> , 2.462	-0.147
$[\text{Ta}^{1+} - \text{Ce}^{3+}]^0$	<u>1.953</u> , 2.507, 2.296, <u>1.972</u> , <u>1.972</u> , 2.446, 2.510, <u>1.993</u>	-0.228
$[\text{W}^{2+} - 2\text{Ce}^{3+}]^0$	<u>1.874</u> , 2.779, 2.170, <u>1.875</u> , <u>1.888</u> , 2.692, 2.374, <u>1.906</u>	-0.695
$[\text{U}^{2+} - 2\text{Ce}^{3+}]^0$	<u>2.198</u> , 2.242, <u>2.157</u> , <u>2.198</u> , <u>2.238</u> , 2.242, 2.242, <u>2.239</u>	-0.442

TABLE II. Bader charges of the dopant M and Ce ion in donor-doped ceria and reference compounds.

Defect	M , [e]	Ce, [e]
Ce_2O_3		+1.99
CeO_2		+2.39
Nb_2O_5	+2.30	
Nb_2O_5	+2.61	
$[\text{Nb}^{1+} - \text{Ce}^{3+}]^0$	+2.61	+2.14
Ta_2O_5	+2.34	
Ta_2O_5	+2.72	
$[\text{Ta}^{1+} - \text{Ce}^{3+}]^0$	+2.78	+2.16
WO_2	+2.21	
W_2O_5	+2.92	
WO_3	+2.90	
$[\text{W}^{2+} - 2\text{Ce}^{3+}]^0$	+2.88	+2.16, +2.17
UO_2	+2.50	
U_2O_5	+2.73	
UO_3	+3.01	
$[\text{U}^{2+} - 2\text{Ce}^{3+}]^0$	+2.80	+2.12, +2.12

U calculation as reported by Sun and co-workers⁷). The negative energy indicates that localization of an excess electron in the form of small polaron is favorable over delocalization state. An excess electron from any donor-type defect (such as O vacancy or donor-type dopant substituting Ce atom) can be trapped in CeO_2 in the form of small polaron.

The favorable defect configurations as a function of E_F for different charge states are found from the formation energy plot as shown in Fig. 9. Stable charge states for Nb_{Ce} and Ta_{Ce} are 0 and 1+ while for W_{Ce} and U_{Ce} they are 0 and 2+. The calculated bandgap of CeO_2 is 2.56 eV such that it is reasonably safe to ensure that the neutral (0) charge state is favorable for n -type. In case of neutral charge state, the defect itself could be $n+$ charged while the excess electron is trapped on the nearest-neighbor Ce atom forming $[\text{M}^{n+} - n\text{Ce}^{3+}]^0$ polaron defect complex having a hydrogenic-like bond as shown in Fig. 10.

For pentavalent Ta and Nb doped ceria, a polaron is localized on the nearest-neighbor Ce atom. For hexavalent W and U doped ceria, two polarons are localized on two nearest-neighbor Ce atoms which are close to each

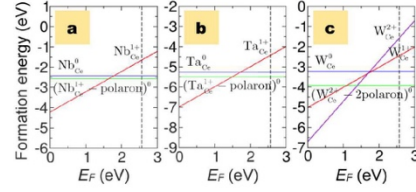


FIG. 9. Formation energies of (a) Nb_{Ce} , (b) Ta_{Ce} and (c) W_{Ce} in different charge states as a function of Fermi level (E_F). The blue, green, red, and purple line indicate neutral charge state M_{Ce}^0 , neutral complex $(M_{\text{Ce}}^{n+} - n \text{ polaron})^0$, 1+ charge state M_{Ce}^{1+} and 2+ charge state M_{Ce}^{2+} , respectively.

TABLE III. Binding energy of removing small polarons from the $(M_{\text{Ce}}^{n+} - n \text{ polaron})^0$ complex. E_b^{1st} and E_b^{2nd} stand for the binding energy of removing the first and the second polaron, respectively.

Configuration	E_b^{1st} [eV]	E_b^{2nd} [eV]
$(\text{Nb}_{\text{Ce}}^{1+} - 1 \text{ polaron})^0$	0.369	
$(\text{Ta}_{\text{Ce}}^{1+} - 1 \text{ polaron})^0$	0.516	
$(\text{W}_{\text{Ce}}^{2+} - 2 \text{ polarons})^0$	0.264	1.107
$(\text{U}_{\text{Ce}}^{2+} - 2 \text{ polarons})^0$	0.182	0.209

other. The $[\text{M}^{n+} - n\text{Ce}^{3+}]^0$ defect complex has an electric dipole moment which will contribute to the electric polarization in doped CeO_2 .

It is interesting to note that, among the studied dopant ions, W-doped ceria shows the highest self trapping polaron energy $E^{\text{ST}} = -0.695$ eV followed by U, Ta Nb with $E^{\text{ST}} = -0.442, -0.228$ and -0.147 eV (Table I). The small polaron occupies only one spin component that is the defect induced state below conduction band as shown in Fig. 11. For Nb, Ta, and W doped ceria, all eight neighboring O atoms move inward to the dopant because the dopants are slightly smaller than Ce. The bond length of $M\text{-O}_i$ ($i = 1, 2, 3, \dots, 8$ as indicated in Fig. 10a) is dis-

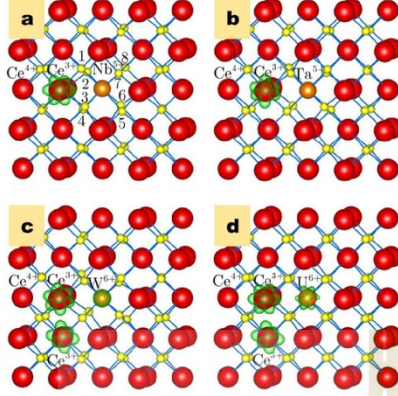


FIG. 10. Calculated spin densities of the favorable configuration of (a) $(\text{Nb}_{\text{Ce}}^{1+} - 1 \text{ polaron})^0$, (b) $(\text{Ta}_{\text{Ce}}^{1+} - 1 \text{ polaron})^0$, (c) $(\text{W}_{\text{Ce}}^{2+} - 2 \text{ polarons})^0$, and (d) $(\text{U}_{\text{Ce}}^{2+} - 2 \text{ polarons})^0$, respectively. The position of the first-nearest neighbor O atoms surrounding the dopant M is labeled by $i = 1, 2, 3, \dots, 8$ as indicated in the Figure (a). The distance from the dopant M to O_i atom ($M-\text{O}_i$) is listed in Table I.

torted from 2.343 Å of pristine CeO_2 and listed in Table I. In Nb, Ta, and W doped ceria, four $M-\text{O}_i$ bonds that form a tetrahedral configuration around the dopant are obviously shorter than 2.343 Å of pristine CeO_2 . This indicates a more covalent character of the four $M-\text{O}_i$ bonds while the remaining four oxygens form the dangling bonds. Our result is in good agreement with the DFT calculation of Muhich et al.²¹. On the other hand, U doped ceria shows no covalent character and U tends to move toward the two Ce^{3+} . Therefore, the $M-\text{O}_i$ bonds that share the O atom with the Ce^{3+} are shorter than the Ce^{4+} .

In order to compare our results with the oxidation number of referenced Ce compounds, Bader charge analysis^{22,23} has been carried out and the results have been listed in Table II. The referenced cerium(III) (Ce_2O_3) and cerium(IV) (CeO_2) oxide has Bader charge of +1.99 and +2.39 $|e|$, respectively. For Nb and Ta doped ceria, the dopant gives an excess electron to a neighboring Ce forming a polaron as shown in Fig. 10(a) and (b) with the Bader charge value of +2.14 and +2.16 $|e|$, respectively, that are close to the value of cerium(III) (Ce_2O_3). In other words, the oxidation state of neighboring Ce is changed from Ce^{4+} to Ce^{3+} . With polaron formation, the Bader charge of Nb and Ta are +2.62 and +2.78 $|e|$ which is close to niobium(V) (+2.61 $|e|$) and tantalum(V) (+2.72 $|e|$) oxide, respectively. For W and U doped ceria, the two neighboring Ce atoms are also

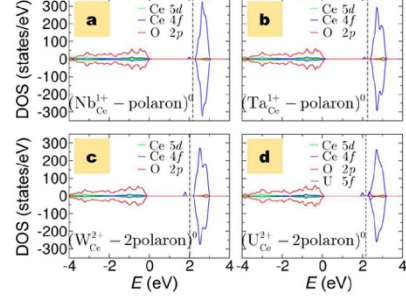


FIG. 11. Density of states (DOS) from spin-polarized calculations of (a) $(\text{Nb}_{\text{Ce}}^{1+} - 1 \text{ polaron})^0$, (b) $(\text{Ta}_{\text{Ce}}^{1+} - 1 \text{ polaron})^0$, (c) $(\text{W}_{\text{Ce}}^{2+} - 2 \text{ polarons})^0$, and (d) $(\text{U}_{\text{Ce}}^{2+} - 2 \text{ polarons})^0$, respectively. The valence band maximum is set to zero and the dashed line represents Fermi level. The localized state (small polaron) is slightly below the conduction band.

reduced to Ce^{3+} due to the two polarons formation as shown in Fig. 10(c) and (d), respectively. The W and U center becomes more positive with the value of +2.88 $|e|$ (+2.90 $|e|$ for tungsten(VI) oxide) and +2.80 $|e|$ (+3.01 $|e|$ for uranium(VI) oxide), respectively.

Interactions between small polarons and the donor defect M_{Ce}^{n+} in $\text{Ce}_{1-x}M_x\text{O}_2$ are examined by calculating the binding energy that is the energy required to separate a small polaron from the $(M_{\text{Ce}}^{n+} - n \text{ polaron})^0$ complex. The binding energy of removing the first and the second small polarons are given by

$$E_b^{1st} = E_{\text{tot}}[(M_{\text{Ce}}^{n+} - (n-1) \text{ polaron})^+] + E_{\text{tot}}[\text{polaron}] - E_{\text{tot}}[(M_{\text{Ce}}^{n+} - n \text{ polaron})^0] - E_{\text{tot}}[\text{bulk}] \quad (6)$$

and

$$E_b^{2nd} = E_{\text{tot}}[(M_{\text{Ce}}^{n+} - (n-2) \text{ polaron})^{2+}] + E_{\text{tot}}[\text{polaron}] - E_{\text{tot}}[(M_{\text{Ce}}^{n+} - (n-1) \text{ polaron})^+] - E_{\text{tot}}[\text{bulk}], \quad (7)$$

respectively, where $E_{\text{tot}}[(M_{\text{Ce}}^{n+} - n \text{ polaron})^0]$ is the total energy of the supercell containing $(M_{\text{Ce}}^{n+} - n \text{ polaron})^0$ complex ($n = 1$ for Nb and Ta, $n = 2$ for W and U), $E_{\text{tot}}[(M_{\text{Ce}}^{n+} - (n-1) \text{ polaron})^+]$ is the total energy of the supercell containing $(M_{\text{Ce}}^{n+} - (n-1) \text{ polaron})^+$ complex, $E_{\text{tot}}[(M_{\text{Ce}}^{n+} - (n-2) \text{ polaron})^{2+}]$ is the total energy of the supercell containing $(M_{\text{Ce}}^{n+} - (n-2) \text{ polaron})^{2+}$ complex, $E_{\text{tot}}[\text{bulk}]$ is the total energy of the perfect bulk supercell and $E_{\text{tot}}[\text{polaron}]$ is the total energy of an isolated small polaron. The results of the calculated binding energies are shown in Table III indicating that small polarons are strongly bound to the M_{Ce}^{n+} defect. We found that removing the second polaron from $(\text{W}_{\text{Ce}}^{2+} - 2 \text{ polaron})^0$ and

$(U_{\text{Ce}}^{2+} - 2 \text{ polaron})^0$ complexes requires more energy than removing the first one.

In general, the first-principles simulations are in qualitative agreement with our experimental findings. For Nb- and Ta-doped ceria the f -electron is localized on the nearest Ce site to the donor ion. In case of W- and U-doped ceria, the two Ce^{3+} ions are found on the nearest and next-nearest sites to the donor defect but they do not form a co-axial $\text{Ce}^{3+}\text{-M}^{6+}\text{-Ce}^{3+}$ defect complex as was intuitively suggested based on our low- T dielectric data. The energy scale of the BSP binding energy to the donor defect is of the same order of magnitude as the one estimated from the experimental data. However, the large difference in the E_b^{1st} values for Nb- and Ta-doped CeO_2 (Table III) is not supported by the experimental data (Fig. 3). The origin of the large discrepancy with the experimental data may be too small supercell used in our DFT simulations and/or the type of the electron correlation functional employed. For example, Sun et al. reported much smaller values of the BSP binding energy to the oxygen vacancy obtained by the hybrid functional-based first-principles simulations⁷.

IV. CONCLUSIONS

Early reports on the electron transport of donor-doped and partially reduced ceria have helped to shape a robust opinion that the f -electron localization in CeO_2 is driven by the electron-phonon interactions in the form of small polarons²⁴⁻²⁶. Since then CeO_2 has become (and still remains) a textbook example of the small polaron transport in metal oxides with the number of the first-principles simulations far exceeding the experimental reports.

More recent experimental and simulation results on ceria suggest that the other source of electron localization,

i.e., the Anderson localization caused by defects and random fields, has been overlooked^{5,7,27}. The experimental findings that do not fit with the small polaron scenario are the absence of the SP ‘overcrowding’ effect^{5,28}, a very large scatter in the activation energy of the electrical conductivity^{5,29-31}, a strong dependence of the activation energy on the type of the donor defect and other impurities^{27,32,33}, an absence of the correlation between the SP binding energy and the SP optical absorption band^{5,27}.

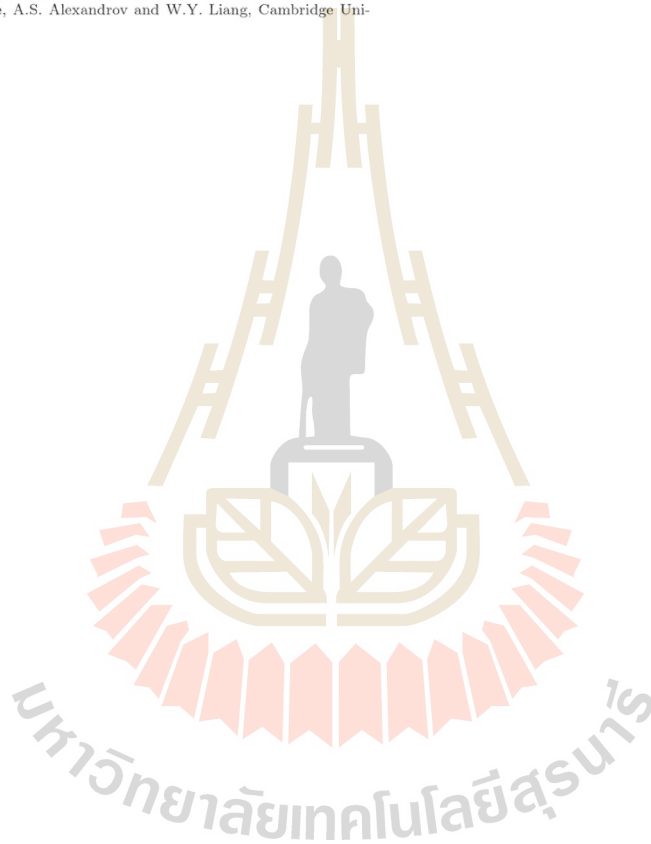
Both the experimental data and the first-principles simulations confirm the localized nature of the charge carriers in the donor-doped ceria³⁴⁻³⁶. We argue, however, that in contrast to the SP scenario, the main driving force for the localization in the real-case ceria is the Anderson localization stemming from the random fields and strong Coulomb interaction between the f -electrons and the (donor) defects.

Probably one of the most important results of this study is the very low activation energy of the BSP dynamics in ceria as revealed by the low- T dielectric spectroscopy. It appears that the ‘hopping’ energy of the SP bound to the donor defect is more than an order of magnitude smaller than the binding energy of the $\text{Ce}^{3+}\text{-M}^{5+/6+}$ defect complex. This may indicate that the SP effects in ceria are order of magnitude weaker than previously thought. We hope that these experimental findings will be taken as a reference standard for more refined and accurate first-principles simulations of electron localization in ceria.

This work was supported by internal NIMS project funds PA5160 and PA4020. The work of N.V. was supported by King Mongkut’s Institute of Technology Ladkrabang under grant 2562-01-05-46. N.V. and T.K. would like to acknowledge the ‘Academic Melting-Pot’ program. P.T. was funded by Development and Promotion of Science and Technology Talents Project (DPST) Scholarship, Thailand.

-
- * kolodiaznyi.taras@nims.go.jp
- ¹ P. W. Anderson, Phys. Rev. **109**, 1492 (1959).
 - ² P. K. Gosh and W. E. Spear, J. Phys. C., **1**, 1347-1358 (1968).
 - ³ T. Holstein, Ann. Phys. **8**, 343-389, (1959).
 - ⁴ H. L. Tuller and A. S. Nowick, J. Phys. Chem. Solids, **38**, 859-867 (1977).
 - ⁵ T. Kolodiaznyi, T. Charoonsuk, Y.-S. Seo, S. Chang, N. Vittayakorn, J. Hwang, Phys. Rev. B, **95**, 045203 (2017).
 - ⁶ P. W. Anderson, Nature (London) Phys. Sci. **235**, 163 (1972).
 - ⁷ L. Sun, X. Huang, L. Wang, A. Janotti, Phys. Rev. B, **95**, 245101 (2017).
 - ⁸ T. Kolodiaznyi, H. Sakurai, A. A. Belik, O. V. Gornostaeva, Acta Materialia, **113**, 116-123 (2016).
 - ⁹ G. Kresse and J. Hafner, Phys. Rev. B **48**, 13115 (1993).
 - ¹⁰ D. Sanchez-Portal, E. Artacho, and J. M. Soler, Solid State Commun. **95**, 685 (1995).
 - ¹¹ W. Kohn and L. J. Sham, Phys. Rev. **140**, A1133 (1965).
 - ¹² F. Fuchs, J. Furthmüller, F. Bechstedt, M. Shishkin, G. Kresse, Phys. Rev. B, **76** 115109 (2007).
 - ¹³ P. E. Blöchl, Phys. Rev. B **50**, 17953 (1994).
 - ¹⁴ G. Kresse and D. Joubert, Phys. Rev. B **59**, 1758 (1999).
 - ¹⁵ J. P. Perdew, K. Burke, and M. Ernzerhof, Phys. Rev. Lett. **77**, 3865 (1996).
 - ¹⁶ J. Hubbard, Proceedings of the Royal Society of London. Series A. Mathematical and Physical Sciences **276**, 238-257 (1963).
 - ¹⁷ A. Janotti, J. B. Varley, M. Choi, and C. G. Van de Walle, Phys. Rev. B **90**, 085202 (2014).
 - ¹⁸ A. Janotti and C. G. Van de Walle, Phys. Rev. B **76**, 165202 (2007).
 - ¹⁹ T. G. Stratton, H. L. Tuller, J. Chem. Soc. Faraday Trans. **83**, 1143-1156 (1987).
 - ²⁰ Z. C. Orel and B. Orel, physica status solidi (b) **186**, K33 (1994).

- ²¹ C. Muhich and A. Steinfeld, *J. Mater. Chem. A* **5**, 15578 (2017).
- ²² D. A. Andersson, S. I. Simak, N. V. Skorodumova, I. A. Abrikosov, and B. Johansson, *Phys. Rev. B*, **76**, 174119 (2007).
- ²³ G. Balducci, J. Kaspar, P. Fornasiero, M. Graziani, M. S. Islam, and J. D. Gale, *J. Phys. Chem. B* **101**, 1750 (1997).
- ²⁴ I. K. Naik and T. Y. Tien, *J. Phys. Chem. Solids*, **39**, 311-315 (1978).
- ²⁵ I.K. Naik and T.Y. Tien, *J. Electrochem. Soc.*, **126**, 562-66 (1979).
- ²⁶ H.L. Tuller and A.S. Nowick, *J. Electrochem. Soc.*, **126**, 209-217 (1979).
- ²⁷ T. Charoonsuk, N. Vittayakorn, T. Kolodiaznyi, *J. Appl. Phys.*, **123**, 165704 (2018).
- ²⁸ E.K.H. Salje, Polarons and bipolarons in WO_{3-x} and $\text{YBa}_2\text{Cu}_3\text{O}_7$, in *Polarons and Bipolarons in High- T_C Superconductors and Related Materials*, edited by E.K.H. Salje, A.S. Alexandrov and W.Y. Liang, Cambridge University Press, Cambridge (1995).
- ²⁹ M. C. Göbel, G. Gregori, J. Maier, *Solid State Ionics*, **215**, 45-51 (2012).
- ³⁰ R. N. Blumenthal, R. L. Hofmaier, *J. Electrochem Soc.*, **121**, 126-131 (1974).
- ³¹ R. N. Blumenthal, R. K. Sharma, *J. Solid State Chem.*, **13**, 360-364 (1975).
- ³² M.R. De Guire, M.J. Shingler and E. Dincer, *Solid State Ionics*, **52**, 155-163 (1992).
- ³³ P. V. Ananthapadmanabhan, S. B. Menon, D. S. Patil, N. Venkatramani, *J. Mat. Sci. Lett.*, **11**, 501-503 (1992).
- ³⁴ M. Nakayama, H. Ohshima, M. Nogami, M. Martin, *Phys. Chem. Chem. Phys.*, **14**, 6079-6084 (2012).
- ³⁵ E. Shoko, M. F. Smith, R. H. McKenzie, *J. Phys. Chem. Solids*, **72**, 1482-1492 (2011).
- ³⁶ J.J. Plata, A. M. Marquez, J. F. Sanz, *J. Phys. Chem. C*, **117**, 14502-09 (2013).



CURRICULUM VITAE

Name Pannawit Tipsawat

Date of Birth November 25, 1993

Place of Birth Bangkok, Thailand

Education

2016 – present MSc candidate

School of Physics, Suranaree University of Technology, Nakhon Ratchasima, Thailand, Project supervisor: Assoc. Prof. Sirichok Jungthawan.

2012 – 2016. BSc in Physics

School of Physics, Suranaree University of Technology, Nakhon Ratchasima, Thailand, Project supervisor: Prof. Santi Maensiri, Grades: 3.77/4 (First class honors).

2009 - 2011. High school

Ratchasima Wittayalai, Nakhon Ratchasima, Thailand, Grades: 3.94/4.

Grants and Fellowships

2012 – present. the Development and Promotion of Science and Technology Talent Program (DPST) scholarship at Ministry of Science and Technology, Thailand.

2016 – 2017. the DPST short term (6 months) researcher scholarship at National Institute for Materials Science (NIMS), Japan (Sept. 1, 2016 - Feb. 28, 2017).